"FATIGUE LIFE ESTIMATION OF LANDING GEARS OF FIGHTER AIRCRAFT USING FINITE ELEMENT ANALYSIS"

Submitted in partial fulfillment of the requirement
For the award of Degree of

MASTER OF ENGINEERING
In
(Production Engineering)

Submitted by

AMIT KUMAR SONI
(University Roll No. 9066)
(College Roll No. 13/Pro/04)

Under the Guidance of

PROF. VIJAY GAUTAM
Assistant professor

DEPARTMENT OF MECHANICAL ENGINEERING
DELHI COLLEGE OF ENGINEERING BAWANA ROAD,
NEW DELHI (DELHI UNIVERSITY)

2010-11

Certificate

This is to certify that the Master of Engineering Major Project entitled ***"Fatigue Life Estimation of Landing Gear of A Fighter Aircraft Using Finite Element Analysis"*** *submitted by Mr. AMIT KUMAR SONI, Department of Mechanical Engineering, Delhi College of Engineering, Delhi University, Delhi, embodies the original work carried out by him under my supervision and guidance. His work has been found excellent for the partial fulfilment of the requirement of the Degree of Master of Engineering in Production Engineering.*

The project has been carried out during the session 2010-11.

Internal Guide
(Prof. Vijay Gautam)
Assistant professor
Department of Mechanical Engineering
Delhi Technical University Formally
(Delhi College of Engineering)
Bawana Road, Delhi-42

External Guide
(R. P. Khapli)
Chief Manager (Design)
Head of Design Mechanical System &
Flight Analysis Group
Aircraft Upgrade Research and Design Centre
Hindustan Aeronautics Limited,
Nasik-422207

ACKNOWLEDGEMENT

It is distinct pleasure to express my deep sense of gratitude and indebtedness to my guide Prof. Vijay Gautam, Department of Mechanical Engineering, Delhi technical university formally Delhi College of Engineering, for his invaluable guidance, encouragement and patient review.

I am equally grateful to Shri R.P.Khapli, Chief Manager (Design), Head of Mechanical System & Flight Analysis Group, AURDC, HAL, Nasik who provides full hearted support, encouragement and helped me in solving all the practical problems and kept me going through the project work.

I remain grateful to Shri P.K. Khanwalkar, General Manager (AURDC), Hindustan Aeronautics Limited, Nasik for the permission to carry out this project work in HAL, Nasik Division.

I am thankful to Design Stress Department of AURDC, for their wholehearted support and technical advice. I sincerely extend my thanks to Mr. Nilesh Chaudhari, Manager (Design) & Mr. Sachin Shrivastav, Dy. Manager (Design) AURDC, HAL Nasik for their guidance and all assistance during my work.

I am grateful to Prof B.D. Pathak, HOD (Mechanical & Prod. Engg.), Prof S. Maji, Dean TRD, Prof S. K. Garg with other faculty members for providing necessary help and support from the department. I am also thankful to my friend Mr. Mukesh Shukla and Rishu Sharma for their unconditional support and motivation for this major project.

(AMIT KUMAR SONI)
University Roll No: 9066
College Roll No. 13/Pro/04
M.E. (Production Engineering)
Department of Mechanical Engineering
Delhi College of Engineering, Bawana Road, Delhi-42
Date:

ABSTRACT

The Total Technical Life (TTL) of fighter aircraft "Article 29L" is 1800 flying hrs. However the TTL of Main Landing Gear (MLG) and Nose Landing Gear (NLG) is only 2000 landing. Considering average sortie duration of 45 minutes, the life of LGs should have been ideally 2400 landings. So there is need to increase the life of LGs.

In older days the stress analysis and life extension study was carried out considering the experimental stress analysis approach and testing, which is time consuming and require huge testing setup. In order to bridge this gap and to reduce the effort, it is proposed to estimate the life of the under carriage by Integrated Approach of Finite Element (FE) Analysis.

The determination of the fatigue life of an engineering structure is based on two precepts. These are knowledge of the structure itself and knowledge of how that structure is loaded. The information required for fully understanding these two singularly complicated items is significant hence utmost care is taken to estimation of life of LGs.

In this work Finite Element (FE) Analysis 3-D geometric modeling developed using CATIA software. The assembly model was imported in PATRAN software and 3-D mesh was generated using HYPERMESH. Connectivity between the components is provided using the surface to surface contact element. Contact elements are capable of transferring the displacement as per contact status and stiffness of contacting body. The FE model was solved using NASTRAN software for stress and displacement, as per fatigue test load data available. Further fatigue analysis has been carried out using MSC Fatigue software for fatigue life estimation.

To validate FE stress analysis, results were compared with classical calculations and Rejuvenation zones of MLG. Thus determine cumulative fatigue damage hot spots can be rejuvenated locally and more no of landing (life of LGs) can be extended accordingly and avoid the experimental stress analysis approach and testing for life extension.

Key Words: Landing Gear, TTL, *FEM Analysis, Fatigue Life Estimation*

CONTENTS

LIST OF FIGURES

LIST OF TABLES

LIST OF ABBREVIATIONS

σ	Bending Stress
τ_t	Twisting Stress
σ_n	Normal stress
τ_q	Shear Stress
σ_m	Mean Stress
σ_a	Alternate Stress
σ_{min}	Minimum Stress
σ_{max}	Maximum Stess
µ	Micron
µm	Micrometre
30	(30/100) % OF CARBON(C)
2D	Two Dimensional
3D	Three Dimensional
A	Grade for high quality
AURDC	Aircraft Upgrade Research & Design Centre
A_k	Material constant
°C	Degree Centigrade
CLG	Centre line Landing Gear
CAD	Computer Added Design
D	Outer diameter
d	Inner diameter
FD	Flight Direction
FEM	Finite Element Method
FEA	Finite Element Analysis
G	Manganese (Mn)
GOST	Russian Standard

HAL	Hindustan Aeronautics Limited
I	Moment of Inertia
I_P	Polar Moment of Inertia
KH	Chromium (Cr)
K_f	Fatigue Notch Factor
K_t	stress concentration factor
LG	Landing Gear
M_b	Bending Moment
M_t	Twisting Moment
MLG	Main Landing Gear
MPC	Mid Point Contact
mm	Millimetre
N	Normal Load
N2	Nickel (not more than 2%) (Ni)
NLG	Nose Landing Gear
OPS	Oleo-Pneumatic Spring
Py	Vertical Force/Load
Px	Drag Force
Q	Shear Load
q	notch sensitivity,
R	R-ratio
r	Notch Radius
S	Silicon (Si)
S-N	Stress –No. of cycle
UTS	Ultimate Tensile Stress
V5	Version 5
X	Initial life of test sample
N2	Nickel (not more than 2%) (Ni)

CHAPTER 1: INTRODUCTION

Landing Gear generally referred as under-carriage, is a vital element of both civil and fighter aircraft. Under-carriage system is design to perform safe take-off and Landing of aircraft. It includes both Main Landing Gears (MLG) & Nose Landing Gears (NLG) and is designed with optimum weight, keeping in mind that it should not fail during service life of aircraft. Hence utmost care is required during designing and assigning/computing the life of the landing gears.

Under-carriage life is independent with aircraft life and defined in terms of number of landings during the service/operational life. It was noticed that number of landing assigned to under-carriage is expired well before the TTL/calendar life of aircraft. Thus life extension of under-carriage of an aircraft is vital activity and big challenge for aircraft designers. As under-carriage is subjected to high fatigue load the determination of the life of such engineering structure is based on the two precepts knowledge of the structure and loading condition of structure.

In earlier days the stress analysis and life extension / estimation study was carried out considering the experimental stress analysis approach and testing, which is time consuming and require huge testing setup. In order to bridge this gap and to reduce the effort, it is proposed to use Integrated Approach of Finite Element (FE) Analysis for life extension of under-carriage.

Finite Element (FE) Analysis is a computer simulation and has become powerful tool for numerical solution to a wide range of engineering problems. With aid of statistical design and advances in computer technology, FEA can provide quick and accurate solution to complex problem with relative ease. Therefore, FEA is employed for determining the stress and fatigue hot spots. This will help to minimize the number of tests and give focussed attention to the critical spots in the tests during full scale testing of Landing gears.

Further, under the duty cycle loading as experienced by the landing gears, the stress critical hot spot need not be the fatigue critical hotspots. Therefore in the analysis, fatigue life calculations become mandatory. FE structural analysis of the under-carriage component of a fighter aircraft are shown in this project in the subsequent pages. The stress critical hot spots are identified and indicated in the pictures. Further the fatigue critical hot spots are identified by carrying the fatigue analysis and the results are shown. The life of the main landing gear and nose landing gear is estimated and given.

1.1 OBJECTIVES OF PROJECT

The objective of the project is to gain the knowledge of the Fatigue life estimation / extension program of aircraft under-carriage system and Finite Element (FE) based stress analysis. The following objectives are specified:

- Implementation, and adaptation of modeling & Analysis through FEA based technologies for the components in Aerospace industries
- To identify stress hotspots (Stress critical) and stress level for MLG & NLG using computer simulation for different load cases.
- A comparative study of stress value calculated by classical method with result of computer simulation.
- To identify fatigue hot spots (potential locations of crack initiation) for MLG & NLG using computer simulation.
- To estimate corresponding fatigue life of MLG & NLG.

1.2 PROBLEM STATEMENT

i. To conduct the Finite Element based static stress analysis for all the loading conditions of the MLG and NLG and develop a methodology in identification of stress critical areas (stress hot spots),

ii. To conduct the Finite Element based Fatigue analysis to predict the crack initiation location (potential locations of crack initiation) with the loads as given in the repeated test program.

iii. Identify the fatigue hot spots, draw fatigue life plot and predict the corresponding fatigue life of the landing gear.

1.3 PLAN OF WORK

Project includes four steps i.e. CAD Modeling, Meshing, Stress Analysis & Fatigue analysis for Nose Landing Gears and Main Landing Gears of fighter aircraft article 29L.

In this work 3-D geometric modeling of detail structural components and assembly of MLG & NLG was developed using CATIA software from 2D drawings available with HAL. The assembly model was imported in PATRAN software and 3D mesh was generated using hyper mesh. Connectivity between the components is provided using the surface to surface contact element. Contact elements are capable of transferring the displacement as per contact status and stiffness of contacting body. The total number of elements and node in assembly are 166627 and 48520 respectively. The FE model was solved using NASTRAN software for stress and displacement, as per fatigue test load data available. Further fatigue analysis has been carried out using MSC Fatigue software for fatigue life estimation. The stress result were compared with stress value calculated classical method also hot spot zone were compared with rejuvenated zone of MLG and found matching.

1.4 ORGANIZATION OF THE THESIS

The thesis contains five chapters and travels from introduction to conclusion. Chapter 1 in the thesis covers the basic objective of the project and the problem statement. This unit gives the overview of the whole work and expected outcome. The literature review is clearly given in next section. This unit gives the basic idea about under-carriage system of aircraft, fatigue life and FEM. The recent advancements in these areas are also covered in this unit. The work done in past is clearly stated.

Chapter 3 gives the details of material and machine used for the work. This section also defines the CAD software & FEM software used like CATIA, Hyper-Mesh NASTRAN-PATRAN & MSC Fatigue. In later part of this chapter, experimental as well as analytical procedure is also discussed in detail. With the procedure and assumption referred in this unit, the results are clearly stated in terms of graphs and tables in chapter 4. FE structural analyses of the Main Landing Gear & Nose Landing Gear components of aircrafts are shown. The stress critical hot spots are identified and indicated in the pictures. Further the fatigue critical hot spots are identified by carrying the fatigue analysis and the results are shown. The analysis gives the clear picture of stress hotspots & fatigue hot spots, stress distribution fatigue life plot. The fatigue life of the Main Landing Gear and Nose Landing Gear are estimated and given. The thesis ends with conclusion, future scope of work and bibliography.

CHAPTER 2: LITERATURE REVIEW

2.1 LITERATURE SURVEY

2.1.1 Books

2.1.1.1 Currey Norman S.: Aircraft Landing Gear Design: Principal and Practices.

The book provides basic concepts & principals of aircraft landing gear design and referred to understand the landing gear system of fighter aircraft.

2.1.1.2 Chandrupatala T R, 1991, Prentice Hall of India Pvt. Ltd. New Delhi, Introduction to Finite Element Analysis

2.1.1.3 Cook Robert D., Malkus David S., Plesha Michael E. & Witt Robert J.: Concepts & Applications of Finite Element Analysis.

These books provide in-depth information regarding the basic concepts of finite element analysis and guide lines for Finite Element Analysis for different structures problems.

2.1.1.4 Astakhove M. F.: Aircraft stress analysis (Vol –I)

This book was referred to with view to understand stress analysis of aircraft components and assemblies.

2.1.1.5 Ramamurtham S.: Strength of Material.

This book deals with the fundamental concepts strength of material. During stress calculation by classical method this book was referred.

2.1.2 Technical Papers

2.1.2.1 Ossa E.A., 2006, Failure analysis of a civil aircraft landing gear, Journal of Engineering Failure Analysis 13 (2006) 1177–1183.

2.1.2.2 Bagnoli F. *, Dolce F., Colavita M., Bernabei M., 2008, Fatigue fracture of a main landing gear swinging lever in a civil aircraft, Journal of Engineering Failure Analysis 15 (2008) 755–765

2.1.2.3 L.A.L.,*, Lourenco N.J. , Graca M.L.A., Silva O.M.M. , Campos P.P. de , Dollinger C.F.A. von, 2006 Fatigue fracture of a nose landing gear in a military transport aircraft Franco, Journal of Engineering Failure Analysis 13 (2006) 474–479.

2.1.2.4 Leea Hong-Chul, Hwanga Young-Ha, Kimb Tae-Gu, 2003, Failure analysis of nose landing gear assembly, Journal of Engineering Failure Analysis 10 (2003) 77–84

2.1.2.5 Azevedo C.R. de Farias, Hippert E. Jr., 2002, Fracture of an aircraft's landing gear, Journal of Engineering Failure Analysis 9 (2002) 265-275

These papers provides detail on fatigue fracture of various landing gears and there reason, these papers also help to understand the stress critical areas of landing gears.

2.1.2.6 La Rue J.E., Daniewicz S.R., 2006, Predicting the effect of residual stress on fatigue crack growth International Journal of Fatigue (2006).

The paper states the effect of residual stress on fatigue fracture, it also state high accuracy of analysis can be obtained but at the expense of increased modeling complexity.

2.1.2.7 Kaplan Mitchell P. and Wolff Timothy A.,2001, Fatigue-Life Assessment, International Journal of Fatigue (2001).

The paper gives in-depth information about fatigue life and its assessment.

2.1.3 Manuals

2.1.3.1 Maintenance Manual Book 3 of Article 29L

A detailed description of the aircraft landing gear system is given in this manual along with the parameters and an explanation of the working of the same.

2.1.3.2 Stress Album of MLG and NLG of Article 29L

A detailed description of the type of loading on MLG & NLG and corresponding stresses.

2.2 THEORETICAL BACKGROUND

2.2.1 Introduction to Landing Gear System[7,8]

Modern airliners have one nose landing gear and two main landing gears, some of the larger aircraft have a centerline landing gear (CLG) to support the MLG's when the aircraft is heavily loaded. The basic structure for the landing gear is the same for most commercial airliners; it has a barrel structure (outer cylinder) and a shock-absorber (inner cylinder). A spring is set between the barrel structure and the shock-absorber. The shock absorber is connected to the barrel structure, which in turn connects them both to the aircraft. The active part of the shock absorber is a gas/fluid spring also called an oleo-pneumatic spring (OPS). The OPS is located in the top part of the shock absorber (Figure 2.1).

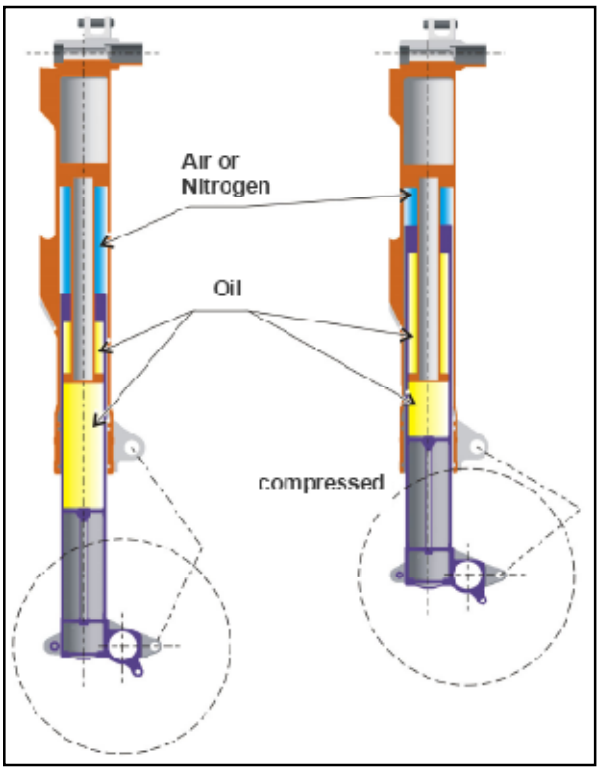

Figure 2.1 Shock absorber during functioning[7,8]

On modern airliners the ground steering is realised by turning the nose wheels, the wheels are turned by an actuator system that turns the inner cylinder

of the NLG. The OPS provides the damping for the aircraft during landing and taxing, it has one of the best damping properties of all spring systems in the market. An OPS consists of two chambers. One is completely filled with hydraulic fluid (oil); the other is partly filled with hydraulic fluid and partly with gas, usually dry nitrogen (Figure 2.1).

During the compression of the landing gear the sliding tube assembly moves into the main fitting assembly. The decrease in volume causes hydraulic fluid to flow through the upper bearing housing and the recoil orifice plate moves and slows the flow of hydraulic fluid. The decrease in volume also causes hydraulic fluid to move through the diaphragm and lift the compression orifice plate: the hydraulic fluid flows through the baffle and into the upper diaphragm tube subassembly (Figure 2.2). This slows the speed of the compression. Hydraulic fluid that moves into the upper diaphragm tube compresses the nitrogen in the main fitting subassembly and the upper diaphragm tube subassembly. As the pressure of the nitrogen increases, the hydraulic fluid in the rod assembly moves against the piston. This slows the speed of the compression even more. When the compression force is decreased the nitrogen pressure in the cylinder pushes the piston to the end of the cylinder: hydraulic fluid moves out of the cylinder and into the rod assembly. The nitrogen pressure in the main fitting subassembly and the upper diaphragm subassembly pushes the hydraulic fluid through the baffle: the compression orifice plate is pushed against the diaphragm and limits the flow of hydraulic fluid through it. This slows the speed of the recoil.

The combined effect gives a smooth dampening. The NLG and MLG have the same system for damping; the OPS on the MLG are larger to cope with the larger loads (Figure 2.1). The functionality of the spring is dependent on the right filling ratio of gas and fluid. If the ratio is wrong the spring either has too little or too much damping. This could result in damage to the landing gear or in the worst case to the aircraft.[7,8]

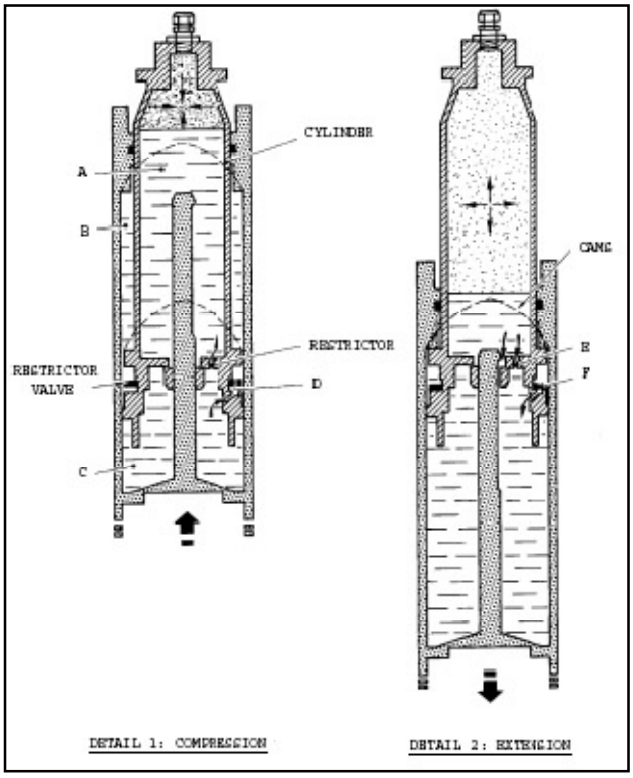

Figure 2.2: shock absorber during compression[7,8].

2.2.2 Landing gear system of aircraft article 29L(selected for project)[15,24]

2.2.2.1 Introduction

The primary purpose of the landing gear is to facilitate movement of aircraft easily on ground while taxing, carry the aircraft weight during take off until it is transferred to the wings and to absorb the shock while landing. The maximum landing weight is of the order of 65 to 70% of the take off weight. Aircraft Landing Gears particularly those of military aircraft are designed for optimum weight. The main purpose of a fighter aircraft is to take off at the shortest possible time, fly and accomplish the mission.

Fighter aircrafts has Tricycle Landing Gear (i.e. it is having 3 landing gears). In this configuration there one Front landing gear is called Nose Landing Gear (NLG) mounted on front frames of fuselage and two rear landing Gear called as Main Landing Gear MLG, mounted near to Center Section of fuselage.

After take-off MLG retracted forward in fuselage well while at the time of landing LG are extended & locked. During landing, most of the time ac lands first on its MLGs and later NLG touches the ground, however there are further possibilities of landings viz. 3-point landing, landing on single MLG, landing with brakes applied, landing with side gust load etc.

For design of LG use of high-strength alloy steel a common practice for major load carrying members. In present design, designer typically used 30KHGSN2A to achieve high strength to weight ratio for LG components.

2.2.2.2 Main Landing Gear (MLG)

MLG of selected aircraft is a complex mechanical assembly (Figure-2.3). Main parts of MLG are Strut, Wheel Turning Unit, Semi fork and Wheel Additional Steering Mechanism with Kinematic Lock. Strut is a welded assembly of three parts, cylindrical in cross section with upper end acting as a pivot point, attached to fuselage structure with the help of removable axle and whose lower end is used as an attachment for turning unit.

The beam is provided with lugs in the middle portion for connecting rod of hydraulic actuating cylinder and bell crank of wheel additional steering mechanism. Provision is made for attachment of ground handling cables used for towing and ground run of the engine. The inner cavities of both the beams and removable axles are used as storage bottles of compressed air for aircraft pneumatic system.

2.2.2.3 Nose Landing Gear (NLG)

The nose LG is arranged along ac centerline of symmetry between frame # 6 to 12 with nose leg attached to frame 7 with the help of axle. It comprises of nose LG leg with shock absorber, two wheels type KT-100 and wheel steering mechanism with its drive. After takeoff, Nose Landing Gear is retracted in the reverse direction (i.e. opposite to the flight direction) into the un-pressurized compartment between frame nos. 6 and 12 of fuselage nose section. The compartment is closed by two hinged doors, provided with tongs-type mechanism actuated by leg itself for their closing & opening. After retraction the

leg is locked & held in this position by mechanical up-lock installed on frame no. 11 along aircraft centerline of symmetry.

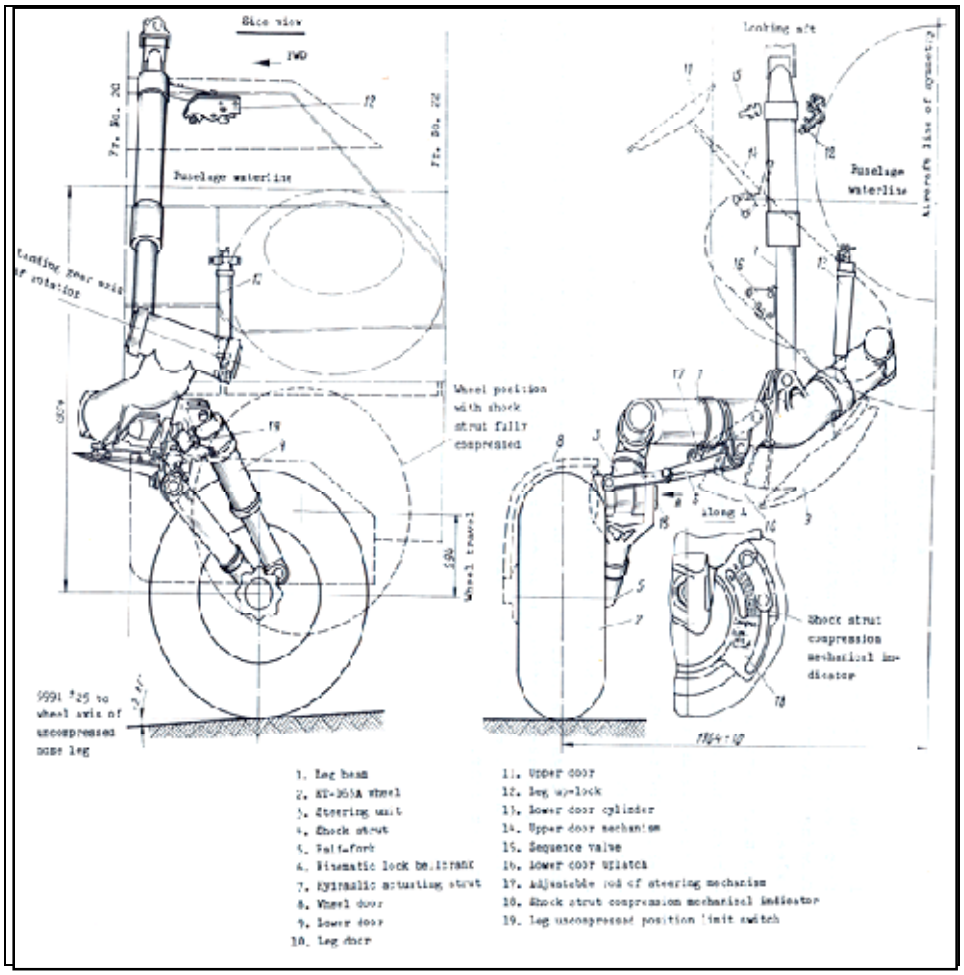

Figure 2.3 Installation and assembly details of the MLG[15,24]

Extension & Retraction operation of NLG Strut is performed by actuating Hydraulic cylinder. Landing gear is also provided with a light to facilitate night landing. The aircraft is steered on ground by wheel steering mechanism MRK 32-25 installed on Nose LG strut. The mechanism counteracts involuntary turns of aircraft during takeoff ground run, landing run and taxing and also ensures turning of the aircraft as per the requirement. Main load carrying members of nose LG are fabricated from steel 30KHGSN2A, heat treated to 170±10 kg/mm^2.

The nose LG leg fork is a welded assembly of two parts with upper portion attached to the head of steering unit with the help of an axle. Lower portion serves as an axle with flanges for installation of nose LG wheels & brakes. In the middle, provision of boss for installation of leg up-lock shackle and lugs for securing connecting rod is made.

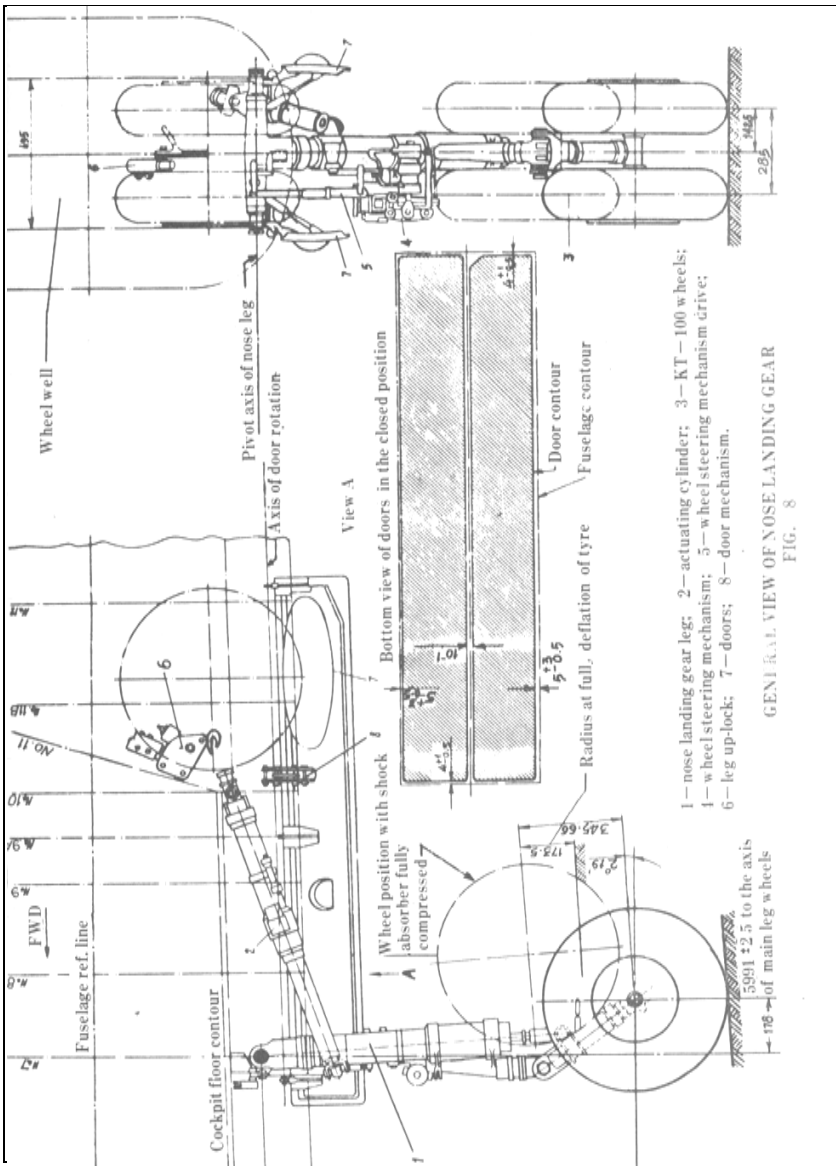

Figure 2.4 Installation and assembly details of the NLG[15,24]

2.2.3 Introduction to Fatigue[6]

Fatigue cracks are caused by the repeated application of loads which individually would be too small to cause failure. Fatigue cracks usually initiate from surface of the component (Fig.39). This is a crack initiation. The crack may then propagate in a direction perpendicular to the direct stress. This is crack propagation. Finally the component may fracture.

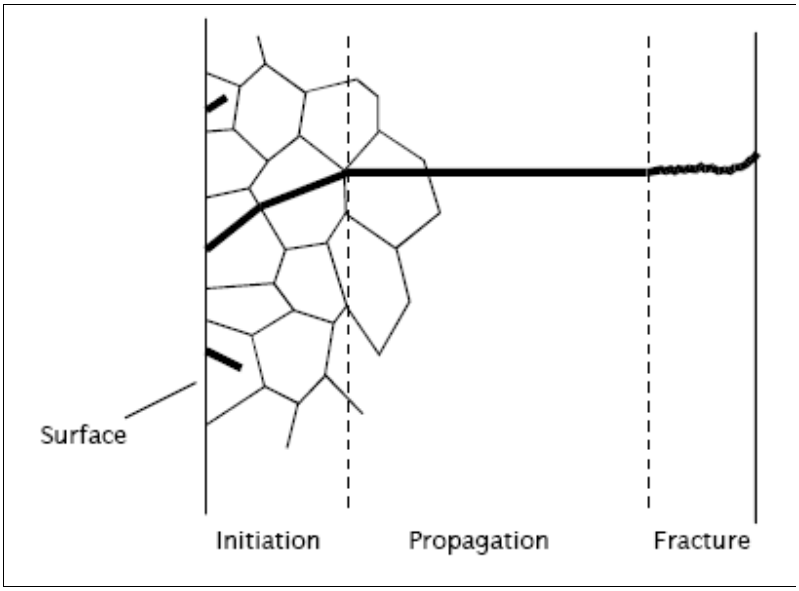

Figure 2.5: Three stages of fatigue failure.[6]

Modern fatigue theories provide separate analysis for each phase. Crack initiation theories are based on assumption that fatigue cracks are initiated by the local strains and stresses on the surface of a component. Crack propagation theories relate crack growth to the stress in the component. MSC Fatigue is a fatigue analysis tool used to predict crack initiation spot.

Final fracture is analyzed using fracture mechanics. Earlier theories treated the whole of the fatigue life as a single entity, and related fatigue life to the calculated engineering stress in the component. Much current research is attempting to describe the whole fatigue process by the study of crack propagation from very small initial defects

2.2.4 Fatigue Life Assessment[3]

The determination of the life of an engineering structure is based on the two precepts. These are knowledge of the structure itself and knowledge of how that structure is loaded. In order to predict the life of the component, therefore the determination of rational inspection intervals require the several engineering disciplines such as mechanics, mechanism, metallurgy, material science, corrosion, inspection methods, statistics, testing methods and design. The individuals tasked with the determination of the component life depend on the knowledge and results of those who can supply the afore mentioned information.

The next area is the determination of these external loads in to internal loads. The internal loads are the loads that manifest themselves throughout the structure. One assume a particular point in time and has a load condition (all the external variables are fixed), and from that one can calculate the loads going through out the structure. These internal loads are then transformed to stresses. The mechanism also needs to discussed. From this we come to know that the structure is statically loaded or dynamically loaded. Finally we see the operating environment. The temperature and the chemical atmosphere determine the operational life of the structure.

2.2.4.1 Fatigue Crack Growth Variables

The fundamental variables involved in any life assessment are those that describe the effects and interaction of material behavior, geometry and stress history on the life of the component. The traditional fatigue methods such as the stress life method, an S-N curve, which plots stress verses number of cycles to failure, is obtained through fatigue testing and is used to define a material-dependent endurance limit. The effects of geometry are established through a fatigue notch factor. It is important to remember that the stresses expected in service are limit stresses expected in service are limit stresses and not ultimate stresses, which have been multiplied by a safety factor to meet static strength requirement.

2.2.4.2 Stress Life Variables[3]

2.2.4.2.1 Constant-amplitude loading and endurance limit

Constant amplitude loading cycles is described in fig-1 by several parameters that are defined in terms of the minimum and maximum stresses applied during the loading cycle. The mean stresses, $б_m$ and the alternating stress $б_a$ is defined as

$$\sigma m = \frac{(\sigma \max + \sigma \min)}{2}$$

$$\sigma a = \frac{(\sigma \max + \sigma \min)}{2}$$

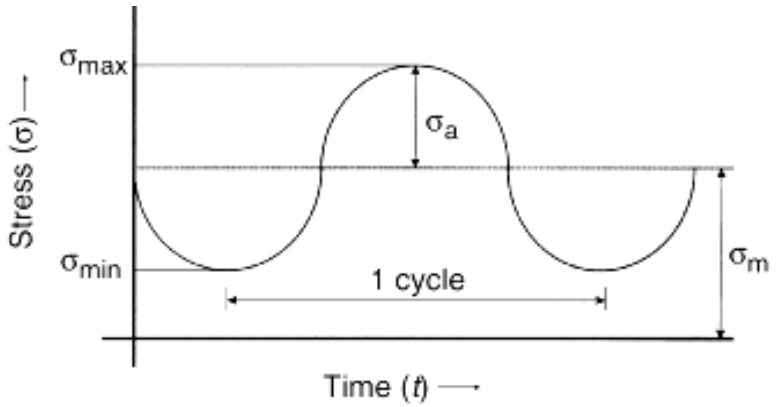

Figure 2.6 Constant Amplitude loading cycle[3]

An additional parameter that is useful for characterizing the type of loading is the R-ratio:

$$R = \frac{\sigma \min}{\sigma \max}$$

A negative R-ratio indicates a tension-compression loading cycle. For an R-ratio of -1, the loading is fully reversed and the mean stress is consequently 0. The reresult of fatigue test run at R= -1 are plotted on S-N curve as shown in fig-2 to establish an endurance limit for the material. For low strength steels, the the endurance limit is established by the portion of the S-N curve that becomes asymptotic as the number of cycles become large. Stress levels below the

endurance limitare considered non-damaging. The endurance limit for low strength steel is roughly 50% of ultimate tensile strength. For high strength steels and aluminum, which do not exhibit a clearly defined asymptote, theendurance limit is defined as the alternating stress level occurring at107 cycles.

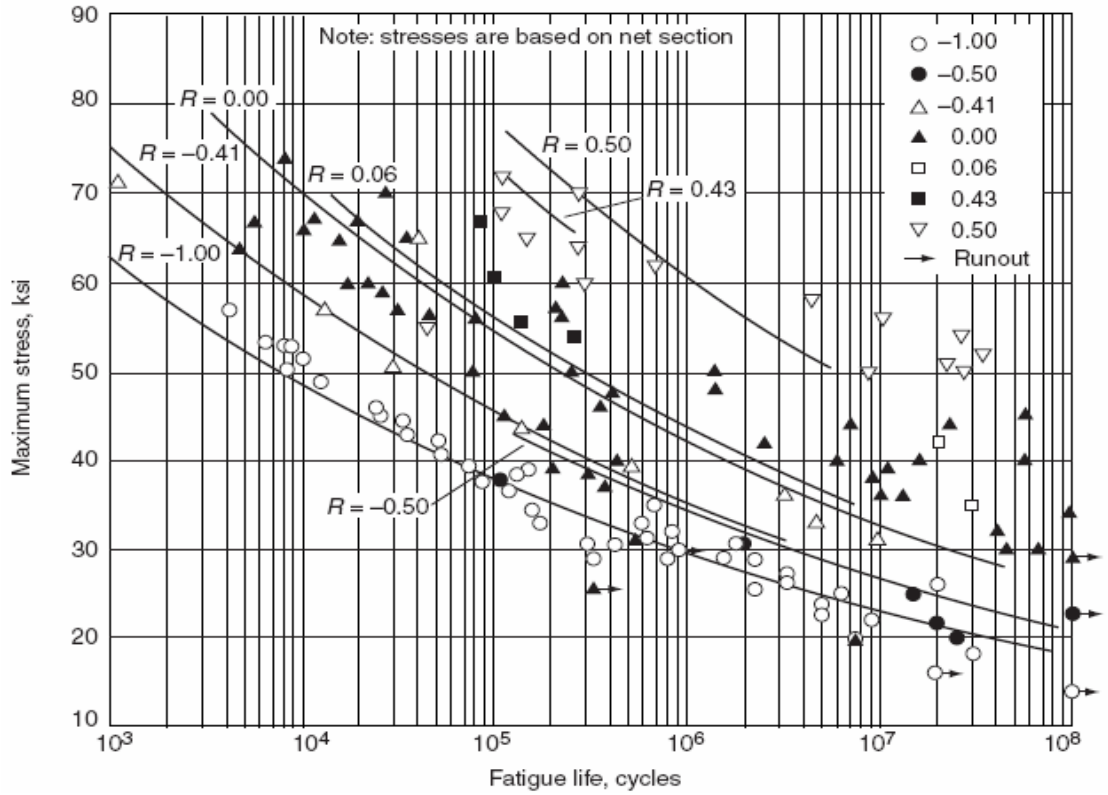

Figure 2.7 *S-N curve for unnotched 2024-T4 aluminum alloy bar*[3]

2.2.4.2.2 Variable-amplitude loading and cumulative damage

While constant-amplitude loading is useful for defining fatigue properties and comparing test data, variable-amplitude loading, such as that shown in fig-3, is more likely to be encountered by structural components in actual service. In order to calculate the life of a component subject to variable loading, a method is needed that relates constant-amplitude fatigue test data to a random stress history. The Palmgren- Miner cumulative damage rule which has the form:

$$\sum_{i=1}^{m} \frac{n_i}{N_i} = 1$$

Provides a simplified approach to this problem, Ni represents the total life of a component for a given stress cycle, ni represents the number of stress cycles actually sustained by the component for the given stress cycle, and the upper limit, m, is equal to the number of unique stress cycles in the stress spectrum. The fraction of damage done by each unique stress cycle is added together to obtain a cumulative damage fraction. The reciprocal of this fraction is equal to the number of stress spectra that the component can withstand before failure. The Palmgren- Miner rule essentially reduces a variable stress spectrum into “blocks” of constant-amplitude stresses to obtain a fatigue life estimate. To accomplish this, two primary assumptions are required. First, the relationship between ni and Ni is assumed to be linear. Second, the fatigue life is assumed to be independent of the order in which the blocks of stresses are applied. These assumptions are valid only under a very limited set of circumstances. For this reason, life estimates obtained from the Palmgren-Miner rule are divided by a large safety factor

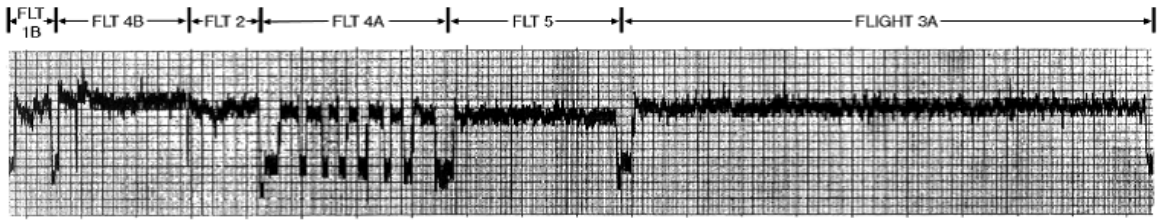

Figure 2.8 *Variable-amplitude loading data*[3].

2.2.4.2.3 Stress concentration and fatigue notch factor

High-stress regions in a structural component are typically located around geometric details, such as a hole, fillet radius, or notch. These local high-stress regions are described in terms of the remote or far-field stress of the component by multiplying the remote stress by a stress concentration factor. Stress concentration factors for various geometric details arederived from the theory of elasticity and/or obtained experimentally. Fatigue tests have shown that the local notch stresses predicted by the stress concentration factor are usually higher than those measured from testing. Therefore, in order to differentiate the

theoretical stress concentration factor from the actual measured stress concentration, the term fatigue notch factor is used to describe the local notch stresses that occur during fatigue loading. For axial or bending fatigue tests, the fatigue notch factor is obtained by dividing the endurance limit of an un notched test specimen by the endurance limit of a notched test specimen. The fatigue notch factor can also be defined in terms of notch sensitivity, q:

$$K_f = q\,((K_t - 1) + 1$$

where Kf is the fatigue notch factor and Kt is the stress concentration factor for the given notch geometry. Notch sensitivity is a measure of how close the experimental results for a particular geometry approach the theoretical results. Fig. 4 displays notch sensitivity versus notch radius for various metals,

$$q = \frac{1}{1 + (A_k / r)}$$

where Ak is a material constant and r is the notch radius. As the notch radius becomes large, the notch sensitivity factor approaches one, resulting in a fatigue notch factor that is equal to the stress concentration factor. For ferrous alloys, Ak can be approximated by the empirical relationship

$$A_k = \left(\frac{300}{S_u}\right)^{1.8} \times 10^{-3} \text{ in.}$$

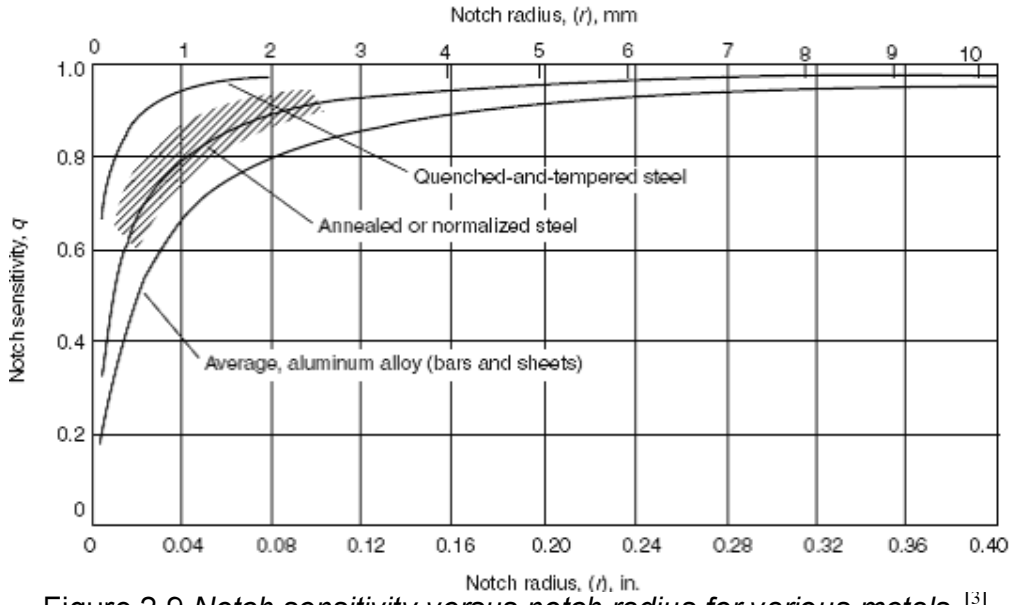

Figure 2.9 *Notch sensitivity versus notch radius for various metals*. [3]

2.2.4.3 Stress spectrum

Increased awareness of the effects of load interaction has demonstrated the importance of defining a realistic loading spectrum for fatigue and damage-tolerance analysis and test. This has led to much effort being expended to quantitatively define how the variation of key spectrum parameters affect crack growth life. The key question remains how closely a design spectrum must simulate real life usage to accurately predict component life.

The first spectra were all block type. It should be noted that the most simplistic block spectrum would have all cycles at a single stress. More complex block spectra would have several different stresses with many cycles at each of the stresses. These block spectra may be stress increasing, stress decreasing, or have the stresses first increase and then decrease. Fig. 5 shows these different types of spectra. There were several reasons for using the block spectra, including; it is easier to program the test equipment, and analytical fatigue techniques such as the Palmgren-Miner Rule did not recognize complex stress sequencing.

Unfortunately, the use of the block spectrum did not accurately reflect the fleet experience, and it should be noted that the fleet experience indicated a shorter life. Therefore, it was necessary to go to a more complex test spectrum to improve the accuracy of the testresults when compared with the lives experienced by the fleet. The more complex stress spectrum was the flight-by-flight spectrum. There are no equipment complexities: personal computers and the computers attached to the laboratory test equipment allow the investigator to use any type of spectra desired.

Problems then occur with the derivation of the stress spectra that best reflects actual use. To define a spectrum that is used to determine component life, care must be taken to ensure ease of analysis and test coupled with realism. For any component (aircraft, automobile, ship, or bridge), the type of loading(s) must be defined and quantified. In all these instances, there are two major types

of loads-operator-induced loads and environmentally induced loads. Operator-induced loads may be maneuver and landing loads for aircraft, The environmental loads may be gust loads, wind loads, for aircraft. The operator-induced loads are determinate, while the environmental loads are probabilistic in nature. Since in many cases these loads occur simultaneously, combining them in a meaningful and consistent manner remains a challenge. It is generally left to the investigator to determine the means of accomplishing this combination.

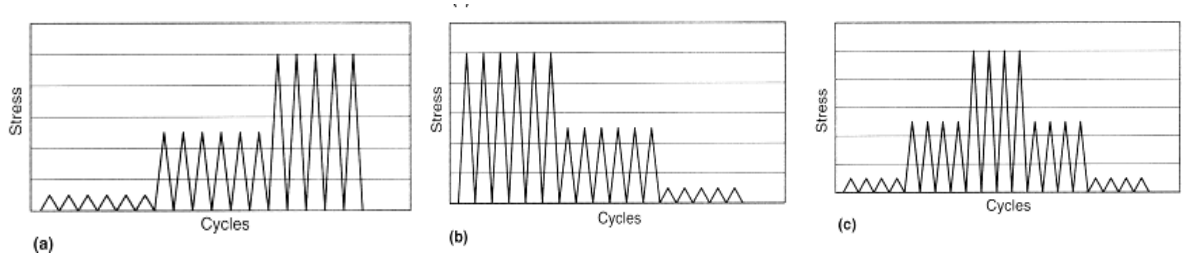

Figure 2.10 *Different types of block spectra. (a) Low-high (b) High-low (c) Low-high-low*[3]

2.2.4.4 Factors affecting the fatigue properties of metals

The main factors affecting the fatigue properties of a component are:

2.2.4.4.1 Stress concentration caused by component design

Fatigue of a component depends on the stress amplitude attained, the bigger the stress amplitude the fewer the stress cycles needed for failure. Stress concentrations caused by sudden changes in cross-section, key-ways, holes or sharp corners can thus more easily lead to a fatigue failure. The presence of the counter shunk hole was considered in one case to have lead to a stress concentration which would have led to a fatigue failure.

2.2.4.4.2 Corrosion

The effect of the corrosion resulting from the salt solution attack on the steel is to reduce the number of stress cycles needed to reach failure for every stressamplitude. The non-corroded steel has a limit of 450 MN-2, the corroded steel has no fatigue limit. The steel can be protected by plating.

2.2.4.4.3 Residual Stresses

Residual stresses can be produced by many fabrication and finishing processes. If the stresses produced are such that the surfaces have compressive residual stresses then the fatigue properties are improved, but if tensile residual stresses are produced at the surfaces then poorer fatigue properties results. The case hardening of steels by carburizing results in compressive residual stresses at the surfaces hence improves the fatigue properties. Rejuvenation/Shot peening also introduced compressive residual stresses.

2.2.4.4.4 Surface Finish / Treatment

The effect of surface finish on the fatigue properties of components is a very significant. Scratches, dents or even surface identification markings can act as stress raisers and so reduce the fatigue properties. Shot peening a surface produces surface compressive residual stresses and improves the fatigue life. Some surface treatment e.g. conventional electroplating can, however, have a detrimental effect on the fatigue properties. This is because the surfaces end up with tensile residual stresses.

2.2.4.4.5 Temperature

An increase in temperature can lead to a reduction in fatigue properties. This is because of oxidation or corrosion of the metal surface increasing. For example, the nickel-chromium alloy Nimonic 90 undergoes surface degradation at temperatures around 700 to 800 0 c and there is a poorer fatigue performance as a result. In many instances an increase in temperature does result in poorer fatigue performance.

2.2.4.4.6 Microstructure of Alloy

The micro structure of an alloy is a factor in determining the fatigue properties. This is because the origins of fatigue failure are extremely localized, involving slip at crystal planes. Because of this, the composition of an alloy and its grain size can affects its fatigue properties. Inclusions, such as lead in steel, can act as nuclei for fatigue failure and so impair fatigue properties.

2.2.4.4.7 Heat Treatment

Heat treatment can change or produce residual stresses within a metal. As mentioned earlier, case hardening improves fatigue properties as a result of producing compressive residual stresses in surfaces. However, some heat treatments can reduce surface compressive stresses and so adversely affect fatigue properties. Some hardening and tempering treatments fall in to this category.

2.3 RECENT WORK

2.3.1 Use of Classical method stress analysis:

Aircraft landing gear life was calculated by classical method. In this method bending stress and shear stress at various sections of structure components were calculated using following important formulae

1. Bending Stress $\sigma_m = \frac{M_b}{Z}$ (i)
2. Twisting Stress $\tau_t = \frac{M_t}{Z}$ (ii)
3. Normal stress $\sigma_n = \frac{N}{A}$ (iii)
4. Shear Stress $\tau_q = \frac{Q}{A}$ (iv)
5. Moment of Inertia $I = \frac{\pi(D^2 - d^2)}{64}$ (v)
6. Polar Moment of Inertia $I = \frac{\pi(D^2 - d^2)}{32}$ (vi)

2.3.2 Use of Rejuvenation Technology/Residual stress measurement:

The Rejuvenation Technology was developed for life extension of aircraft landing gear. The methodologies adopted for life extension of landing gear by

- Identification of Stress Critical Zone
- Measurement of Compressive Residual Stress to assess the fatigue damage on used and CAT 'A' MLG Struts Residual stresses are locked-in

stresses which exist in a structural part without the application of any service or other external loads. Residual Stress can be measurement can be done in any of the method described below,

- Centre Hole Drilling Method
- X-Ray Diffraction Method
- Magnetic Barkhausen Method

2.4 SUMMARY OF PAST WORK

Aircraft article 29L was designed& developed by Russian (OEM) in late 60's&IAF operating article 29L from 1984 onwards till date. The Total Technical Life (TTL) assigned by OEM to article 29L was 1800 hrs.Considering average sortie duration of 45 minutes, the life of MLGs should be ideally 2400landings, but OEM has assigned only 1200 landing life of undercarriage, later life is extended to 2000 by HAL by Rejuvenation Technology. However critical shortage of undercarriages of article 29Lis predicted because 2000 landing life is about to expire and new manufacturing of landing gears not in scopeas aircraft was phased out in late 90s at Russia.

So there is need to further extend the life of landing gear. The bending stress and shear stress at various sections of landing gear components were calculated using classical method earlier was helpful during FEM modelling and care has been taken to maintain the mesh quality in areas where stress levels are higher. This Fatigue analysis will provide a foot forward in this regard.

CHAPTER 3: EXPERIMENTAL PROCEDURE

3.1 DETAILS OF COMPONENTS/APPARATUS/HARDWARES/SOFTWARES

3.1.1 Main Landing Gear (Ref Figure-2.3)[15,24]

After takeoff, Main LGs are retracted across the airflow into side compartment of the fuselage centre section located between frame no. 20 and 22. This compartment is closed with four doors viz. lower door, wheel door, upper door and strut door refer Appendix-D.

Main LGs are

- Manufactured from forgings of high strength alloy steel 30KHGSNA
- X-RAY Inspection of forging & welded joints.
- Heat treatment to obtain UTS=170±10 Kg/mm^2.
- Surface Coating – Zinc Metallizing.
- Assembly & testing using special fixtures & test equipments

3.1.2 Nose Landing Gear (Ref Figure -2.4)[15,24]

After takeoff, Nose Landing Gear is retracted in the reverse direction (i.e. opposite to the flight direction) into compartment between frame nos. 6 and 12 of fuselage nose section later compartment is closed by two hinged doors. Extension & Retraction operation of Nose LG Strut is performed by actuating Hydraulic cylinder. Landing gear is also provided with a light to facilitate night landing.

The aircraft is steered on ground by wheel steering mechanism MRK 32-25 installed on Nose LG strut. The mechanism counteracts involuntary turns of aircraft during takeoff ground run, landing run and taxing and also ensures turning of the aircraft as per the requirement.

3.1.3 Hardwares/Softwares

High Performance HP Z800 Computing Workstation was used for modelling and analysis and Third party design software such as CATIA V5 R15,

HYPERMESH, MSC NASTRAN/ PATRAN and MSC FATIGUE is used in this project work.

FEM has become powerful tool for numerical solution to a wide range of engineering problems. With aid of statistical design and advances in computer technology, FEM can provide quick and accurate solution to complex problem with relative ease. Using this numerical procedure, the uncertainties associated with experiments can be avoided and cost can be significantly reduced. Therefore, FEM is employed to estimate fatigue life of LGs.

3.1.3.1 Introduction to MSC Fatigue[19]

MSC Fatigue is a highly effective tool for fatigue analysis of finite element models. MSC FATIGUE can predict the life of the component under given loading condition and it has capability to detect the prone region in the component for crack initiation. Following flow chart gives the role of MSC FATIGUE in fatigue analysis (Figure-3.1).

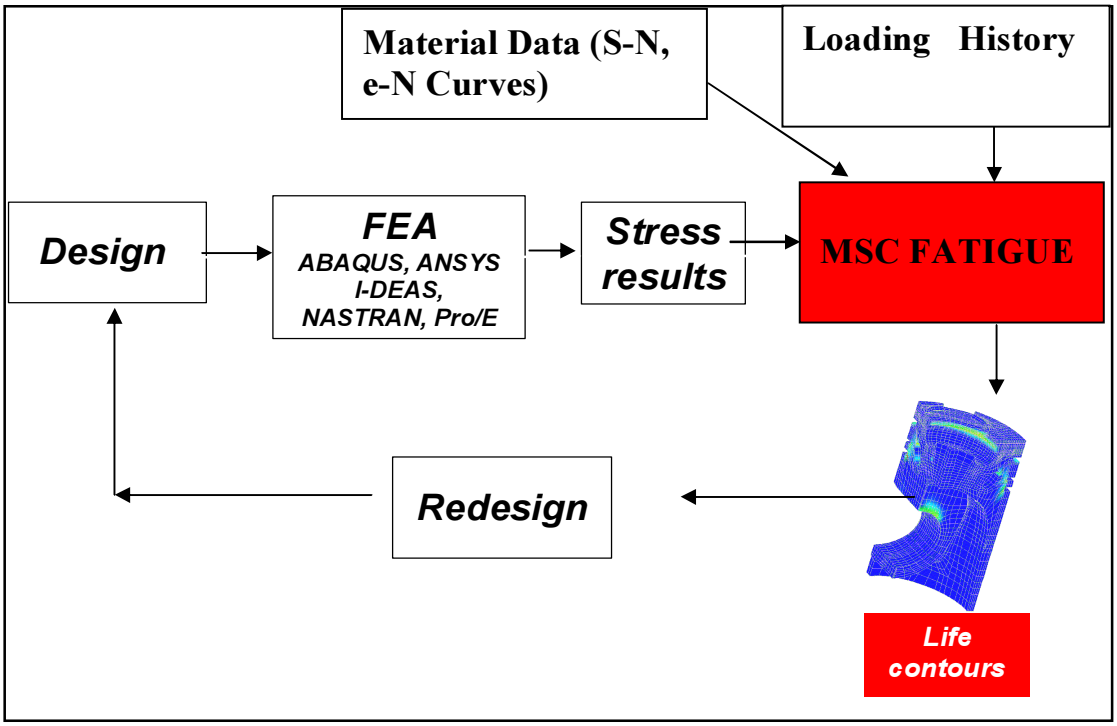

Figure 3.1 Role of MSC FATIGUE in fatigue analysis.

3.2 FATIGUE / STRESS ANALYSIS PROCEDURE

3.2.1 3D CAD Modeling

Generation of 3D models of nose landing gear assembly using CATIA software based on 2D drawings of MLG & NLG.

3.2.1.1 CATIA model of MLG

MLG comprises of 34 components. From 2D scanned drawings, 3D model of components and assembly is generated using CATIA software. The assembly consists of components strut, semi-fork, turning unit, shock absorber, actuating cylinder, stopper, pivot, kinematic linkages etc. The modeling of actuating cylinder and shock absorber are done to simulate in terms stiffness. 3D model of the assembly with its major components and are shown in Figure 3.2 to 3.3.

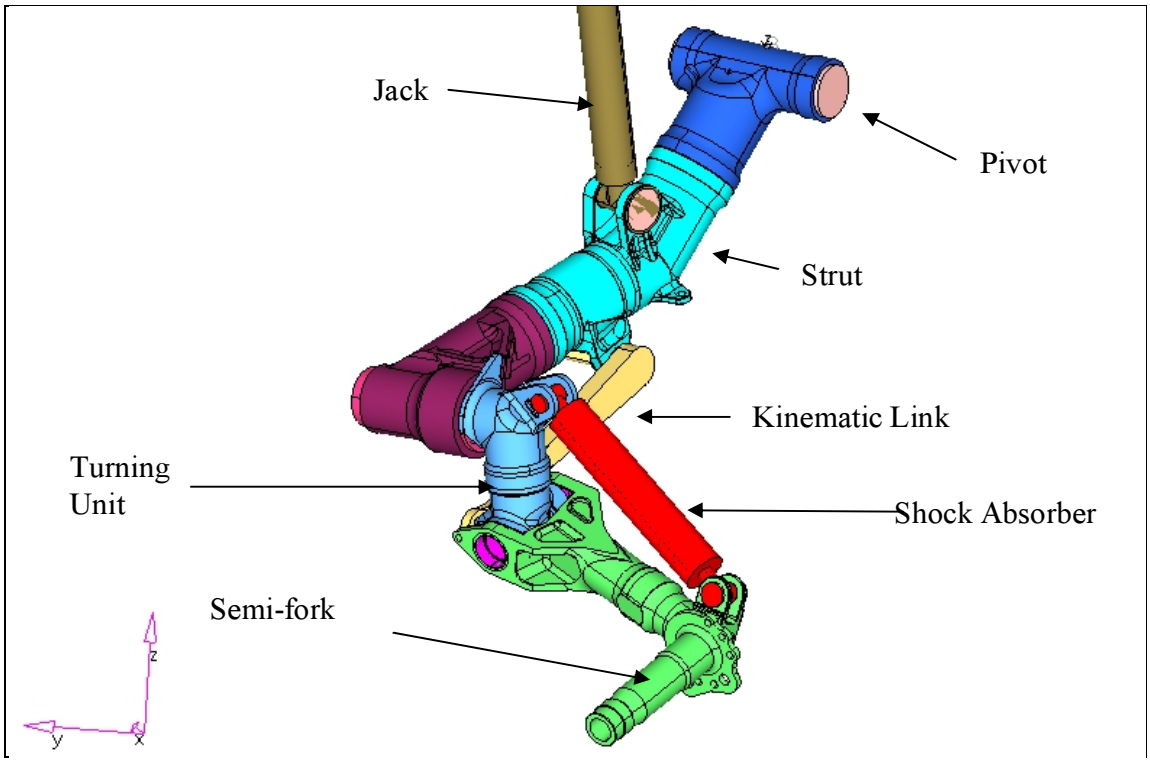

Figure 3.2 3D Solid Model of Main Landing Gear assembly

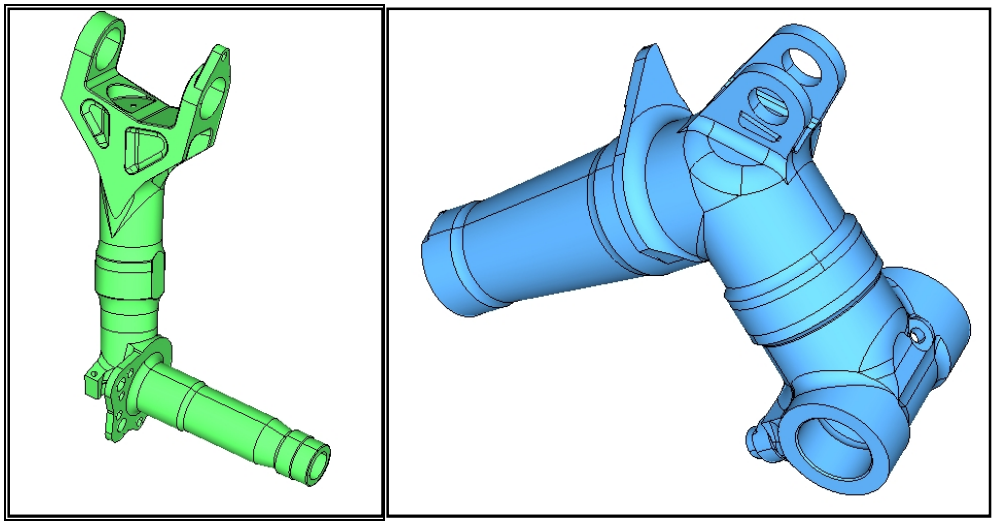

Figure 3.2 Model of Semi-fork &Turning Unit of MLG

3.2.1.2 CATIA model of NLG

NLG comprises of 35 components made of 30 KHAGSN2A materials, from 2D scanned drawings 3D model of components and assembly are generated using CATIA software. 3D model of components and assembly are shown in following Figure 3.4 to 3.7

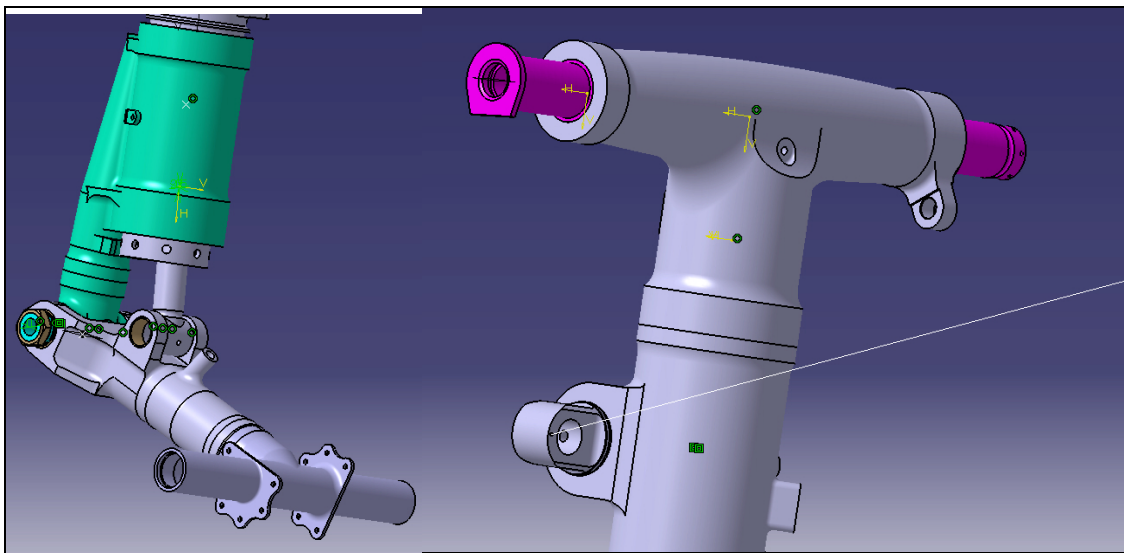

Figure 3.4 Model of wheel fork of NLG Figure 3.5 Model of strut of NLG

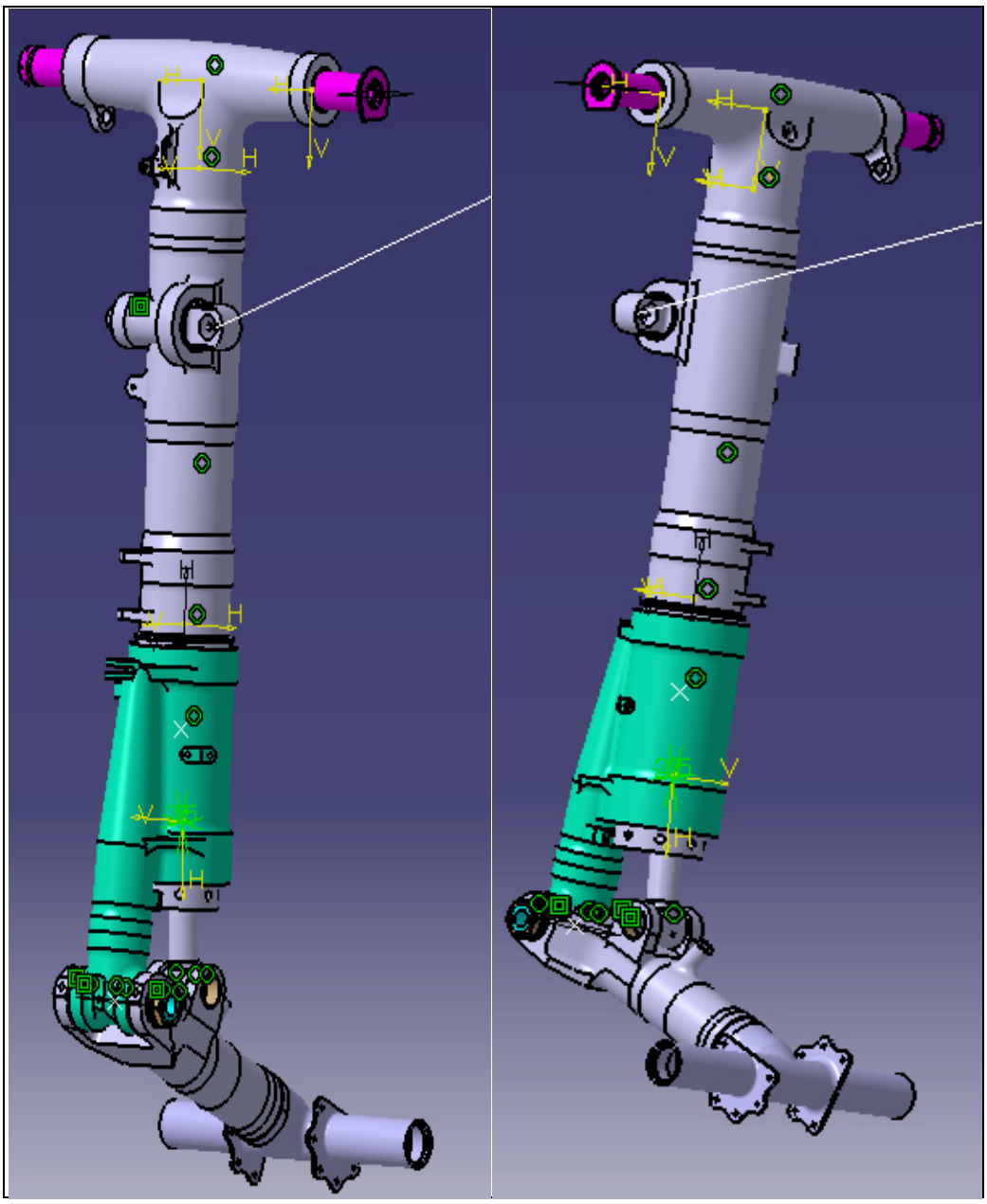

Figure 3.6 Solid Model of Nose Landing Gear assembly

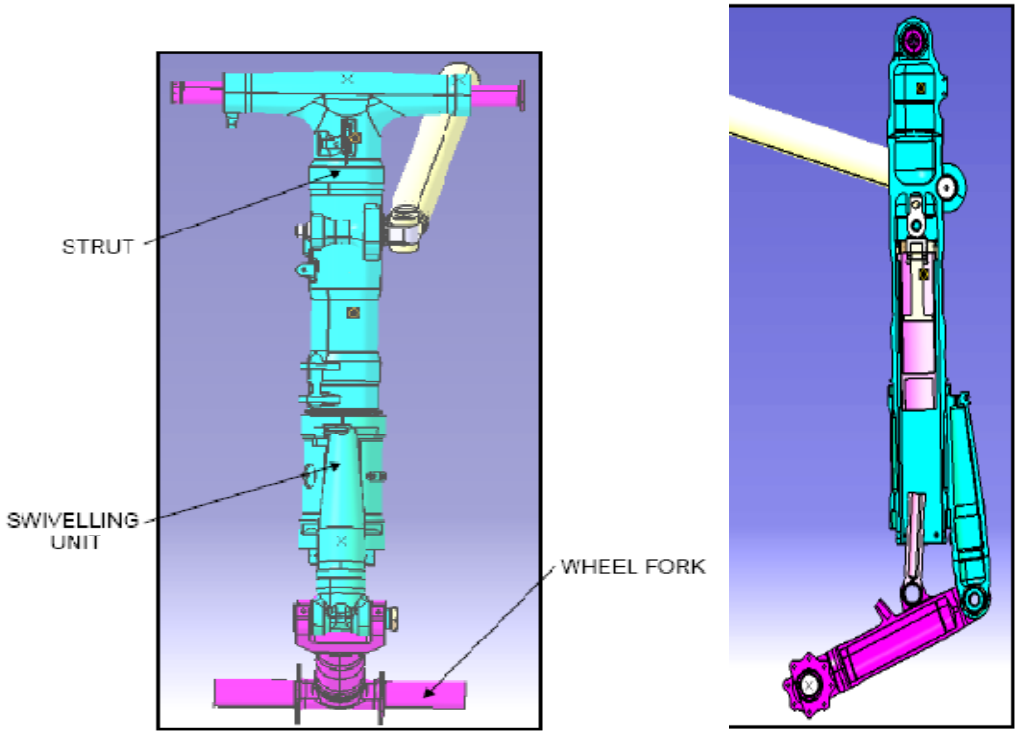

Figure 3.7 Solid Model of NLG with inside view

3.2.2 Finite Element Modeling

3D CAD model generated in CATIA is imported in HYPEMESH in IGES format.

Following steps are carried out for Geometry topology correction

a. Checking and deletion of duplicate surfaces

b. Connectivity is made in different parts of Strut, Turning Unit, Semi-fork, Pivot, and Actuating Cylinder etc.

2-D TRIA mesh generation is carried out in Hypermesh on surfaces of the assembly. Then TET mesh (solid) was generated by converting 2D surface elements to 3-D solid. While generation of 2-D and 3-D elements following quality criterion was adapted.

- ✓ Aspect ratio (AR) lesser than or equal to 3
- ✓ Skew lesser than or equal to 60^{o}
- ✓ Jacobian greater than or equal to 0.7
- ✓ TET Collapse more than 0.25

FE model is imported in PATARN software for further preprocessing. Surface to surface Contact element is used to provide connectivity between mating parts as shown in Figure 3.10.

Contact element transfers the actual displacement and forces as per contact status and stiffness of contacting faces. Contact check is performed in order to ensure that no initial penetration and gap is present in the mating components& convergence is ensured while analysis.

The components of MLG & NLG are modeled with solid elements and beam elements. The element property is given in the Appendix B. These components are in contact with each other and the area of contact is different indifferent loading condition because of change in the piston position. In order to account this surface contact and Mid Point couplings (MPCs) are used. Appendix-C gives the theory of the surface contact and MPCs.

3.2.2.1 Meshed model of MLG

Meshed model of MLG assembly is shown in Figure 3.8

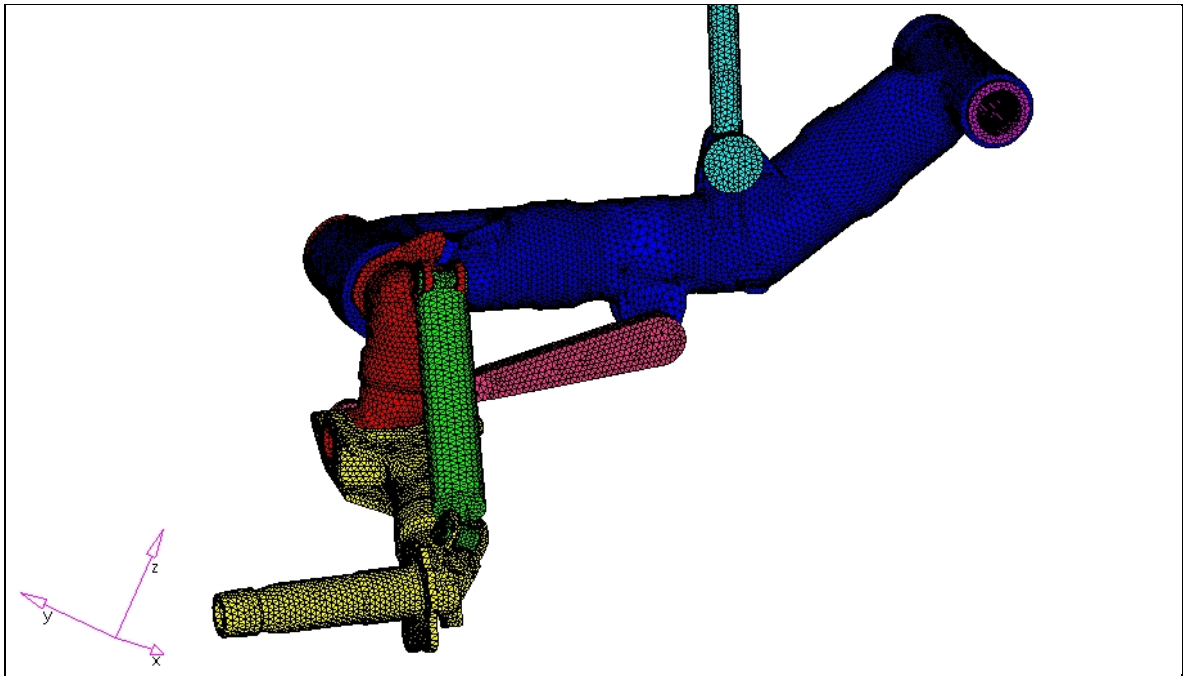

Figure 3.8 Meshed model of MLG assembly

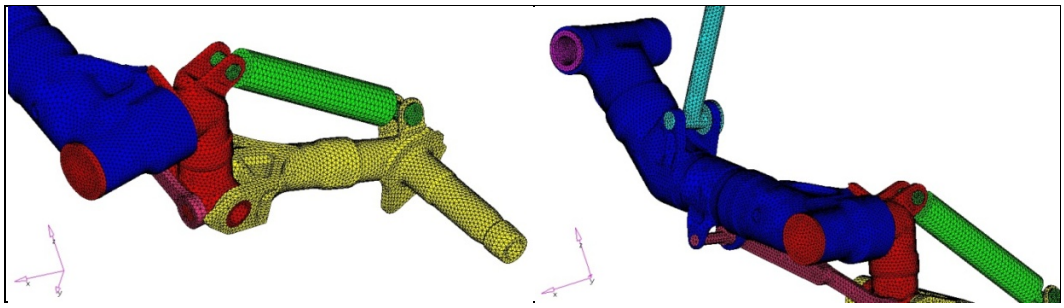

Figure 3.9Meshed model of MLG Assembly

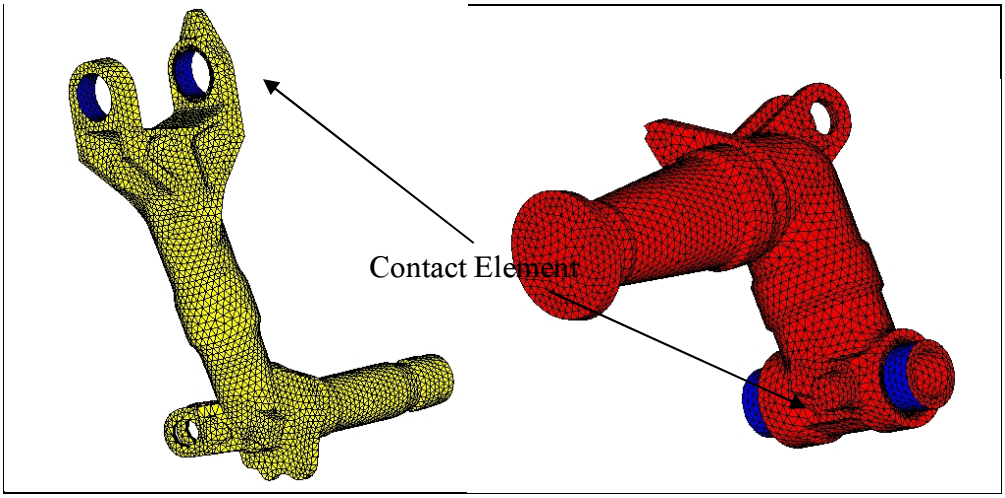

Figure 3.10 Contact element of MLG Assembly

The table 3.1 gives the major load carrying components meshing details and quality criterion for generated mesh. The total number of elements in the assembly is 166627 and total number of nodes is 48520.

Table 3.1 MLG Components meshing details and quality criterion

S.No.	Component	Element Type	Number of elements	Numbers of nodes	Aspect ratio > 3	Jacobian <0.7	Skew> 60^0	TET Collapse
1	Semi Fork	TET	27042	8213	3.89	0	0	0.27
2	Turning Unit	TET	34983	9084	3.53	0	0	0.25
3	Strut	TET	59586	17930	4	2	0	0.3

3.2.2.2 Meshed model of NLG

NLG assembly Meshed model is shown in Figure 3.11 to 3.13

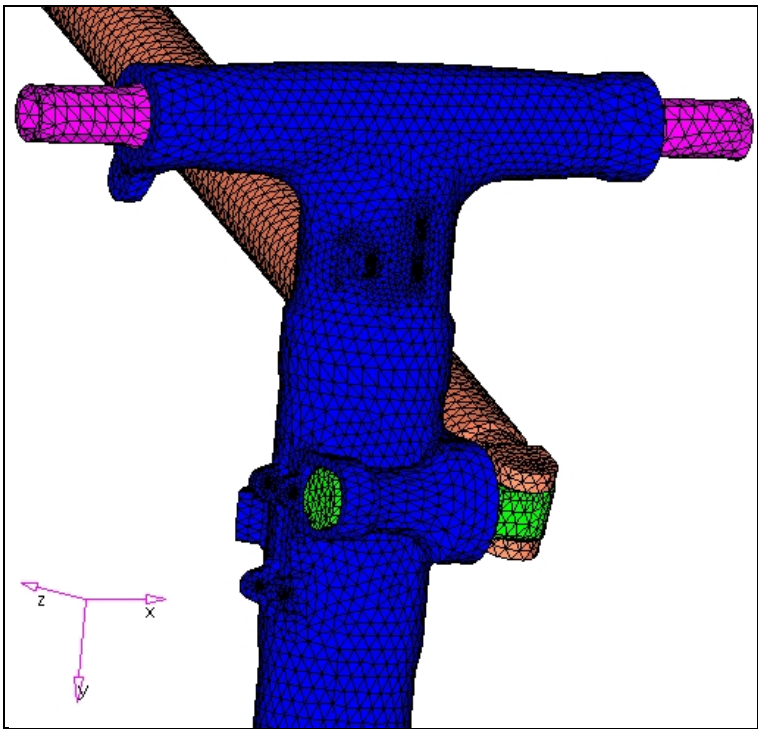

Figure 3.11 Meshed model of NLG wheel fork assembly

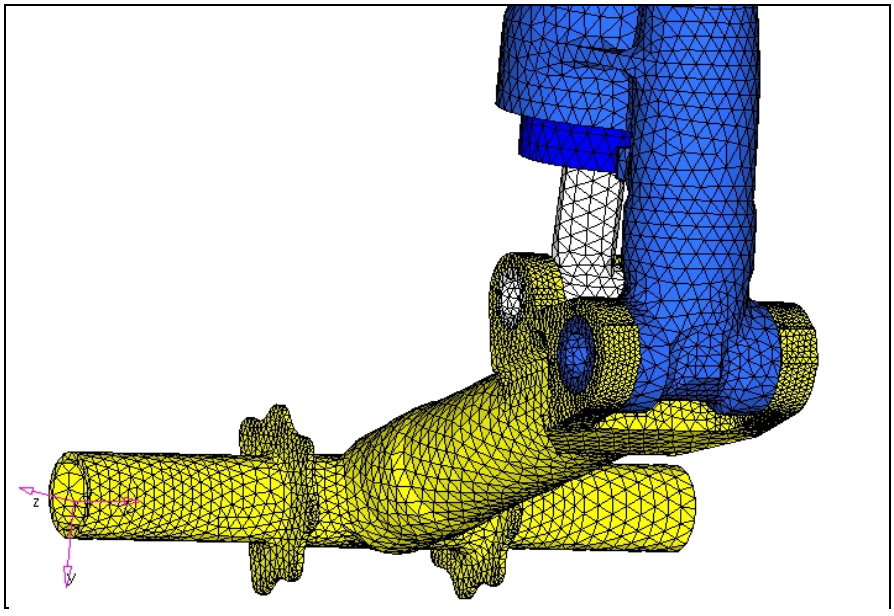

Figure 3.12 Meshed model of NLG assembly

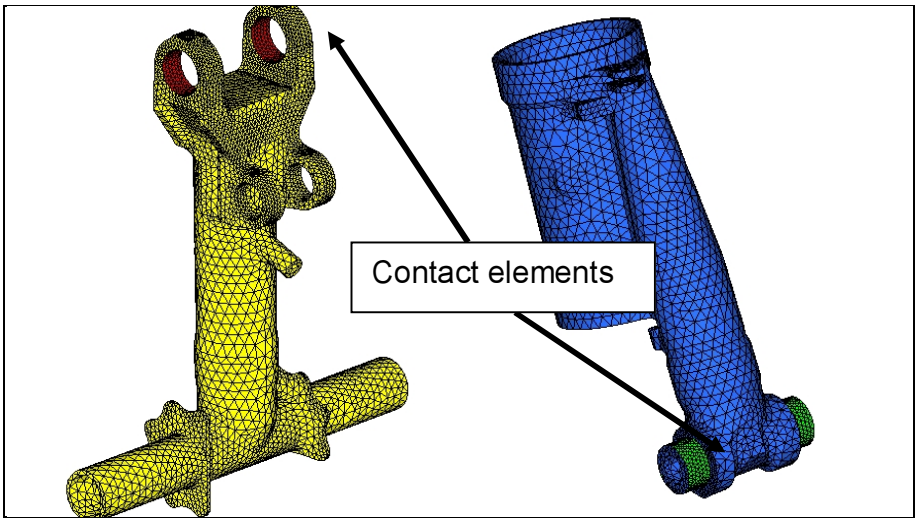

Figure 3.13 Contact element of Meshed model of NLG

The table 3.2 gives the major load carrying components meshing details and quality criterion for generated mesh. The total number of elements in the assembly is127618 and total number of nodes is 40083.

Table 3.2 NLG Components meshing details and quality criterion

S.No.	Component	Element Type	Number of elements	Numbers of nodes	Aspect ratio > 3	Jacobian < 0.7	Skew $>60^0$	TET Collapse
1	Axel	TET	29689	8922	3. 39	0	0^0	0.27
2	Sleeve	TET	17024	5385	3. 83	0	0^0	0.25
3	Strut	TET	3814	1267	4.09	0	0^0	0.23
4	Strut Bolt	TET	5606	1473	3	0	0^0	0.3
5	Connecting Rod	TET	5318	1772	3.30	0	0^0	0.29
6	Cylinder	TET	8261	2560	3.50	0	0^0	0.25
7	Pivot	TET	3667	1250	3.20	0	0^0	0.26

3.2.3. Loadings of landing gear[15,16,17,24]

Loading details are supplied by OEM for both landing gear i.e. MLG & NLG. Four type of loading is defined by OEM for landing gears the same is described in table 3.3.

Table 3.3 Type of loading for MLG & NLG

CASE	DESCRIPTION
$(E'+G')_1$	Landing on two points. At the time of touch down, the wheels are stationary and they start skidding on the run way. This gives rise to a vertical load (+Py) and drag force (+Px) on the wheel.
$(E+G)_2$	Landing on two points. At the time of touch down, the wheels are stationary and they start skidding on the run way. This gives rise to a vertical load (+Py) and drag force (+Px) on the wheel. But, when the wheel starts rolling along with the speed of the aircraft, the drag becomes negative (-Px)
E	Landing on three points. At the instant of landing impact, maximum vertical load (+Py) will be developed on wheels
R1	Drift landing on two points (landing in cross wind (side hit)). At the time of touch down, the wheels are stationary and they start skidding on the run way. This gives rise to a vertical load (+Py) and drag force (+Px) on the wheel. But, when the wheel starts rolling along with the speed of the aircraft, the drag becomes negative (-Px). The side load on one MLG will act in inward direction (+Pz) & on the another MLG in outward direction (-Pz).

3.2.3.1 Loadings of MLG

Loading details are supplied by OEM for repeated testing of the MLG "Ref: Test Program for LG's of Article 32-29L Reg. No. I/29/3228/318. Loading along with its corresponding number of cycle is shown in the Table 3.4. These loading have been considered for FE Stress Analysis. Loading diagram is shown in Figure 3.14 & 3.15

Table 3.4 Loading along with number of cycle for MLG

Load Cases	Case of testing	Number of loadings cycle for each case	Loading while repeated load testing, Kg			Radius R, mm	Compression of shock absorber in mm
			P_Y (±2%)	P_X (±2%)	P_Z (±2%)		
1	$(E' + G')_1$	100	10600	10600	0	-	80
2	$(E + G)_2$	100	10600	-7450	0	-	80
3	E	400	14400	-	0	-	80
4	R_1	500 (+Pz) 200 (-Pz)	10650	-1880	±4260	330	80

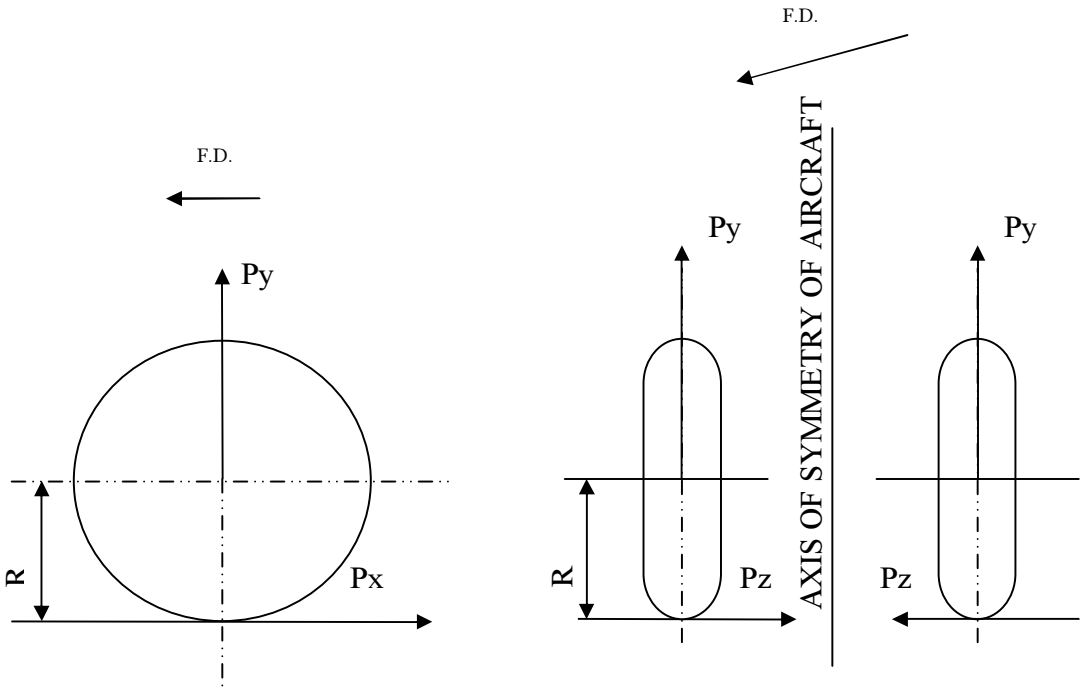

Figure 3.14 MLG Loading Diagram with direction of load

The loads are applied in three perpendicular directions as shown in figure 3.15

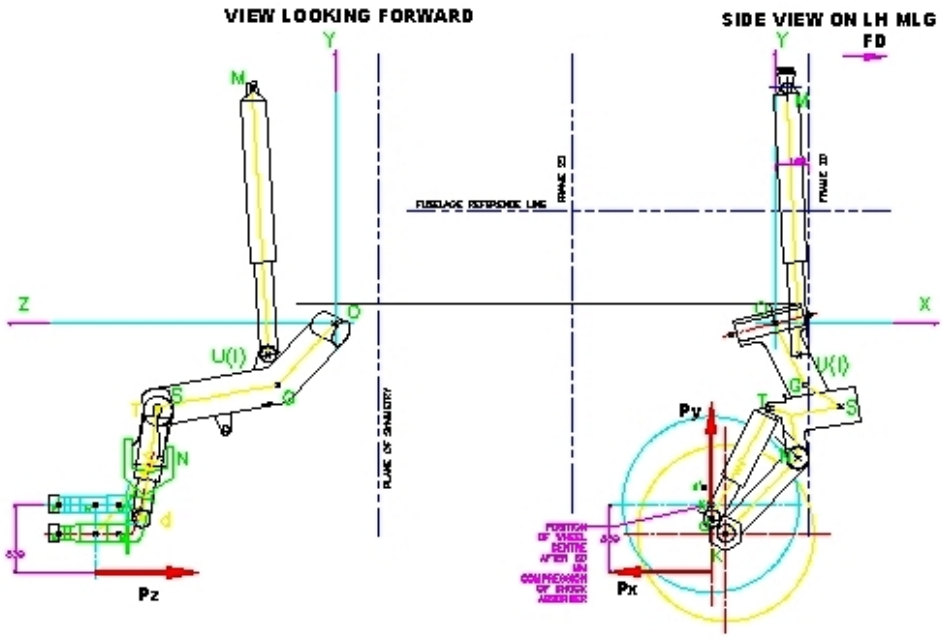

Figure 3.15 Sketch diagram of Load application of Main Landing Gear

3.2.3.2 Loadings of NLG

Loading along with its corresponding number of cycle is shown in table 3.5; these loading have been considered for FE Analysis and Fatigue Testing of NLG. Loading details are supplied by OEM for repeated testing of the NLG "Ref: Test Program for LG's of Article 32-29L Reg. No. I/29/3228/318".Direction of loading is shown in Figure 3.16.

Table 3.5 Loading along with number of cycle for NLG

Sl No	Case of testing	Number of loadings cycle for each case	Loading for two wheels while repeated load testing, Kg			Radius R, mm	Compression of shock absorber in mm
			P_Y (±2%)	P_X (±2%)	P_Z (±2%)		
1.	$(E' + G')_1$	100	4800	4800	0	-	80
2.	$(E + G)_2$	100	3370	-3370	0	-	80
3.	E	400	6750	-	0	-	80
4.	R_1	250 (+Pz) 250 (-Pz)	6400	-	±2230	220	80

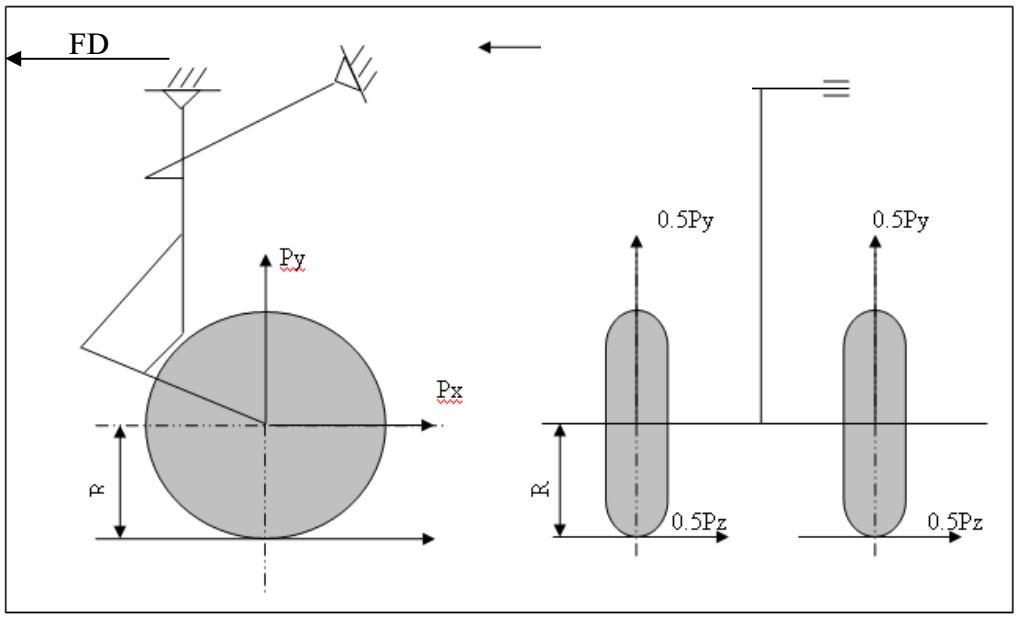

Figure 3.16 NLG Loading Diagram with direction of load

3.2.4. Boundary Conditions

3.2.4.1. Boundary condition of MLG

The strut is connected to the fuselage by pivot and actuating cylinder. Surface to surface contact is defined between the strut and pivot. The pivot is fixed in axial and radial direction as shown in Figure 3.17. Actuator is fixed only in axial direction as shown in Figure 3.18.

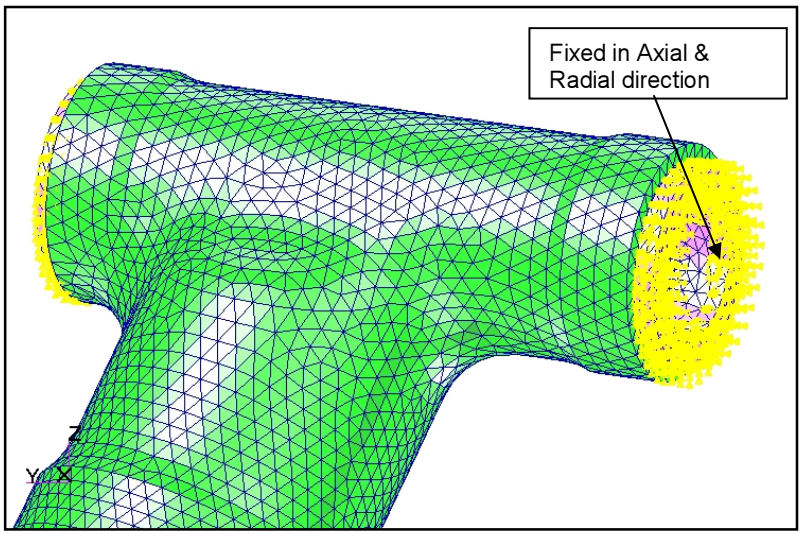

Figure 3.17 Meshed model showing boundary condition on Pivot

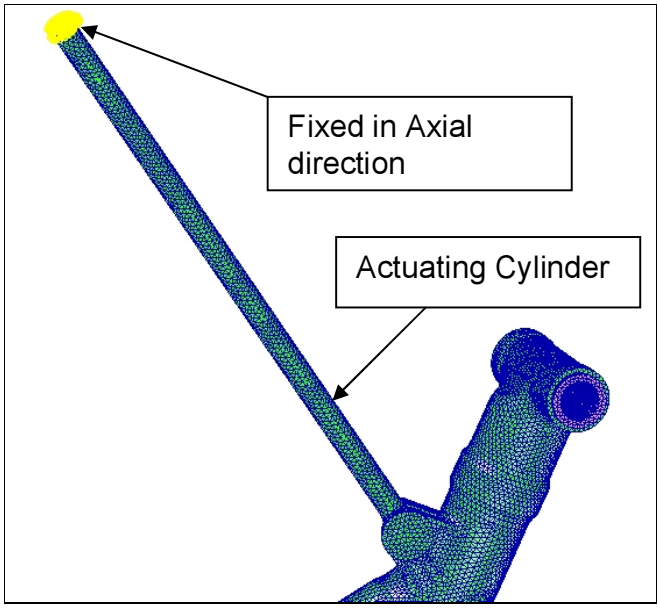

Figure 3.18 Meshed model showing boundary condition on Actuating Cylinder of MLG

3.2.4.2. Boundary condition of NLG

The strut is connected to the nose fuselage through pivot and actuating cylinder. Surface to surface contact is defined between the strut and pivot. The pivot is fixed in axial and radial direction as shown in Figure 3.19. Actuator is fixed only in axial direction as shown in Figure 3.20.

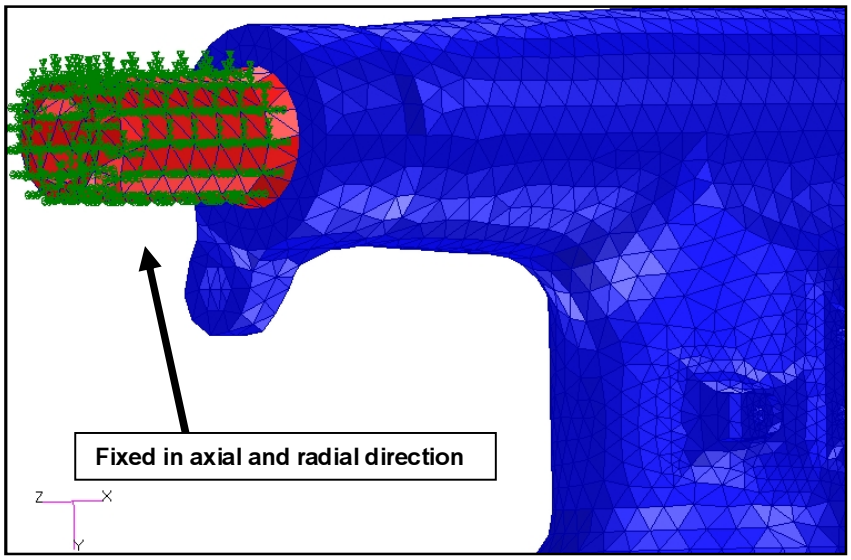

Figure 3.19 Meshed model showing boundary condition on Pivot

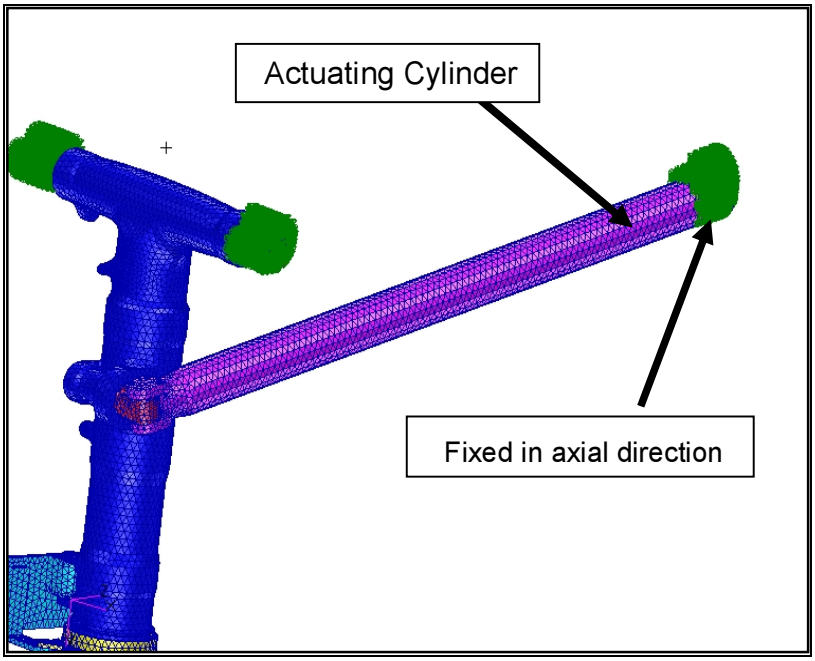

Figure 3.20 Meshed model showing boundary condition on Actuating Cylinder of NLG

3.2.5. Fatigue load test program

The fatigue spectrum of the Landing Gear is as given in stress album. The table also shows the sequence and number of loadings in one block (each block consisting of 1300 cycles for the MLG& 1100 cycle for NLG).

Y= [(3200-X) x 4] / 1300

Where X = initial life of test sample

4 = Scatter factor

Note: The fraction obtained is to be rounded off to next higher no. (viz 3.69 to 4)

Loading for Case 1, 2, 3 & 4 are respectively as shown in Table3.6 for MLG & NLG. Constant amplitude loading spectrum (repeated type) as per Fatigue test schedule is generated using MSC Fatigue software.

Table 3.6 Fatigue Loading along with number of cycle for MLG & NLG

Load Cases	Case of testing	Number of loadings cycle for each case for MLG	Number of loadings cycle for each case for NLG
1	(E'w + G'w)1	100	100
2	(Ew + Gw)2	100	100
3	Ew	400	400
4	R1w	500 (+Pz) 200 (-Pz)	250(+Pz) 250(-Pz)
Total no. of landings per block		1300	1100

3.2.6. Fatigue Loading Sequence

1 block loading is equal to 650 cycles. Each block is repeated n times to find the life of the landing gear. Figure 3.21 shows load sequence for fatigue loading.

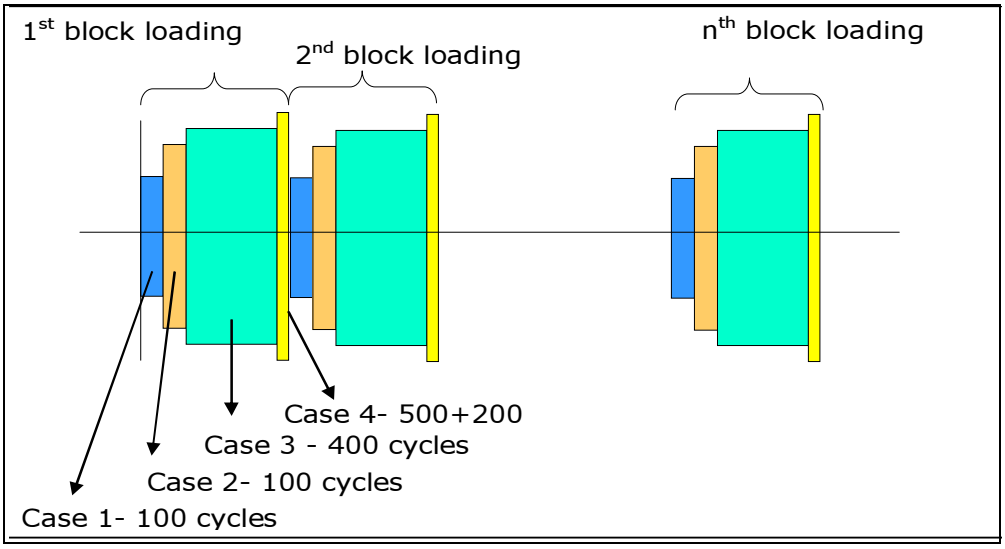

Figure 3.21 Load sequence for the fatigue cycles.

3.2.7. Mechanical Properties of MLG & NLG components material

The material properties to various components are assigned as per drawing details refer Appendix-A, however all the major load carrying components are of 30KHGN2A material. The mechanical properties of 30KHGN2A are shown in Table 3.7 refer Appendix-A.

Table 3.7 Mechanical Properties of material 30KHGN2A

Material Used	E (kg/mm^2)	Poisson Ratio	UTS (kg/mm^2)	Endurance Limit kg/mm^2	Yield Strength kg/mm^2	Density (Kg/mm^3)
30KHGSN2A	21000	0.3	170	73	140	7850

3.2.8. Material Data for Fatigue Analysis[20]

3.2.8.1. Generation of SN Curve for material 30KHGN2A

In Russian material handbook MMT-12 Vol-1 by A T Tumnov has given SN curve for 30KhGSN2A, which is only up-to $76kg/mm^2$. However, the present stress analysis shows maximum stresses are $120kg/mm^2$.(Ref Appendix-A)

Moreover, NAL-Bangalore has also done 30KHGSN2A material testing. Based on above study NAL has supplied SN curve to HAL-Nasik. This SN curve

contains complete information of stress intercept & slope but the endurance limit is not indicated. (Ref Appendix-A)

Therefore, in order to generate complete SN diagram, above curves are merged for doing the Fatigue analysis of MiG-27 undercarriages and a SN curve in MSC PATRAN is generated. The following mechanical properties are used for generation of S-N curve(Ref Figure 3. 22) in MSC Fatigue software.

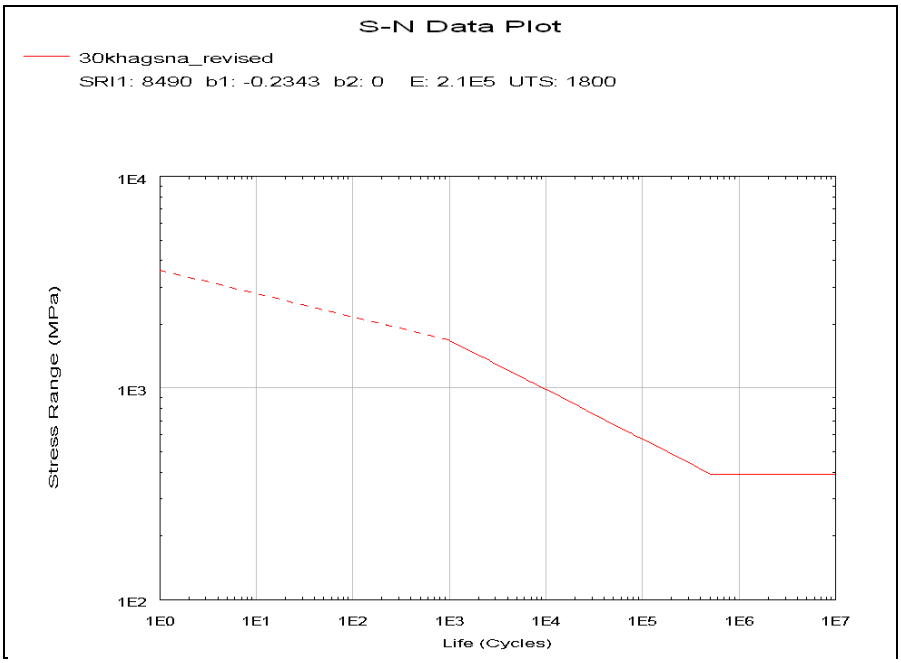

Figure 3.22 S-N curve of 30KHGN2A

3.2.9. Solution Parameters

The stress data of all the loading cases are imported to MSC Fatigue software. Fatigue analysis is carried out by specifying the number of cycles and sequence of loading and the corresponding life of the component is estimated. The following parameters are defined during the fatigue analysis:

i. Cumulative Fatigue life is estimated using Max. Principal Stress Theory

ii. Goodman Criterion is used for prediction of fatigue life based on S-N curve

iii. Modifying factors e.g. surface finish factor - forging, surface treatment – shot peened, reliability factor of 99.9% are considered in present analysis

CHAPTER 4: RESULTS AND DISCUSSION

4.1 STRESS ANALYSIS RESULTS OF MLG

Stress analysis is carried out for all four load cases considering minimum wall thickness required Refer table 4.1 before rejuvenation with the boundary condition mentioned in chapter 3 and material properties in case 4 the load Pz component is acting in positive as well as in the negative direction. Therefore both the cases are analyzed separately.

Table 4.1 Minimum wall thickness of strut

Zone		Wall Thickness as Per drawing Dimension	Min Wall Thickness Required after Rejuvenation
5 & 6	a	9.0	8.5
3 & 4	b	10.5	10.0
	c	10.0	9.5
	d	10.0 & 9.0	8.5
2	e	8.5	8.0
1	f	8.5	8.0

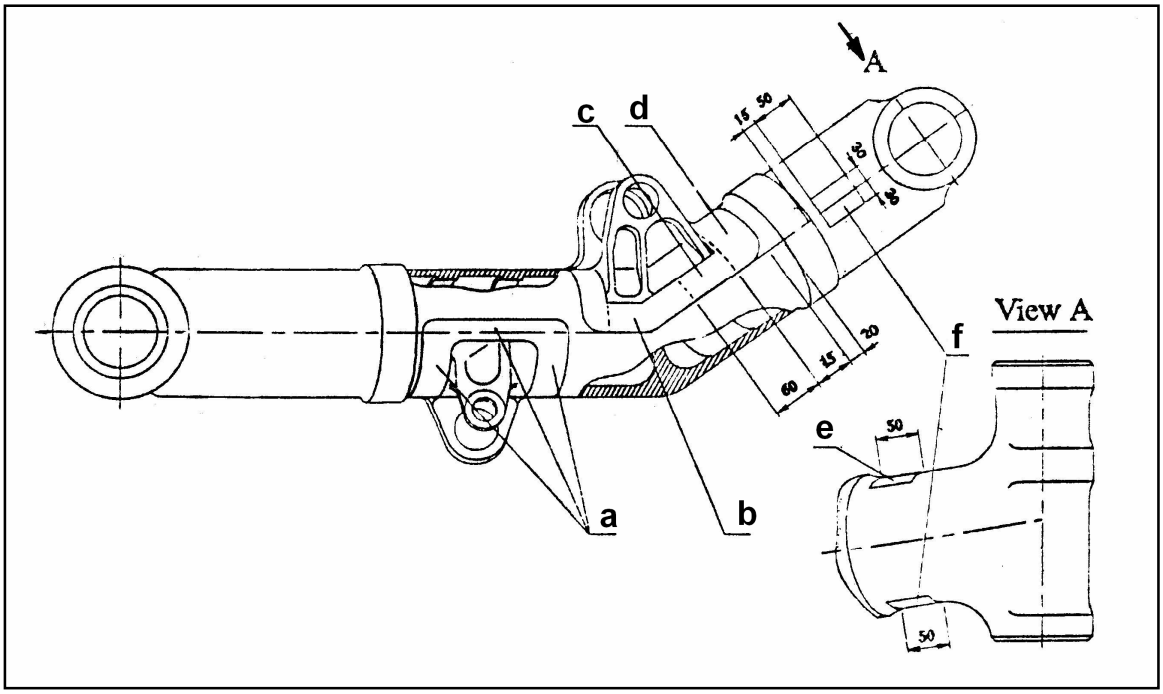

4.1.1 Load Case-1

With the applied loadings and boundary conditions the Maximum displacement & Maximum Principal Stress in case-1 are 78 mm (Figure 4.1) &118 kg/mm^2 (Figure 4.3) respectively. Figure 4.2& 4.4 shows the maximum principal stress plot on critical components.

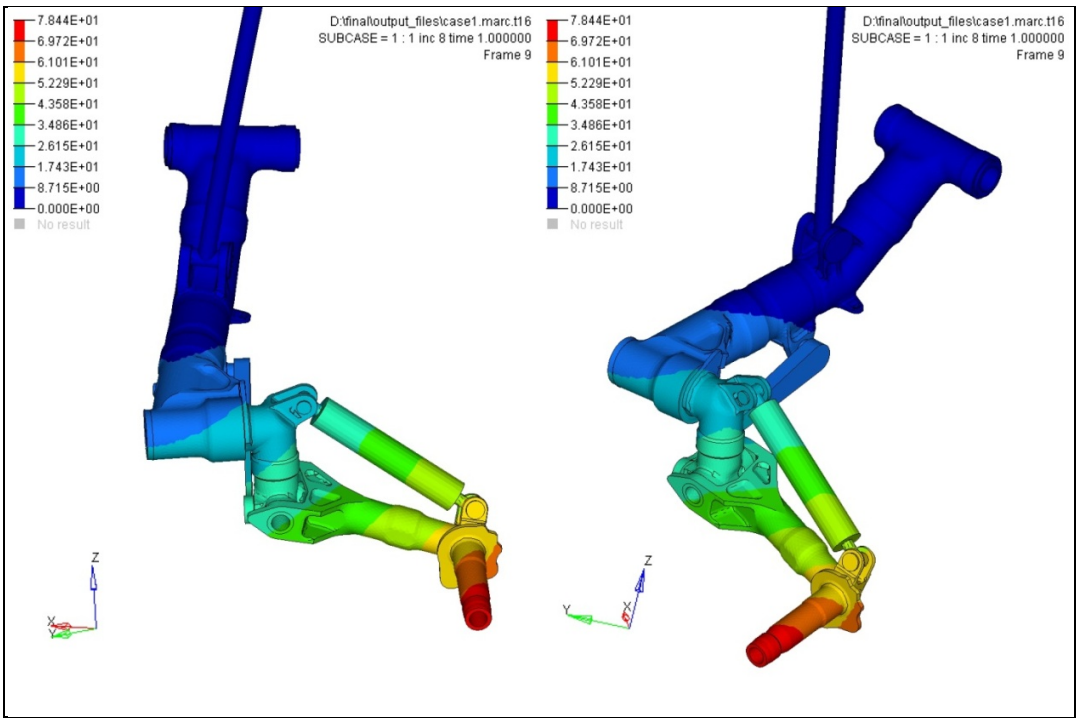

Figure 4.1 Maximum displacement plot for MLG assembly in load case-1

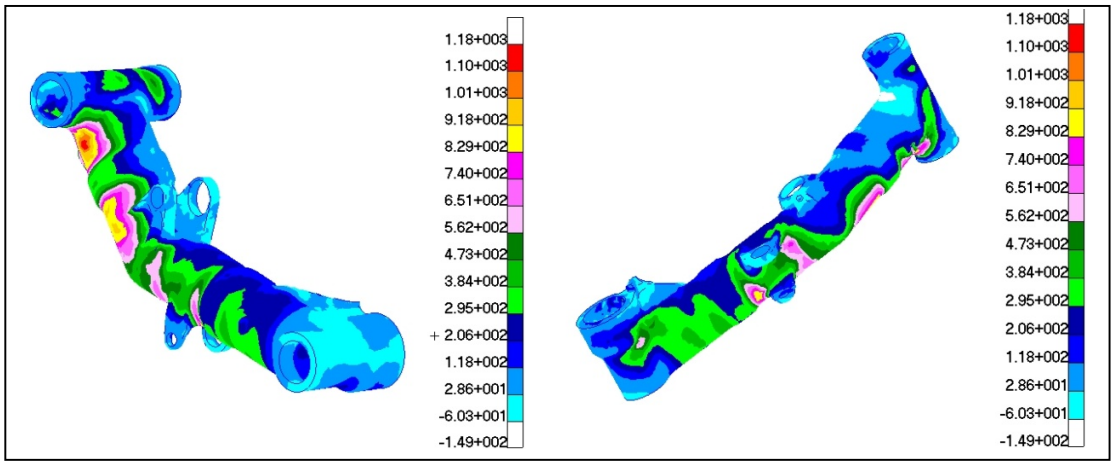

Figure 4.2 Maximum Principal Stress plot for MLG Strut in load case-1

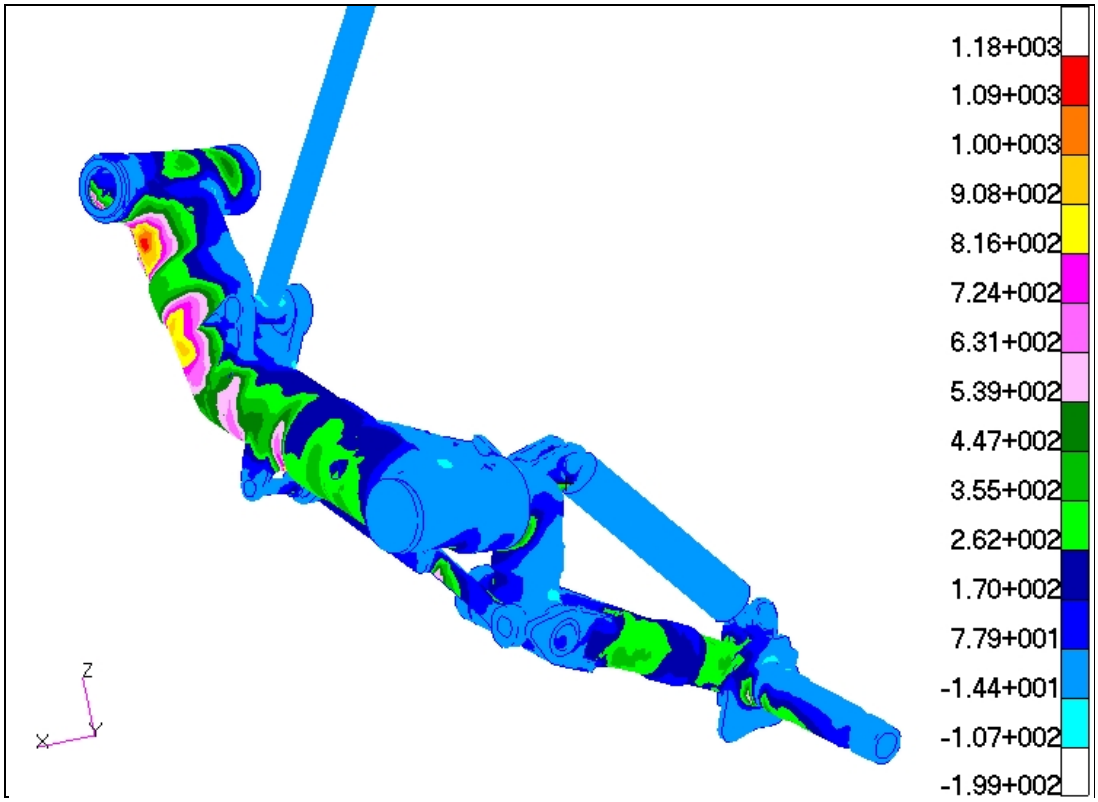

Figure 4.3 Maximum Principal Stress plot for MLG assembly in load case-1

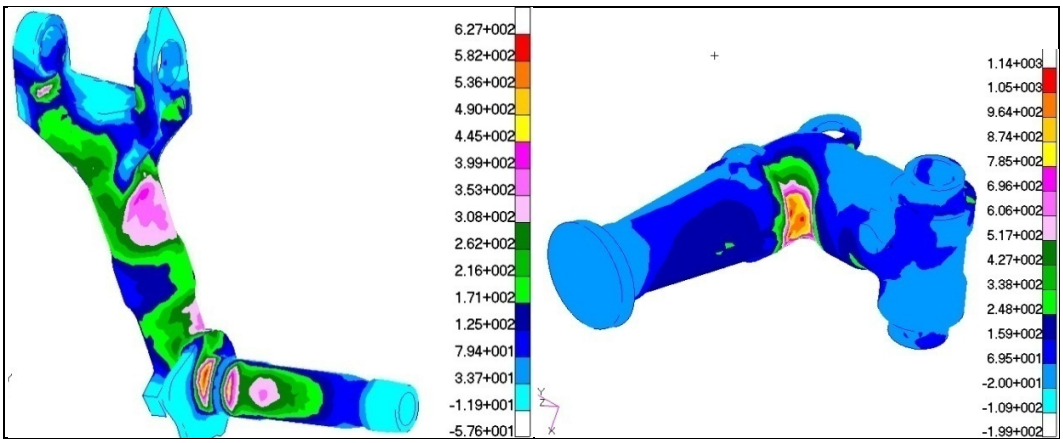

Figure 4.4 Maximum Principal Stress plot for MLG Semi-fork and Turning Unit in load case-1

4.1.2 Load Case-2

Maximum displacement & Maximum principal stress in this case are 53.8 mm (Figure 4.5) and99.3 kg/mm^2 (Figure 4.6) respectively, Figure 4.7 to 4.8 shows the maximum principal stress plot for critical components.

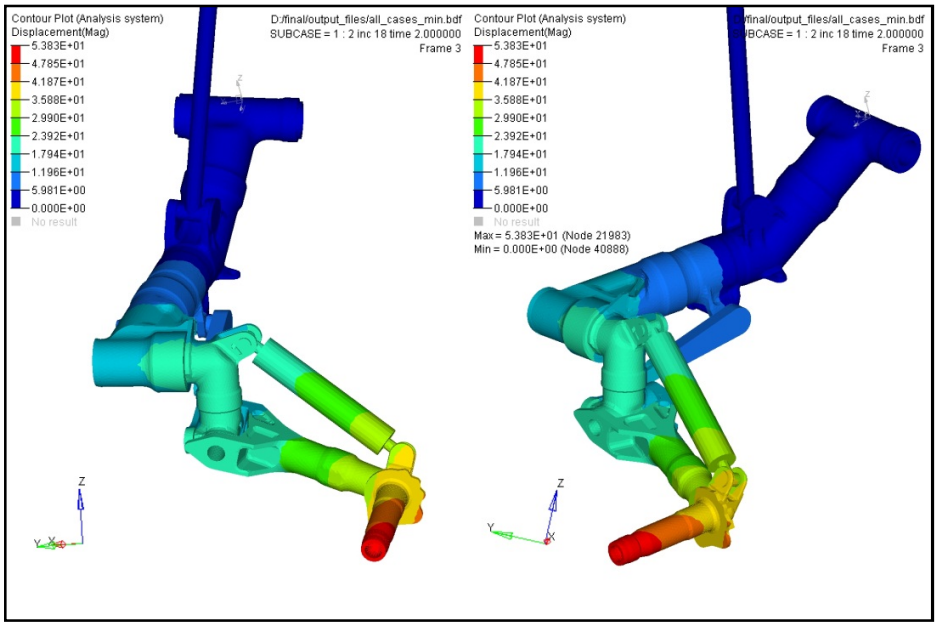

Figure 4.5 Maximum displacement plot for MLG assembly in load case-2

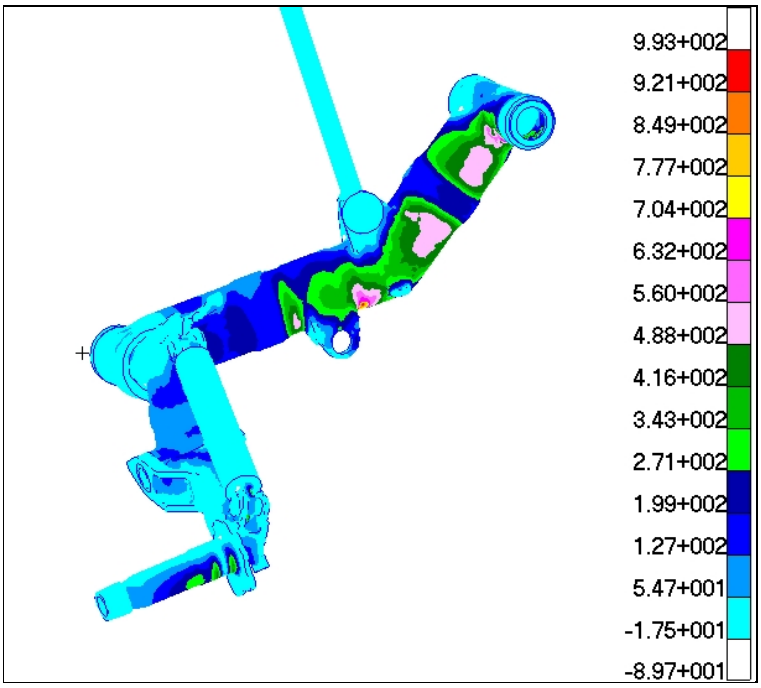

Figure 4.6 Maximum Principal Stress plot for MLG assembly in load case-2

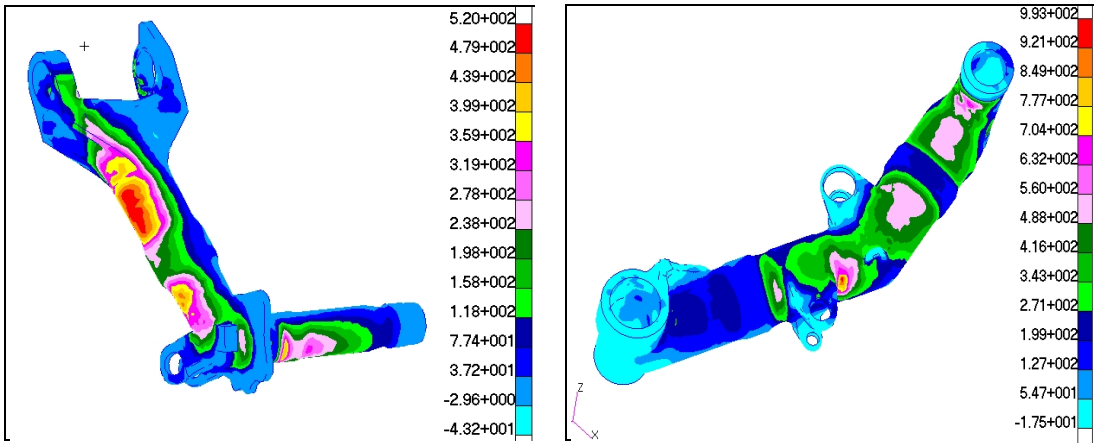

Figure 4.7 Maximum Principal Stress plot for MLG Semi-fork and Strut in load case-2

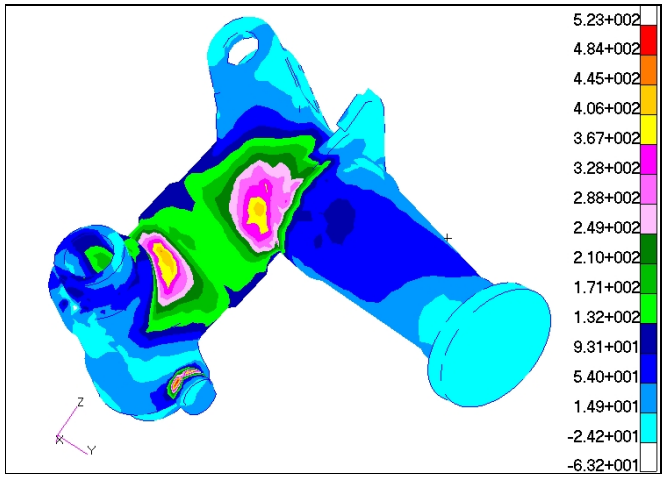

Figure 4.8 Maximum Principal Stress plot for MLG Turning Unit in load case-2

4.1.3 Load Case-3

Maximum displacement & Maximum principal stress are 65 mm (Figure 4.9) & 105kg/mm^2 (Figure 4.10) respectively, Figure 4.11 & 4.12 shows the maximum principal stress plot for critical components.

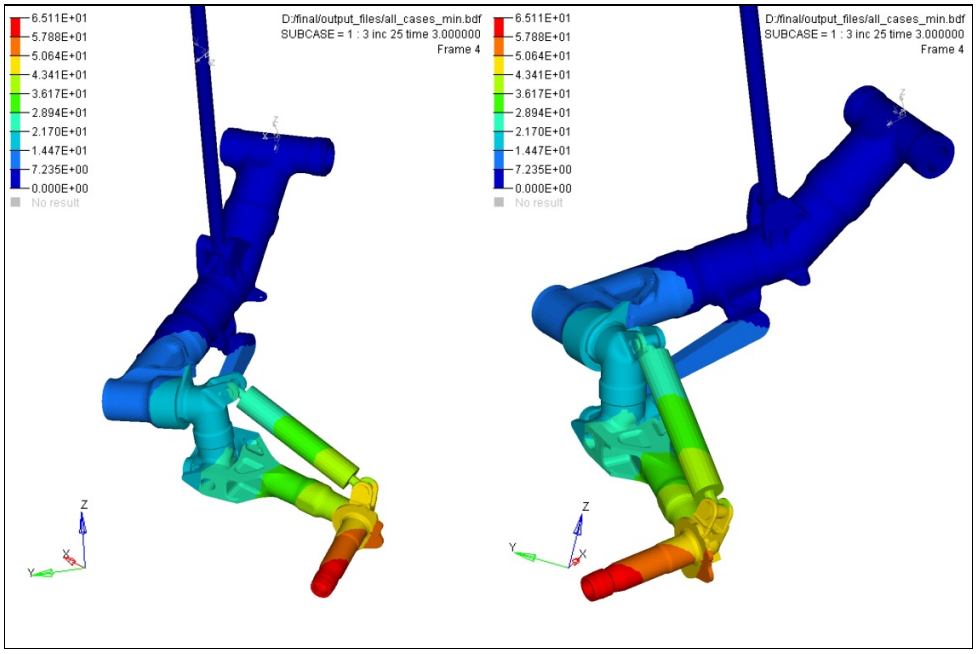

Figure 4.9 Maximum displacement plot for MLG assembly load case-3

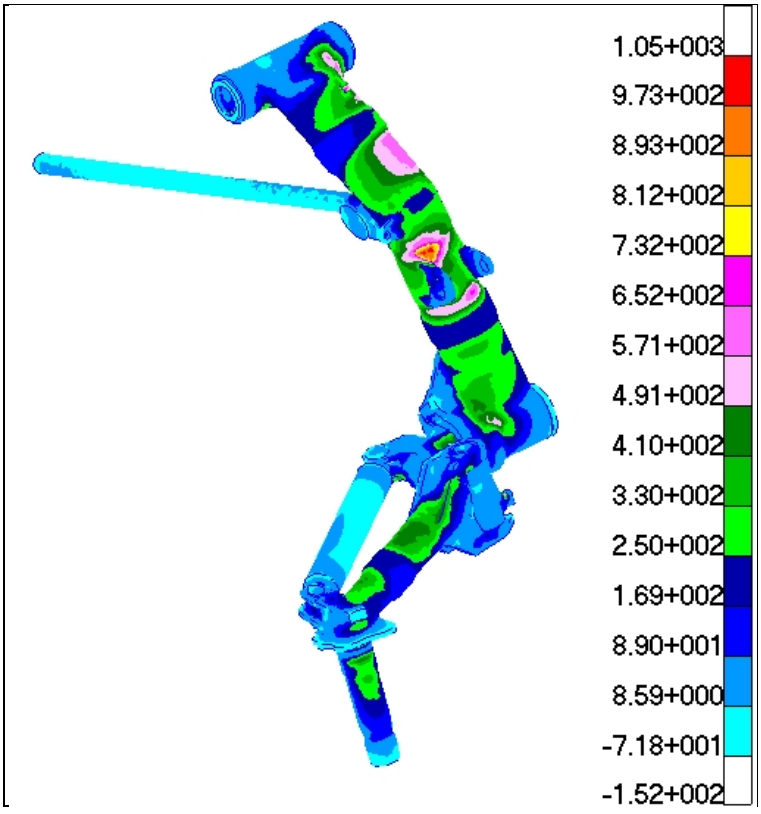

Figure 4.10 Maximum Principal Stress plot for MLG assembly in load case-3

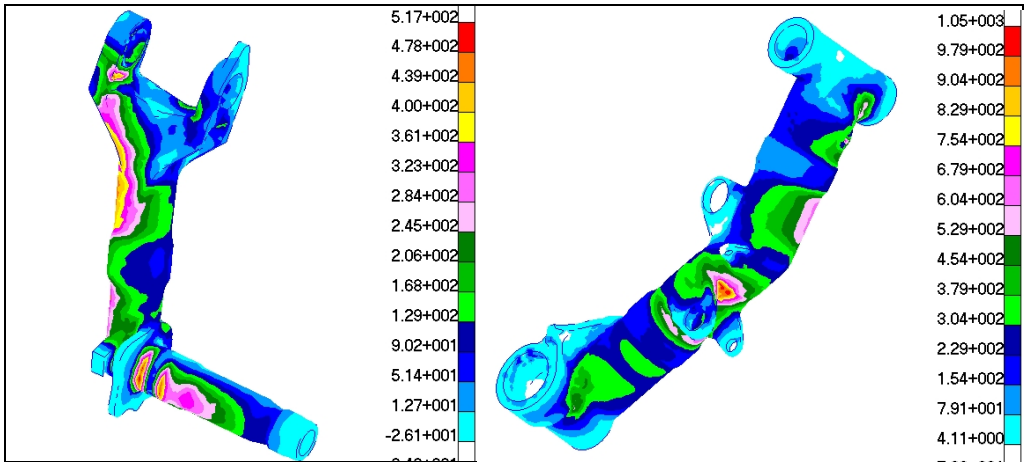

Figure 4.11 Maximum Principal Stress plot for MLG Semi-fork and Strut in load case-3

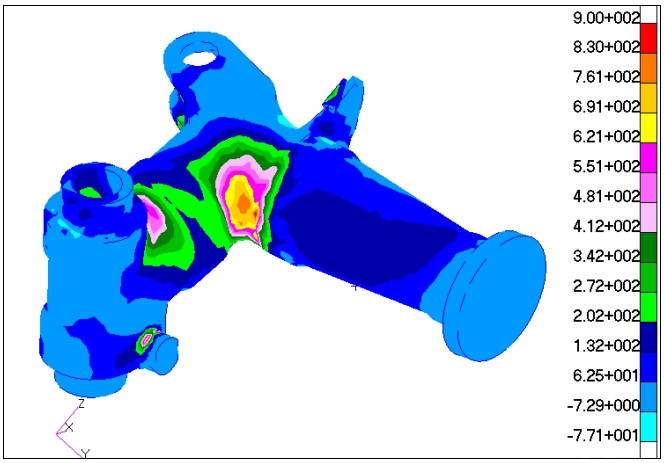

Figure 4.12 Maximum Principal Stress plot for MLG Turning Unit in load case-3

4.1.4 Load Case – 4 (-Pz)

Out of 5 loading cases, load case–4 (-Pz) is the critical one. Maximum displacement & Maximum principal stress are 66 mm (Figure 4.13) and120kg/mm^2 (Figure 4.14) respectively, Figure 4.15 and Figure 4.16 shows the maximum principal stress plot for critical components.

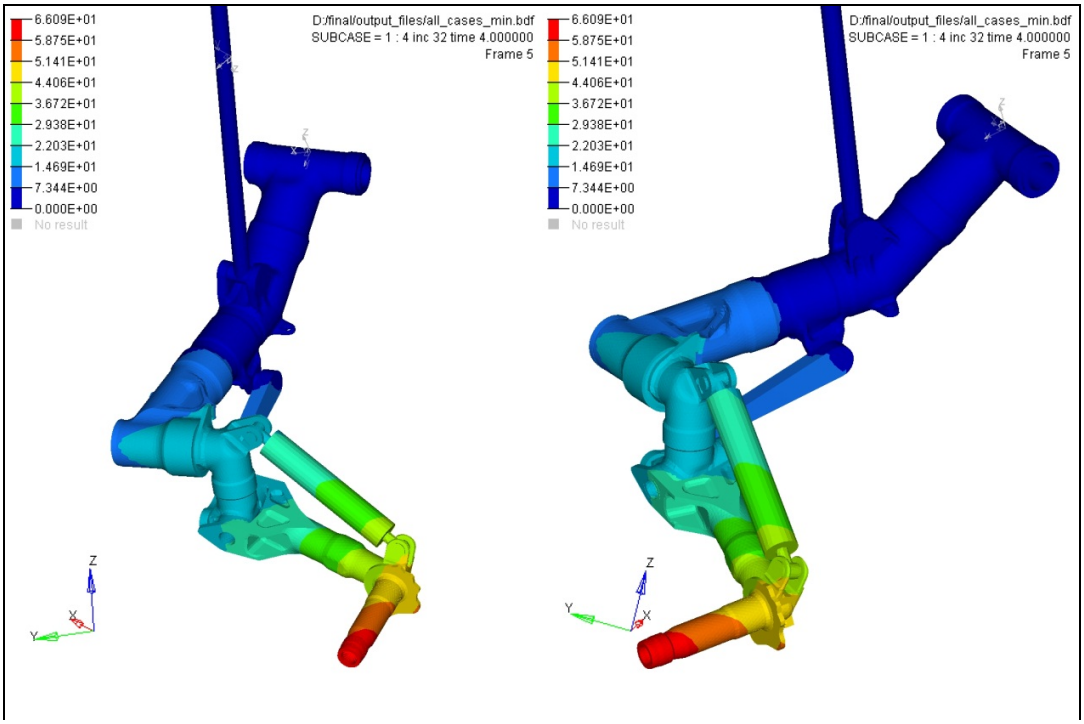

Figure 4.13 Maximum displacement plot for MLG assembly in Load Case – 4 (-Pz)

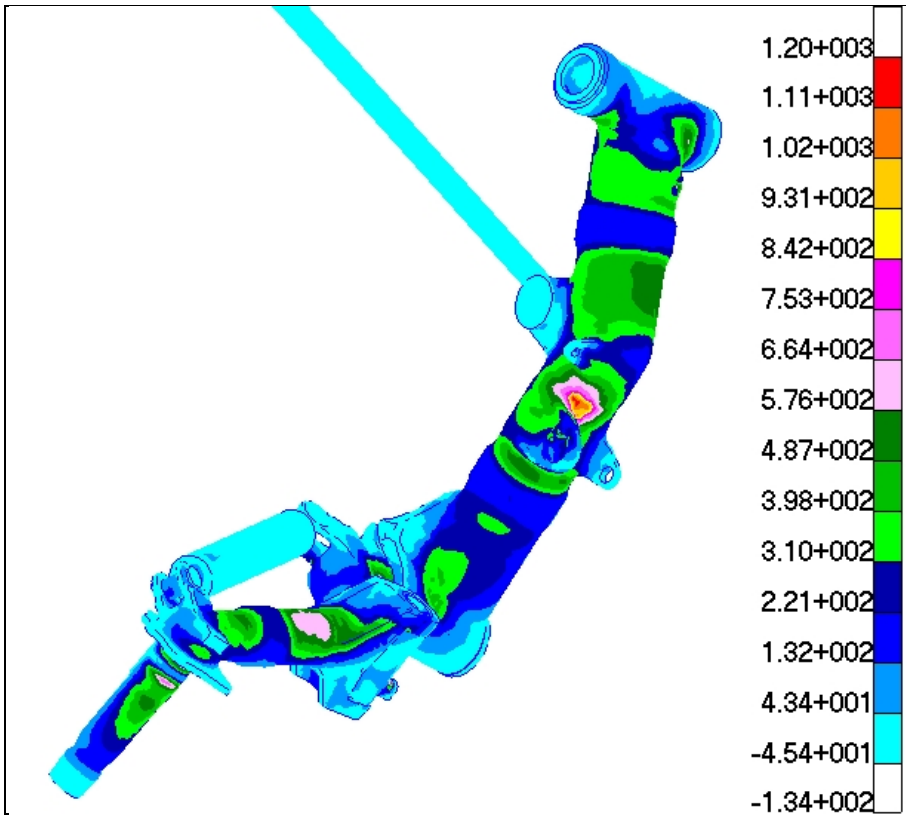

Figure 4.14 Maximum Principal Stress plot for MLG assembly in Load Case – 4 (-Pz)

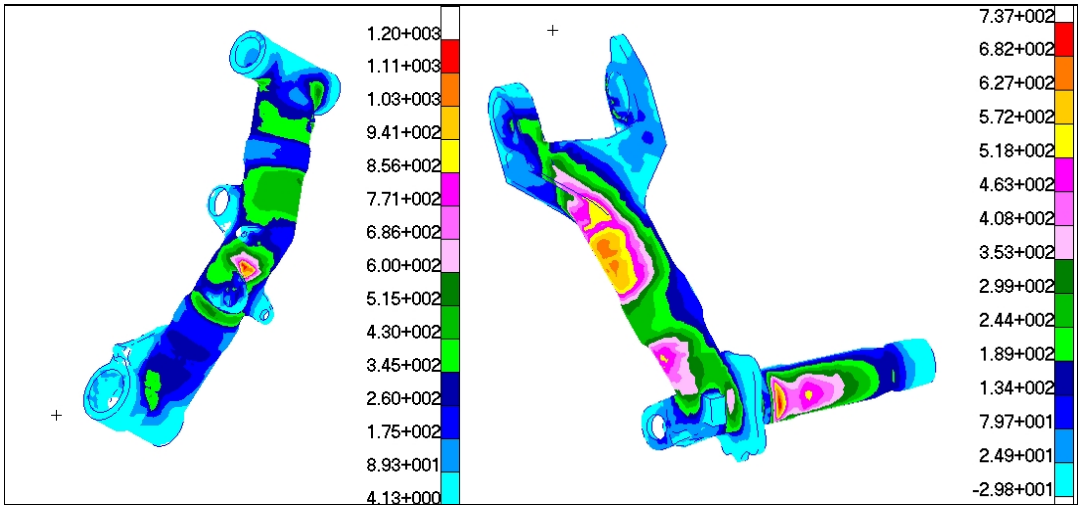

Figure 4.15 Maximum Principal Stress plot for MLG Semi-fork & Strut in load case– 4 (-Pz)

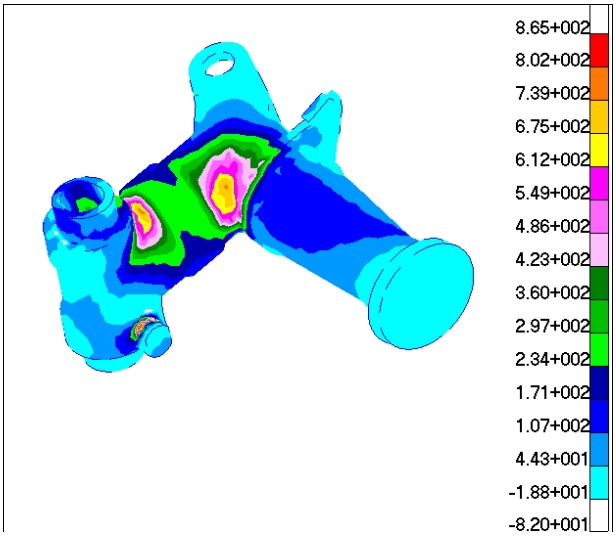

Figure 4.16 Maximum Principal Stress plot for MLG Turning Unit in load case– 4 (-Pz)

4.1.5 Load Case – 4 (+Pz)

Maximum displacement & Maximum principal stress are 30 mm (Figure 4.17) and 53.2kg/mm^2 (Figure 4.18) respectively, Figure 4.19 & 4.20 shows the maximum principal stress plot for individual components.

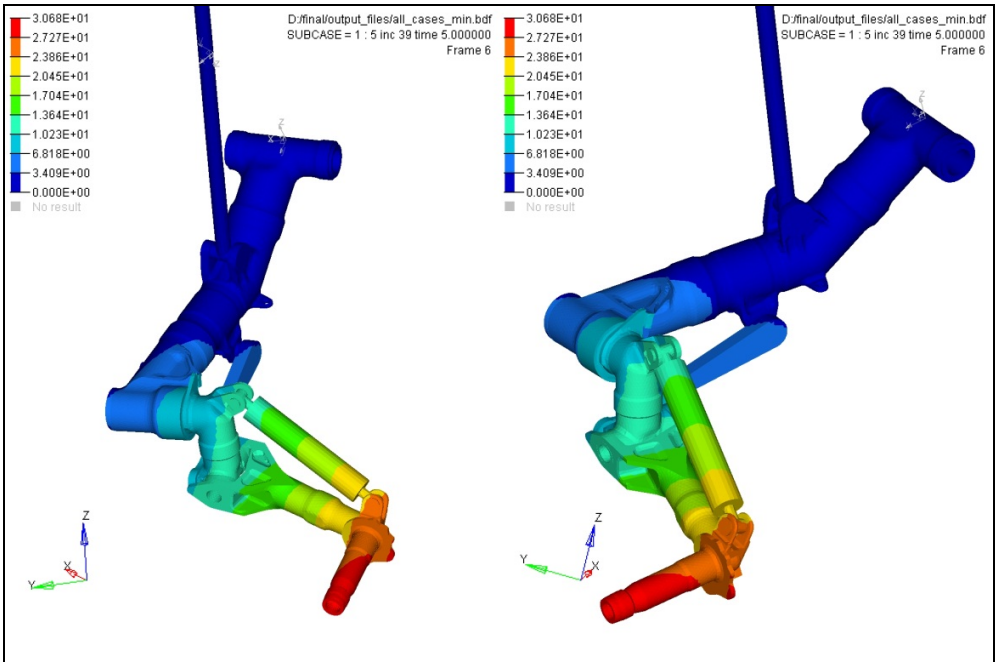

Figure 4.17 Maximum displacement plot for MLG assembly in Load Case – 4 (+Pz)

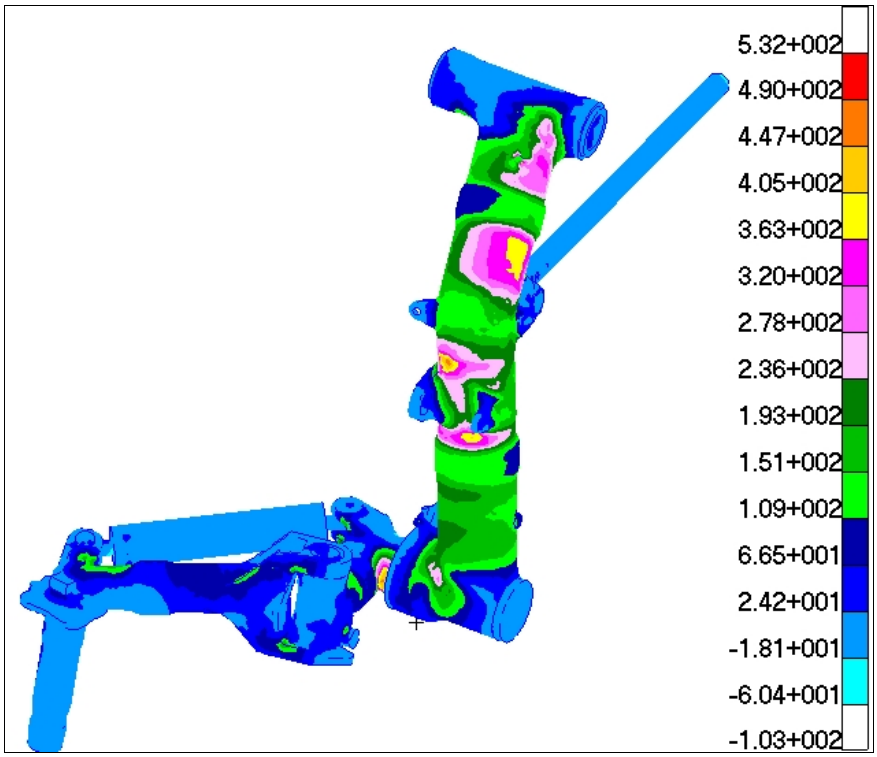

Figure 4.18 Maximum Principal Stress plot for MLG assembly in Load Case – 4 (+Pz)

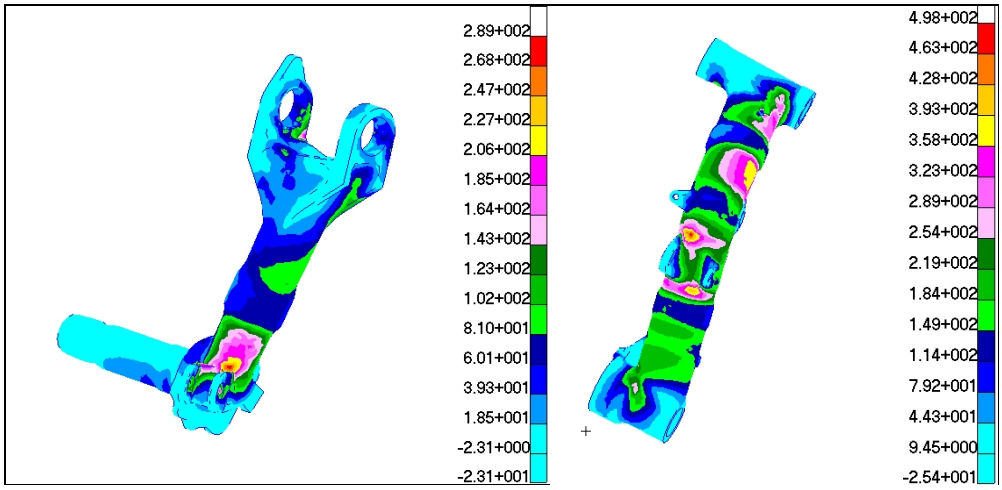

Figure 4.19 Maximum Principal Stress plot for MLG Semi-fork & Strut in load case–4 (+Pz)

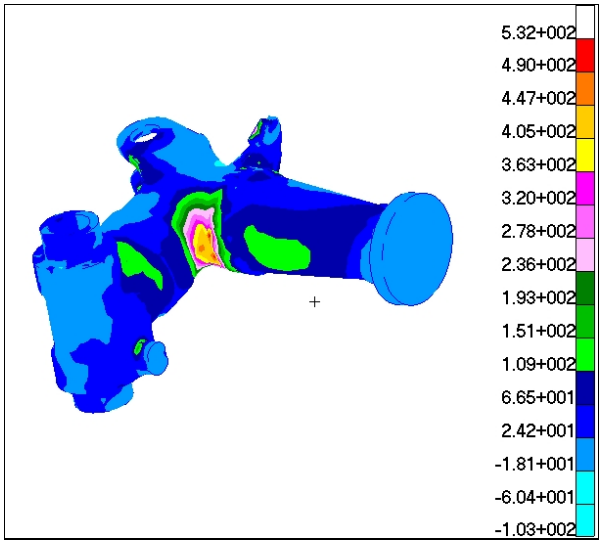

Figure 4.20 Maximum Principal Stress plot for MLG Turning Unit in load case– 4 (+Pz)

4.2 STRESS ANALYSIS RESULTS OF NLG

Stress analysis is carried out for all four load cases with the above mentioned boundary conditions, and material properties. In case-4 the Pz component is acting in positive as well as in the negative direction. Therefore both the cases are analyzed in case-4.

4.2.1 Load Case – 1

Out of four load cases, Load Case-1 is most critical. Maximum displacement & Maximum principal stress are 42 mm (Ref Figure 4.21) & 92.7 kg/mm^2 (Ref Figure 4.22) respectively. Figure 4.23 to 4.2 shows the maximum principal stress plot for critical components.

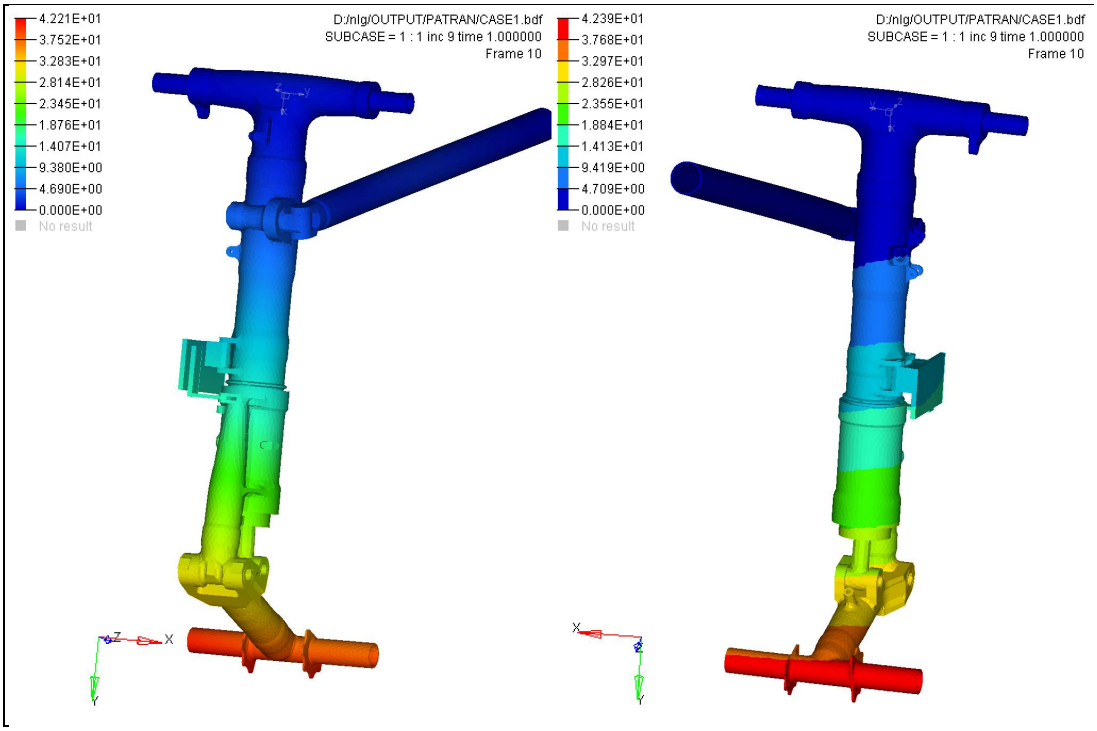

Figure 4.21 Maximum displacement plot for NLG assembly in Load case-1

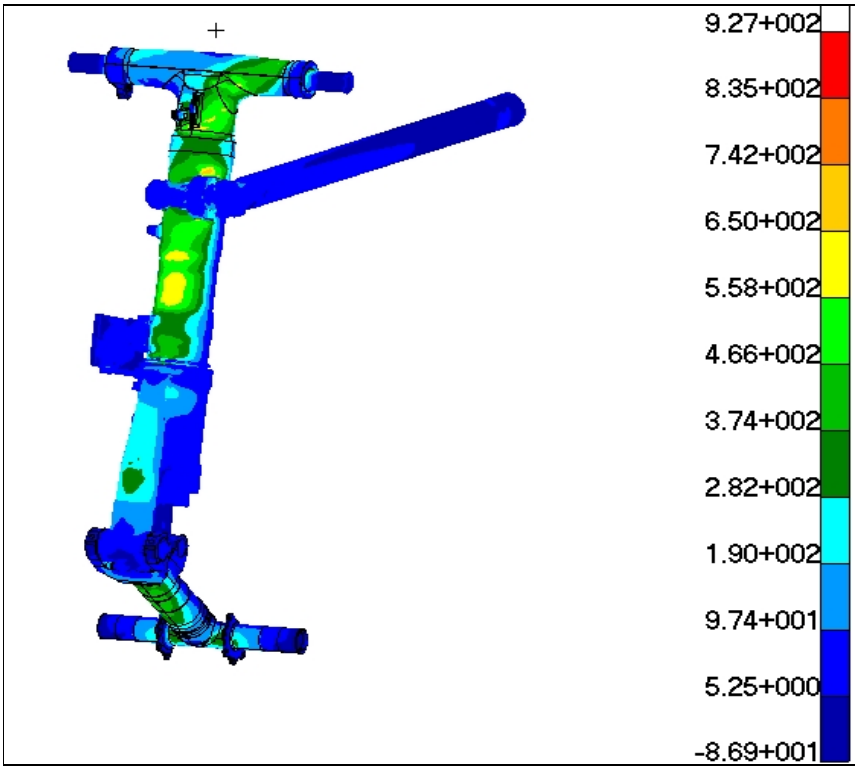

Figure 4.22 Maximum Principal Stress plot for NLG assembly in Load case-1

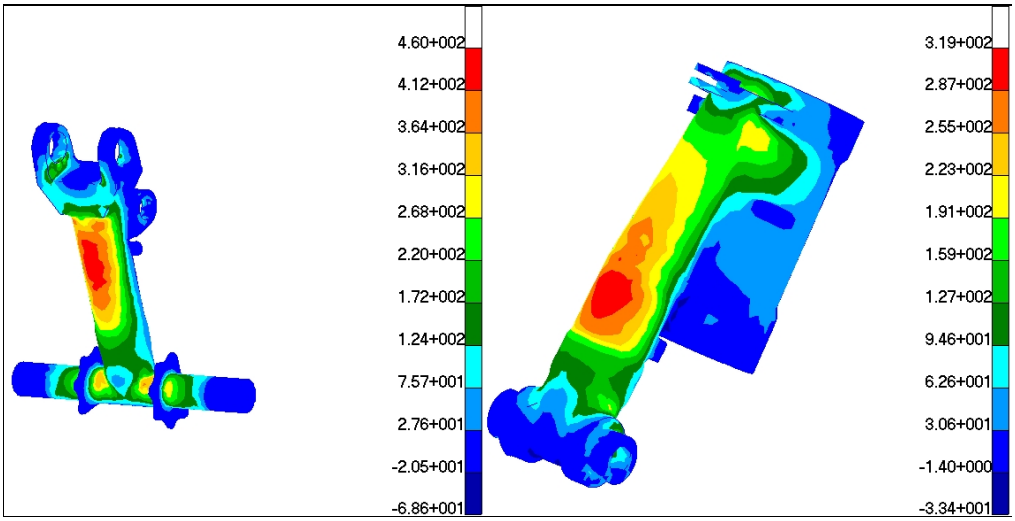

Figure 4.23 Maximum Principal Stress plot for NLG Semi-fork & Swivel Unit in Load case-1

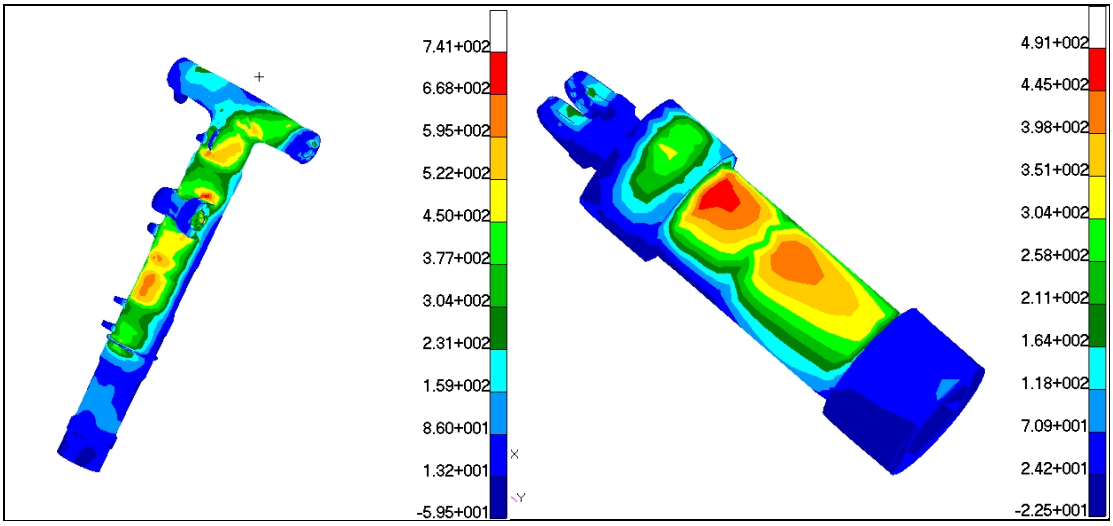

Figure 4.24 Maximum Principal Stress plot for NLG Strut & Cylinder in Load case-1

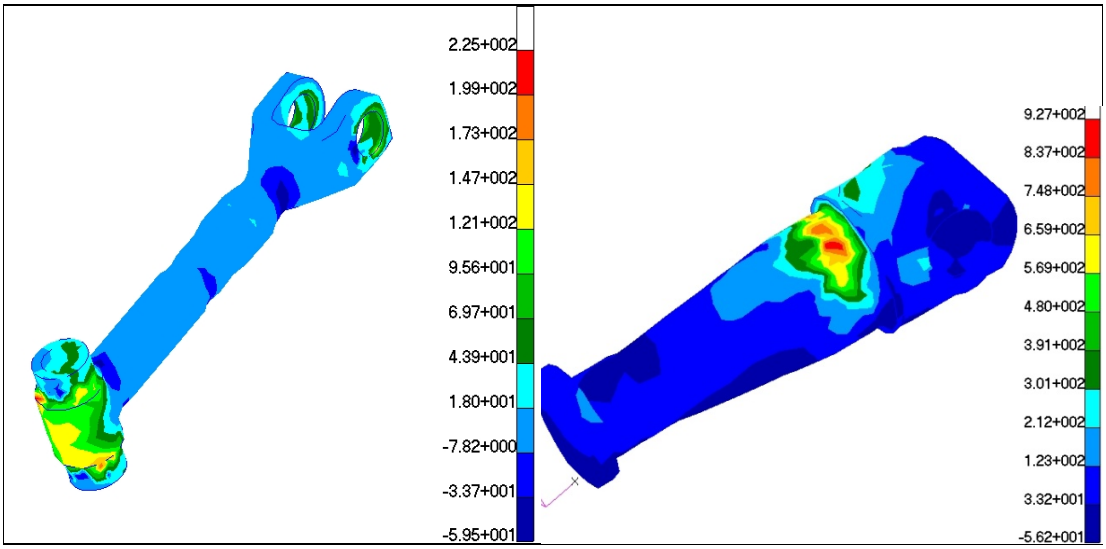

Figure 4.25 Maximum Principal Stress plot for NLG Connecting Rod & Brace Bolt in Load case-1

4.2.2 Load Case – 2

In this case Maximum displacement & Maximum principal stress are 11.9 mm (Ref Figure 4.26) & 39.4 kg/mm^2 (Ref Figure 4.27) respectively. Figure 4.28 to 4.30 shows the maximum principal stress plot for critical components.

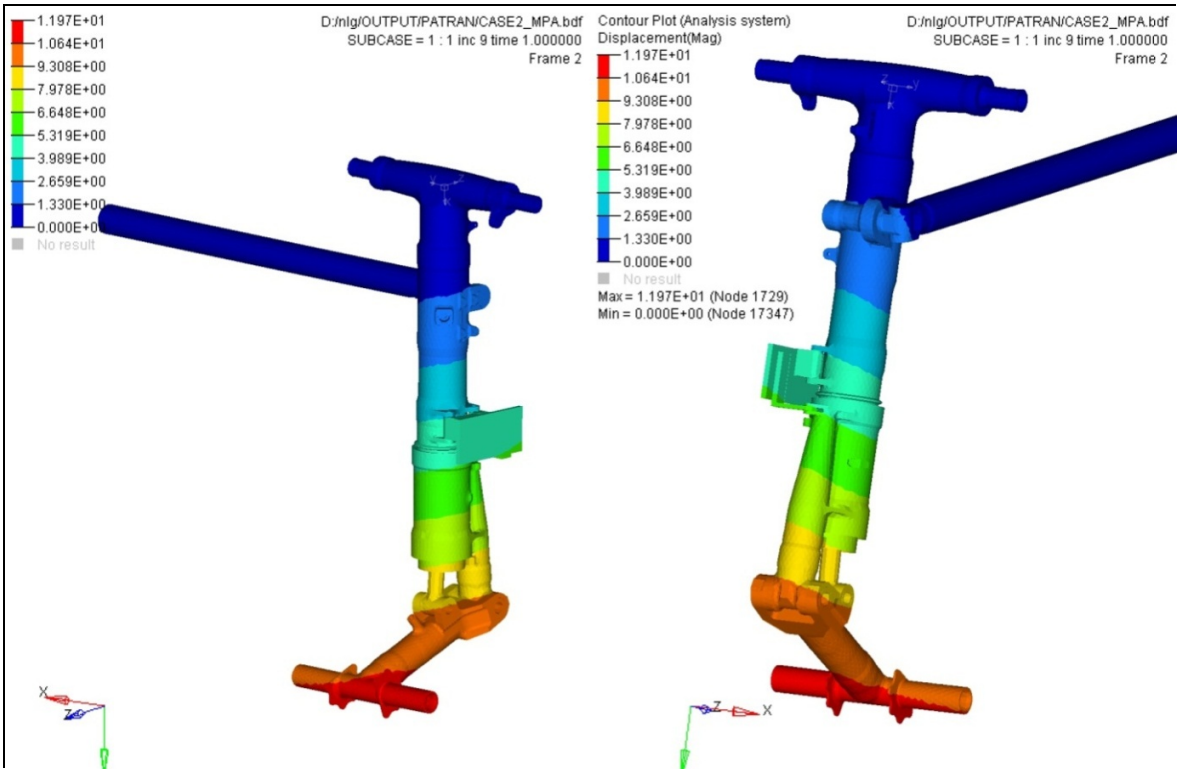

Figure 4.26 Maximum displacement plot for NLG assembly in Load case-2

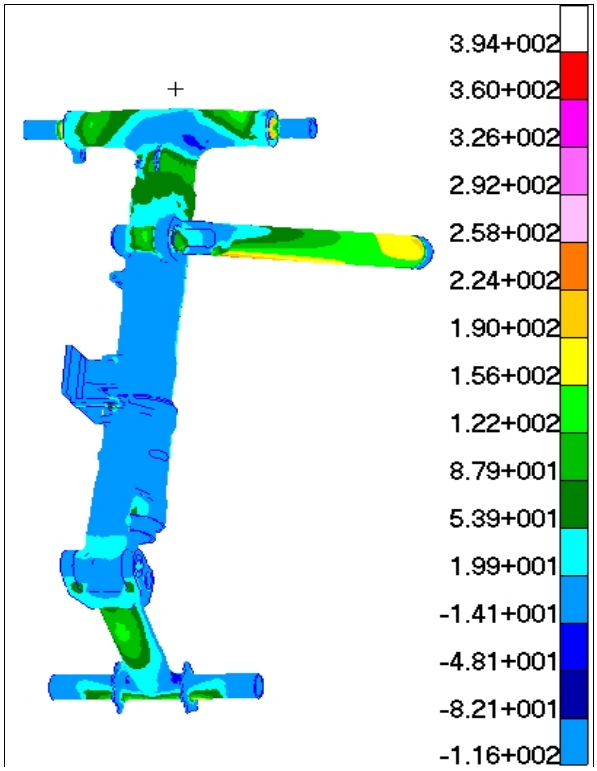

Figure 4.27 Maximum Principal Stress plot for NLG assembly in Load case-2

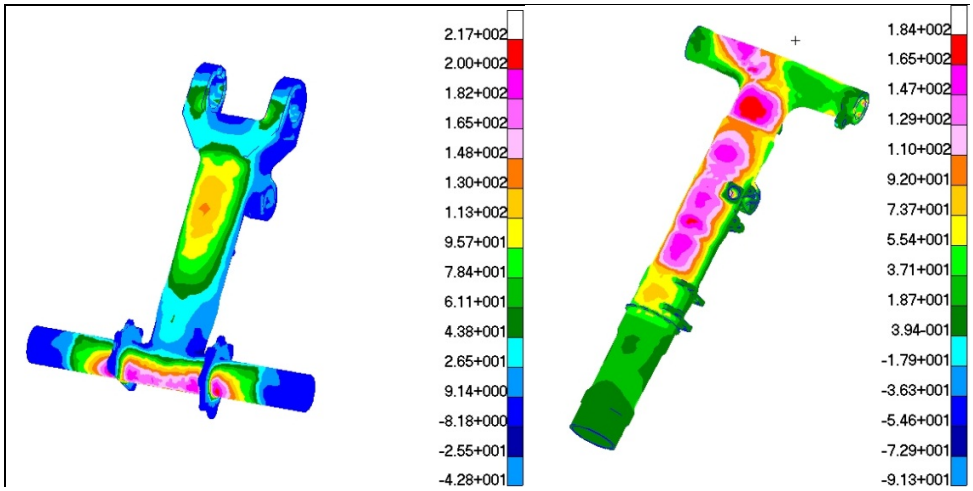

Figure 4.28 Maximum Principal Stress plot for NLG Semi-fork &Strut in Load case-2

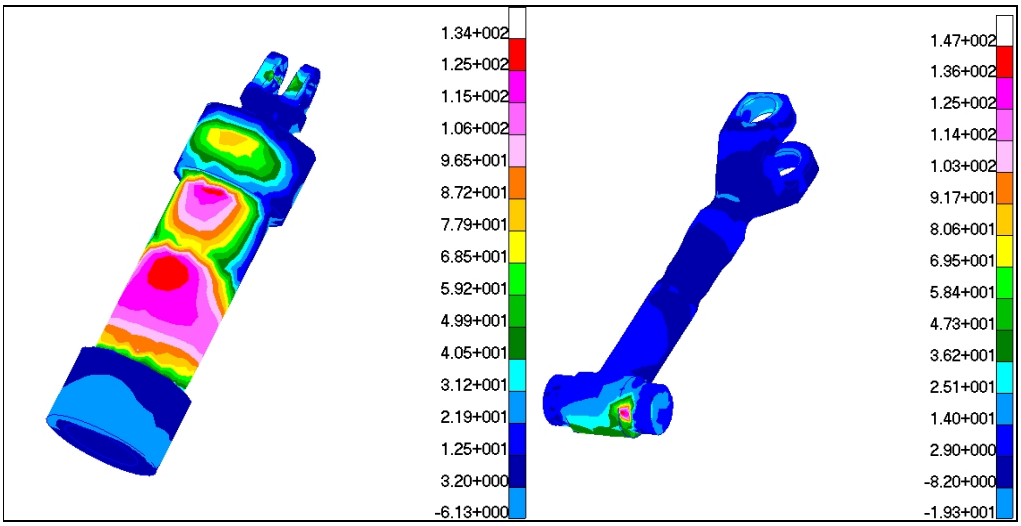

Figure 4.29 Maximum Principal Stress plot for NLG Cylinder & Connecting rod in Load case-2

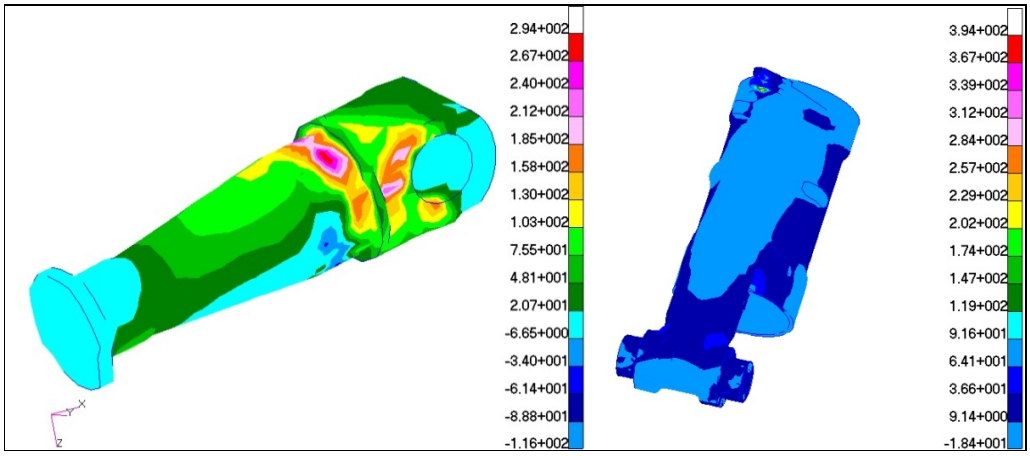

Figure 4.30 Maximum Principal Stress plot for NLG Brace Bolt & Swivel unit in Load case-2

4.2.3 Load Case – 3

Maximum displacement & Maximum principal stress are 17.8 mm (Ref Figure 4.31) & 47.4 kg/mm^2 (Ref Figure 4.32) respectively. Figure 4.33 to 4.35 shows the maximum principal stress plot for critical components.

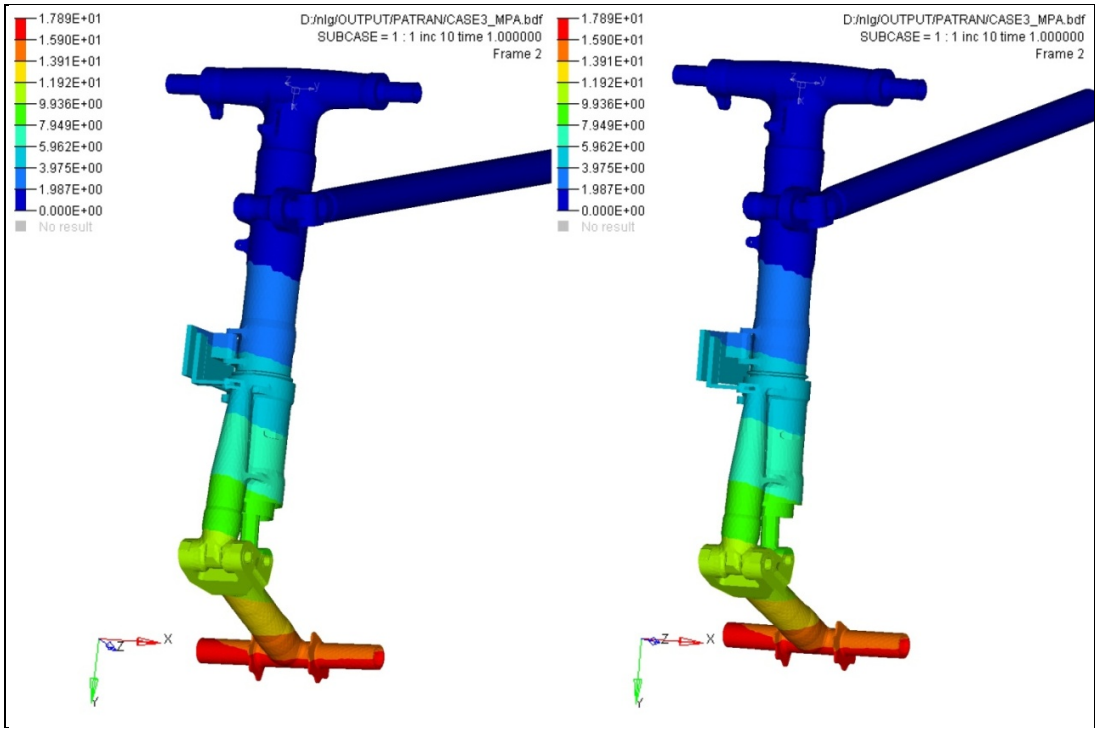

Figure 4.31 Maximum displacement plot for NLG assembly in Load case-3

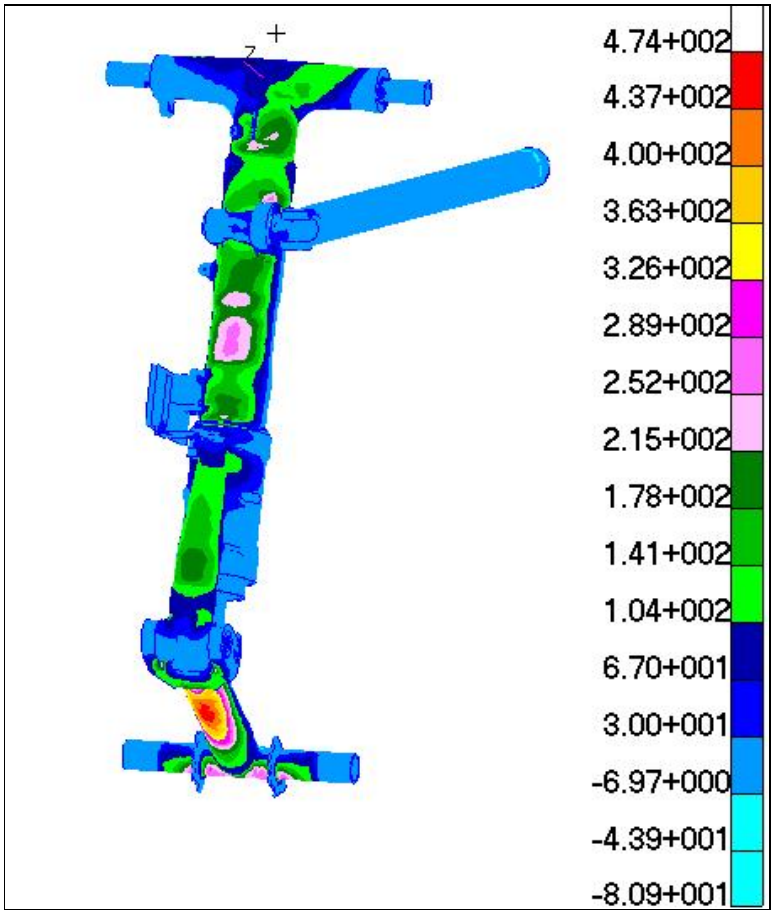

Figure 4.32 Maximum Principal Stress plot for NLG assembly in Load case-3

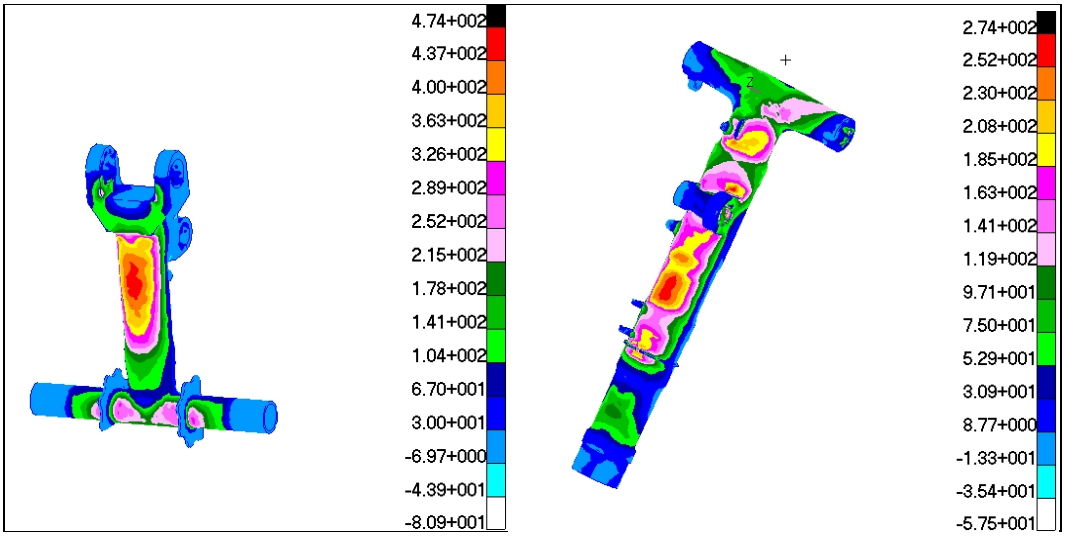

Figure 4.33 Maximum Principal Stress plot for NLG Semi-fork &Strut in Load case-3

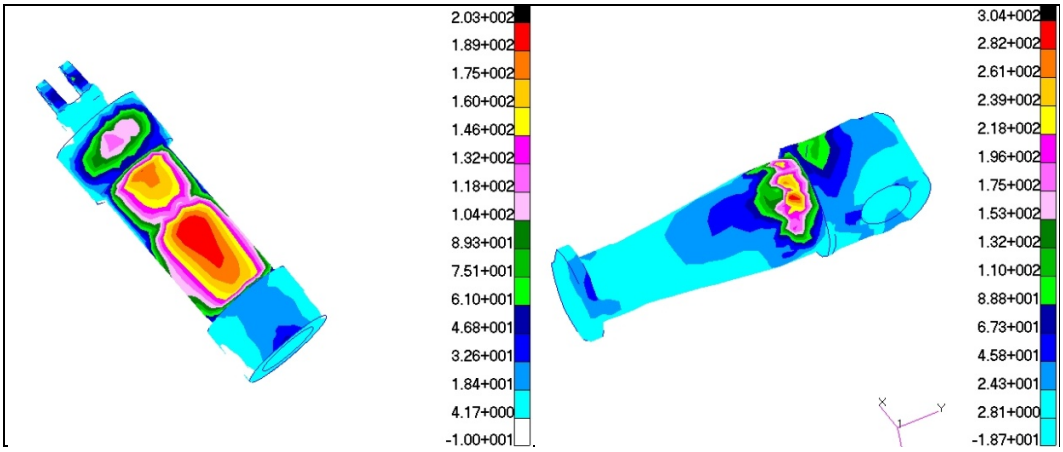

Figure 4.34 Maximum Principal Stress plot for NLG Cylinder & Brace Bolt in Load case-3

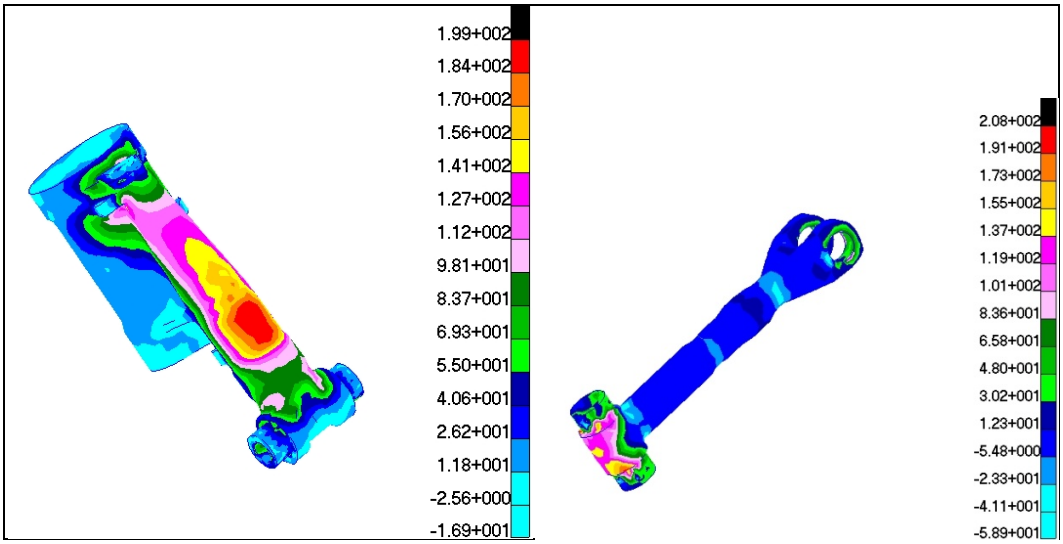

Figure 4.35 Maximum Principal Stress plot for NLG Swivel Unit & Connecting rod in Load case-3

4.2.4 Load Case – 4 (+Pz)

Maximum displacement & Maximum principal stress are 22 mm (Ref Figure 4.36) & 55.8 kg/mm^2 (Ref Figure 4.37) respectively. Figure 4.38 to 4.40 shows the maximum principal stress plot for critical components.

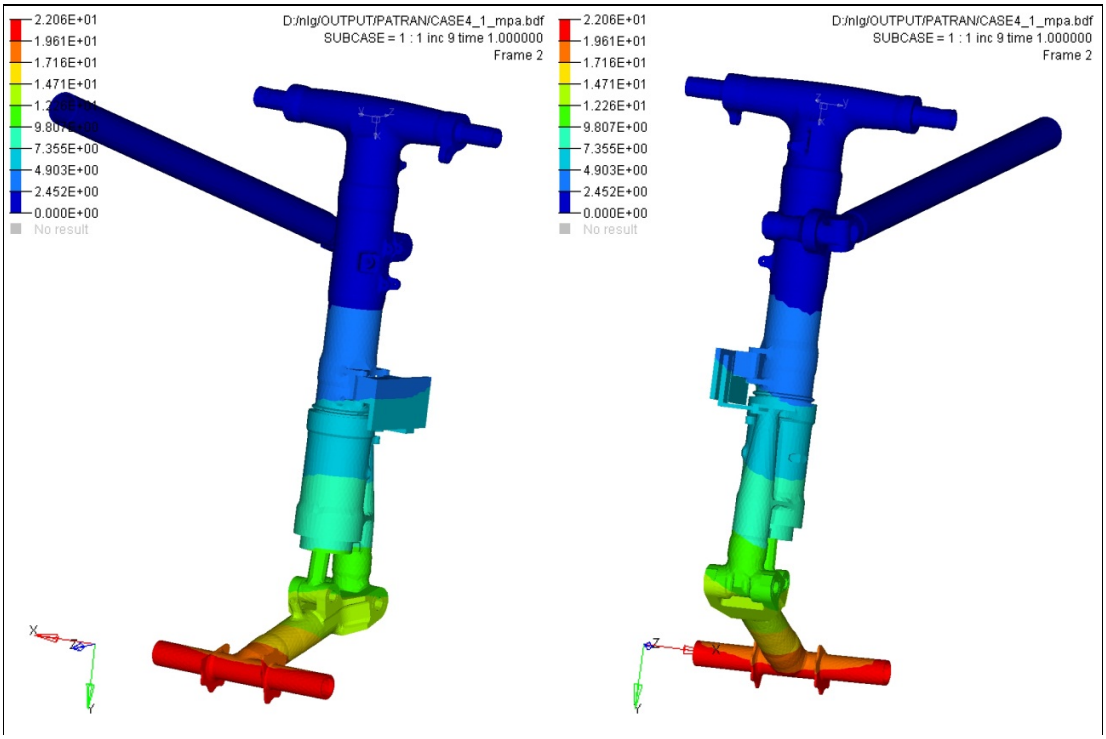

Figure 4.36 Maximum displacement plot for NLG assembly in Load Case – 4 (+Pz)

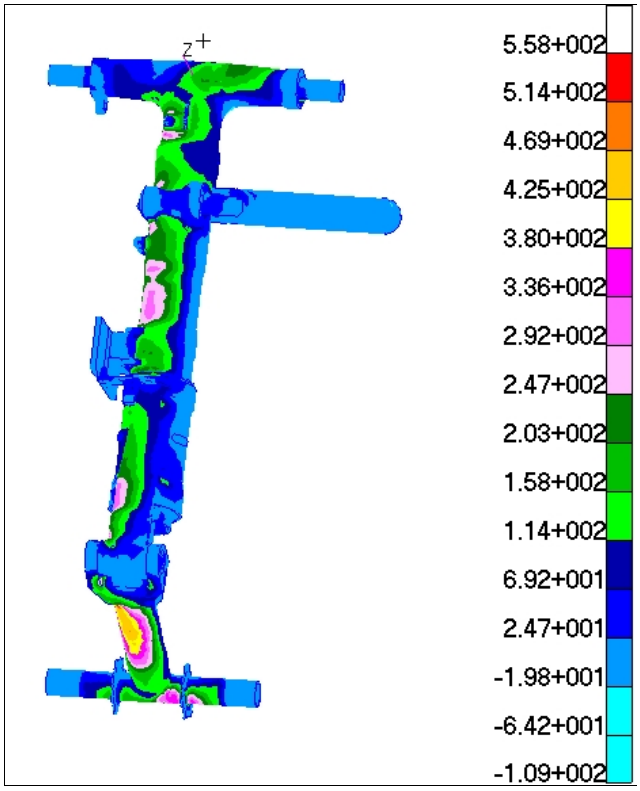

Figure 4.37 Maximum Principal Stress plot for NLG assembly in Load Case – 4 (+Pz)

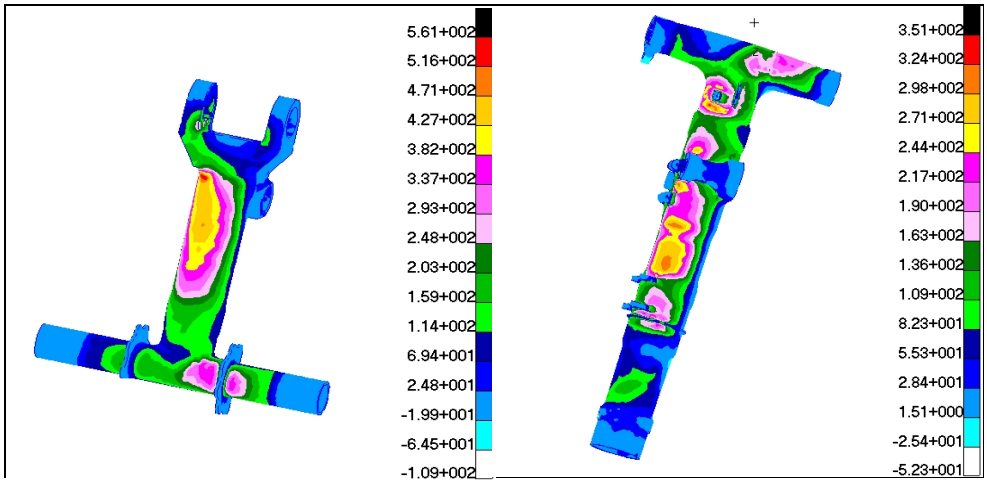

Figure 4.38 Maximum Principal Stress plot for NLG Semi-fork &Strut in Load case-4 (+Pz)

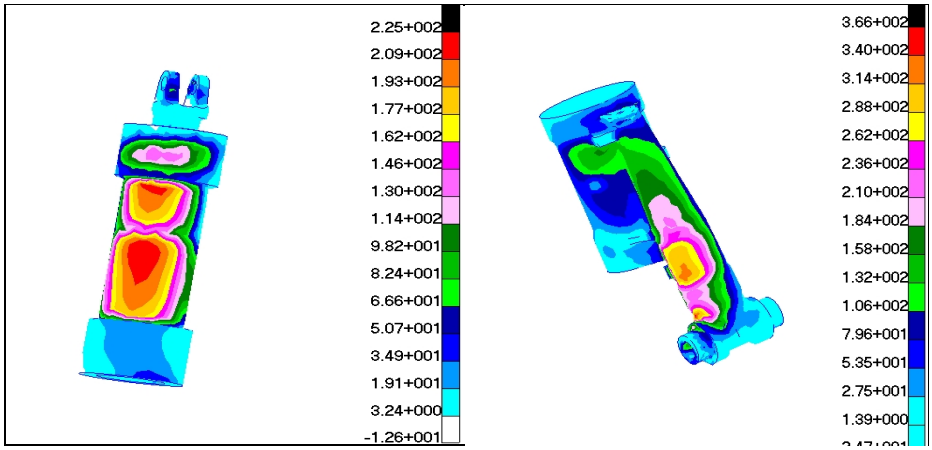

Figure 4.39 Maximum Principal Stress plot for NLG Cylinder & Swivel Unit in Load case-4(+Pz)

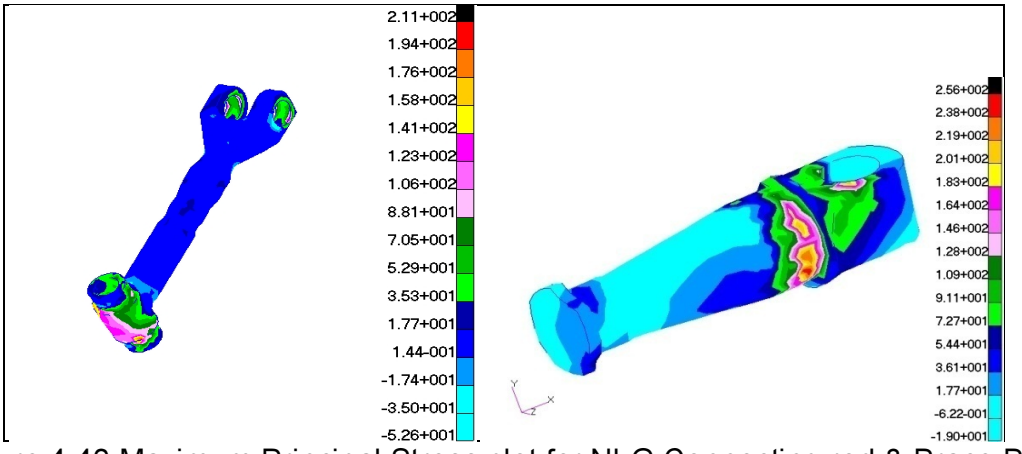

Figure 4.40 Maximum Principal Stress plot for NLG Connecting rod & Brace Bolt in Load case-4 (+Pz)

4.2.5 Load Case – 4 (-Pz)

In this case Maximum displacement & Maximum principal stress are 23.5 mm (Ref Figure 4.41) and51.3 kg/mm^2 (Ref Figure 4.42) respectively. Figure 4.43 to 4.45 shows the maximum principal stress plot for critical components.

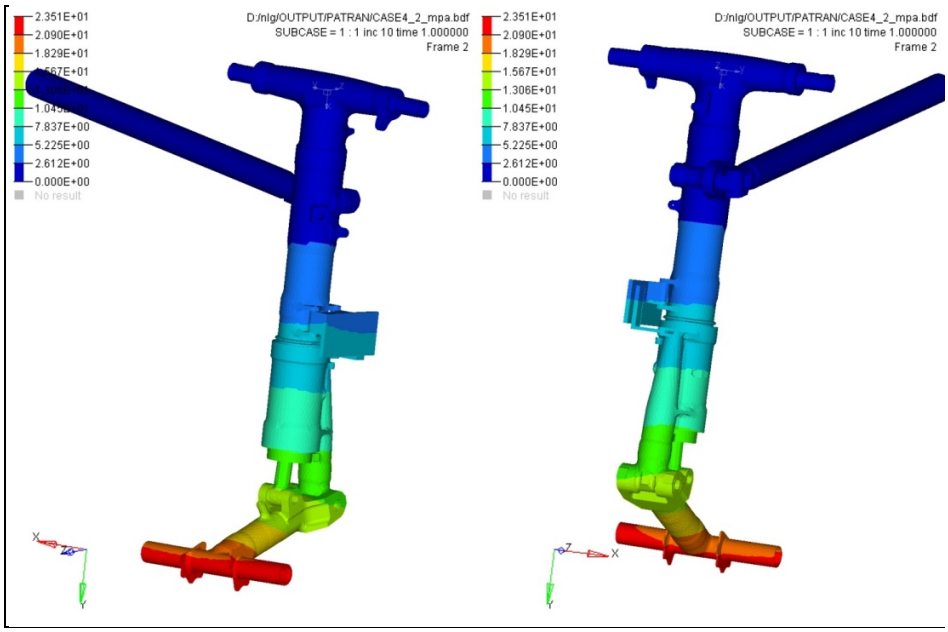

Figure 4.41Maximum displacement plot for NLG assembly in Load Case – 4 (-Pz)

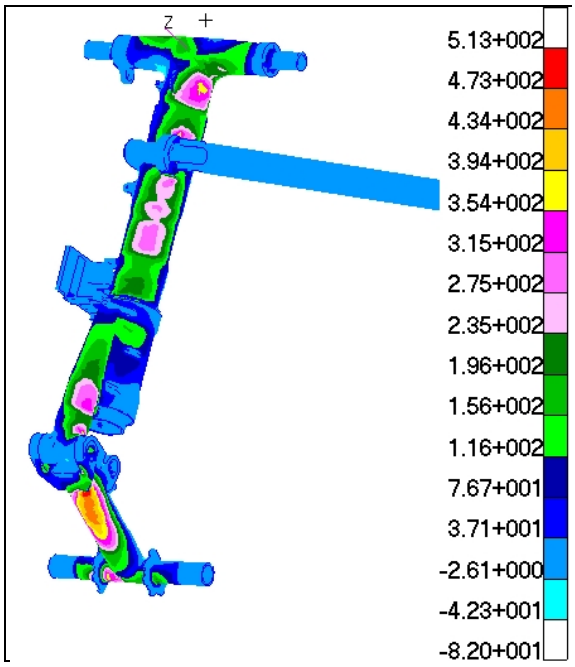

Figure 4.42 Maximum Principal Stress plot for NLG assembly in Load Case – 4 (-Pz)

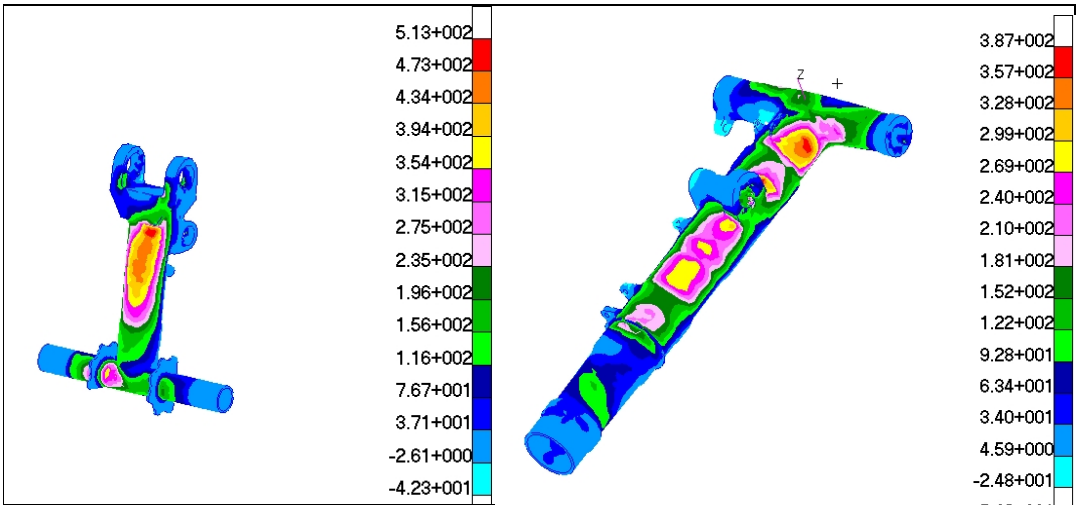

Figure 4.43 Maximum Principal Stress plot for NLG Semi-fork &Strut in Load case-4 (-Pz)

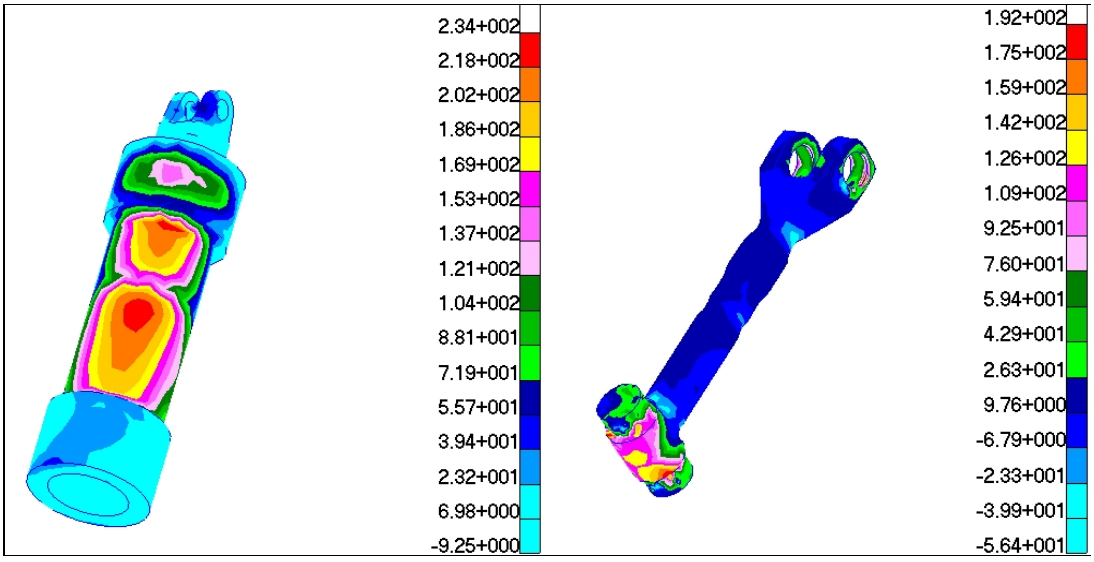

Figure 4.44 Maximum Principal Stress plot for NLG Cylinder & Connecting rod in Load case-4 (-Pz)

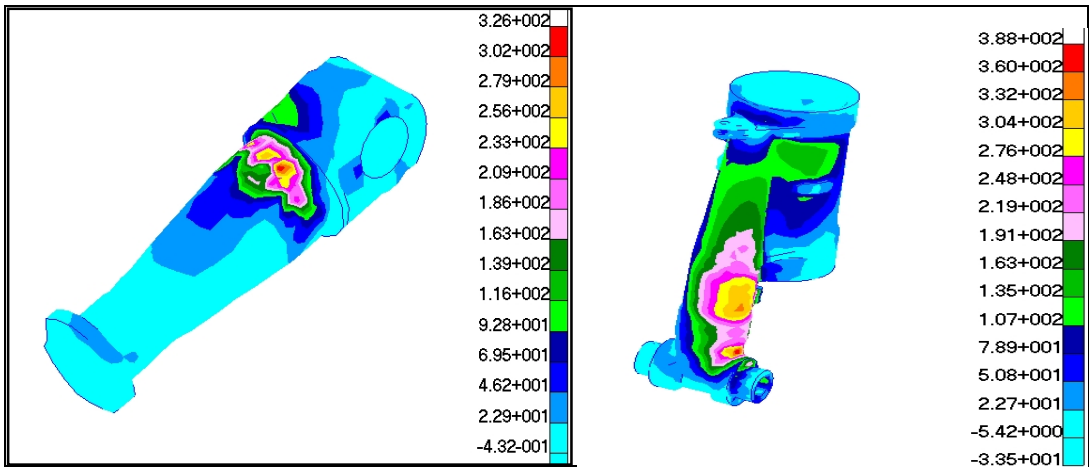

Figure 4.45Maximum Principal Stress plot for NLG Brace Bolt & Swivel Unit in Load case-4 (-Pz)

4.3 Validation of Stress Analysis Results

To validate the FE Stress Analysis following checks has been carried out.

4.3.1 Validation with rejuvenation area

Validation of stress analysis result was carried out with rejuvenated MLG strut. Figure 4.46 to 4.51are showing six zones of rejuvenation on MLG strut and all the rejuvenation zones are found to be matching with stress hot spots at different load cases as shown in the following table-4.2.

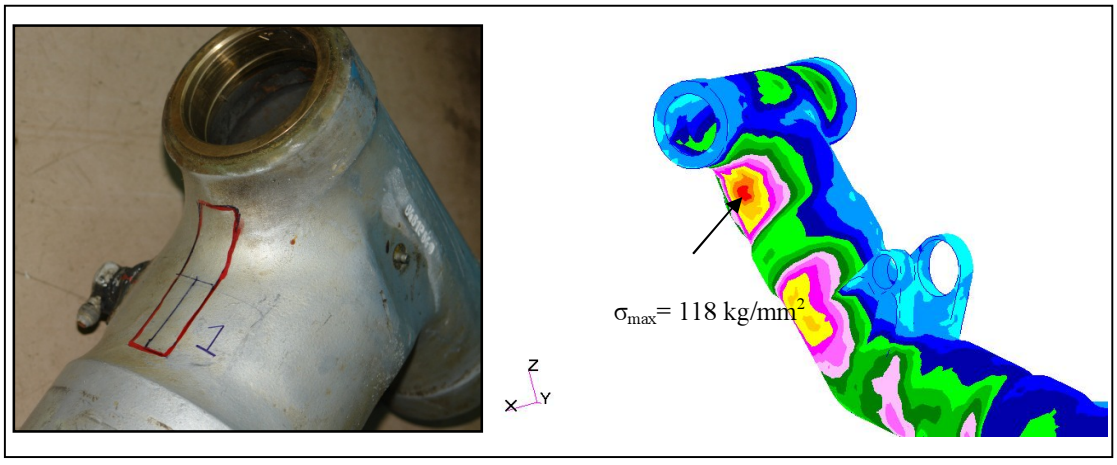

Figure 4.46 Matching of Rejuvenated MLG with stress hot spots (Zone-1)

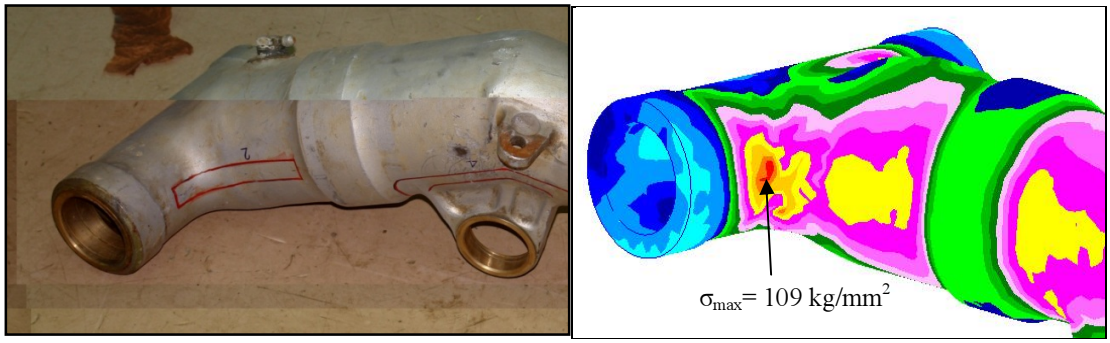

Figure 4.47 Matching of Rejuvenated MLG with stress hot spots (Zone-2)

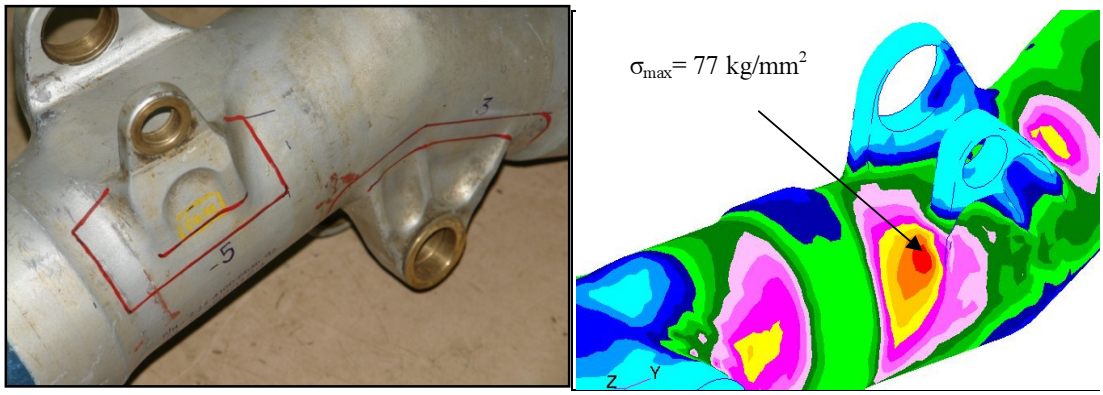

Figure 4.48 Matching of Rejuvenated MLG with stress hot spots (Zone-3)

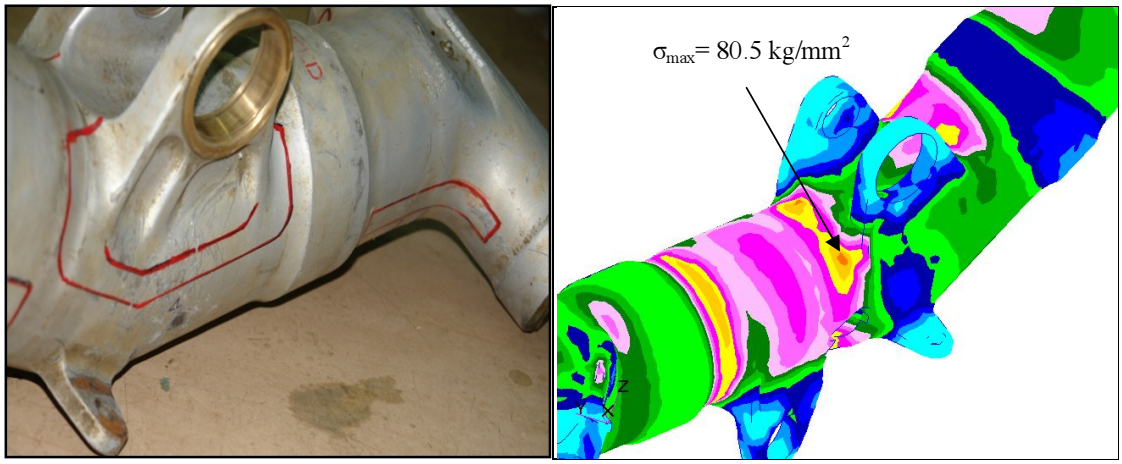

Figure 4.49 Matching of Rejuvenated MLG with stress hot spots (Zone-4)

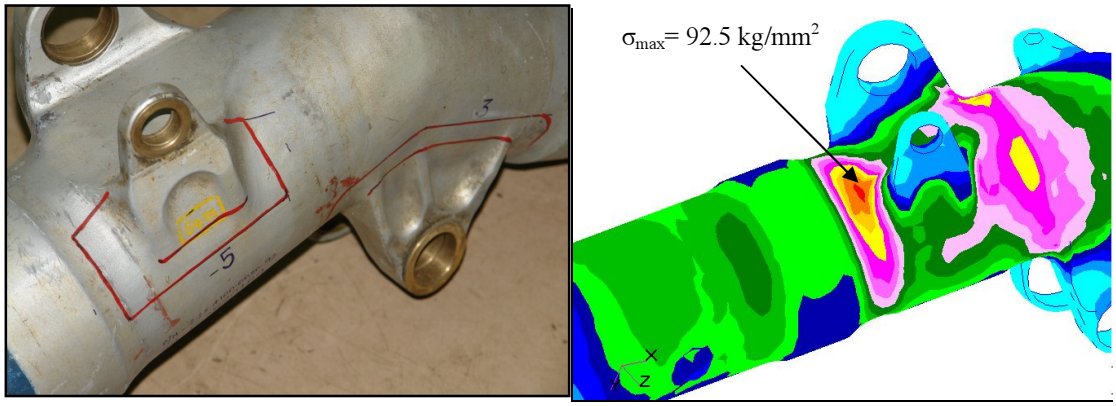

Figure 4.50 Matching of Rejuvenated MLG with stress hot spots (Zone-5)

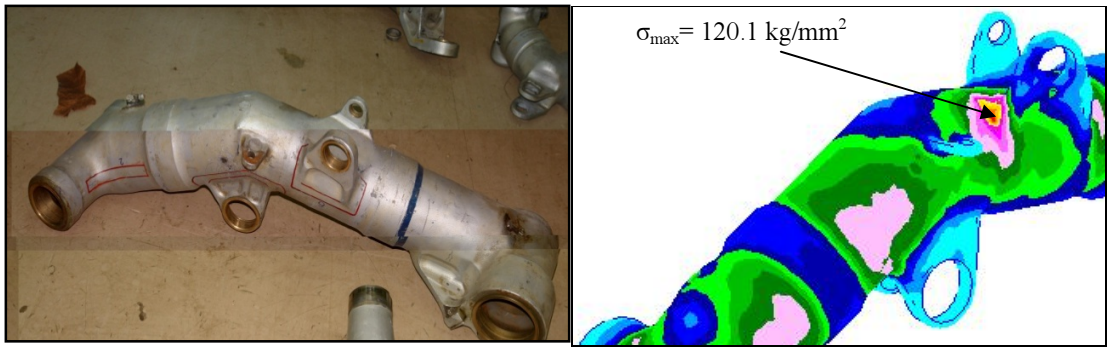

Figure 4.51 Matching of Rejuvenated MLG with stress hot spots (Zone-6)

Table-4.2 Matching rejuvenation zone & stress hot pat with load case

Rejuvenation zone	Load Case
1	(E'w+G'w)1
2	(E'w+G'w)1and(Ew+Gw)2
3	(Ew+Gw)2
4	R1w (+Pz)
5	(E'w+G'w)1
6	(Ew+Gw)2, R1w (-Pz)

4.3.2 Validation with Classical Calculations

Classical calculation for Semi-fork of MLG has been carried out at sections at a distance of 229 and 315 mm from free end. Results have been compared with FE analysis stresses. Table -4.3 shows comparison of results at 229 mm and 315 mm respectively.

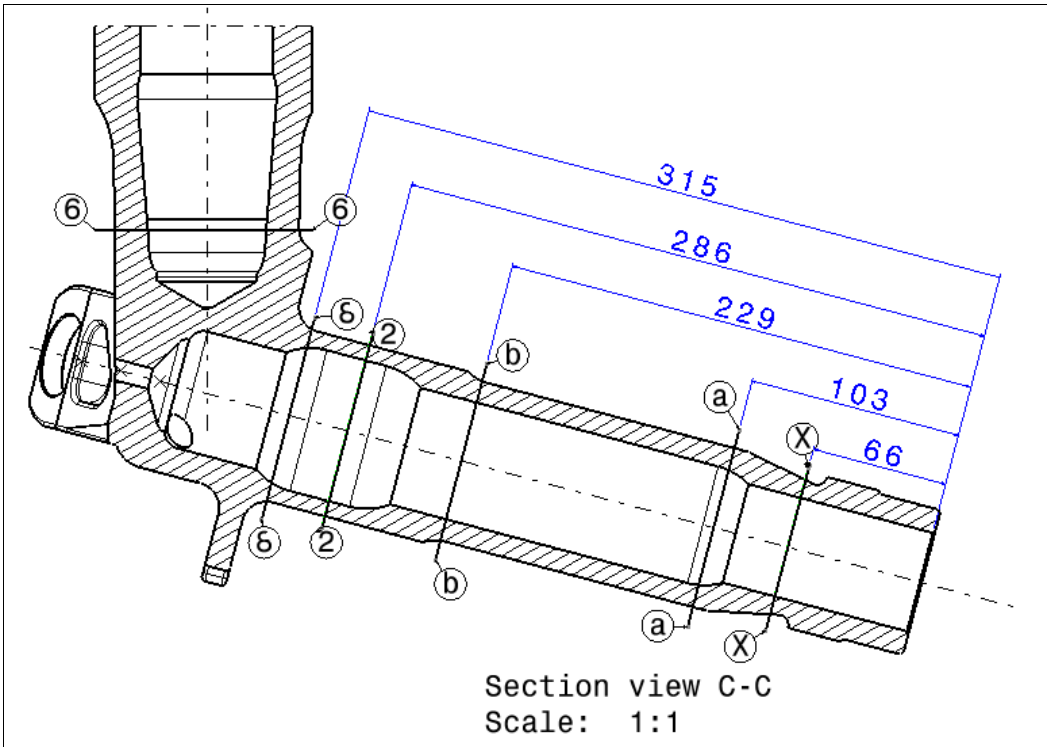

Figure 4.52 Semi-fork of MLG

Table-4.3 Comparison of results for Semi-fork of MLG

Stress	Classical method	FEM	Classical method	FEM
	Section at 229mm		Section at 315mm	
Bending Stress (kg/mm^2)	53	51	37	38.5
Shear Stress (kg/mm^2)	6.0	6.8	2.6	2.8
Von Mises (kg/mm^2)	54	57	37.2	39

Similarly classical calculation for Semi-fork of NLG has been also carried out at sections at a distance of 43 and 108 mm from center of semi fork. Results have been compared with FE analysis stresses and found to be satisfactory. Table-4.3 shows comparison of results at 43 mm and 108 mm respectively.

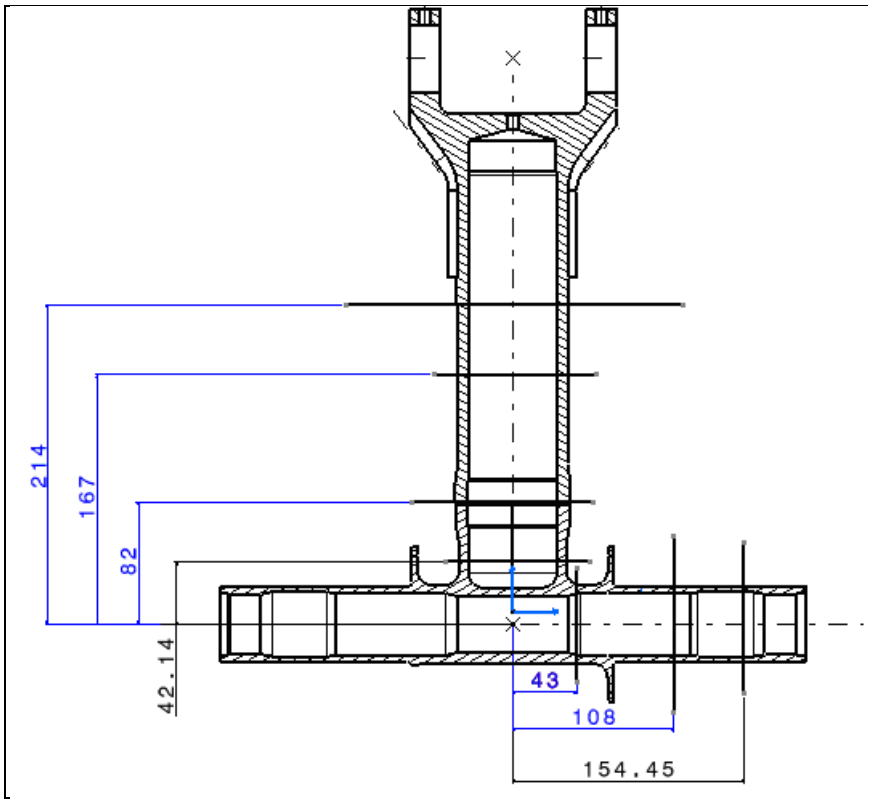

Figure 4.53 Semi-fork of NLG

Table-4.4 Comparison of results for Semi-fork of NLG

Stress	Classical method	FEM	Classical method	FEM
	Section at 43mm		Section at 180mm	
Bending Stress (kg/mm^2)	17.7	19	36	34.2
Shear Stress (kg/mm^2)	5.3	4.2	3.8	4.3
Von Mises (kg/mm^2)	19.9	20.3	36.6	35

4.4 FATIGUE ANALYSIS RESULTS

Fatigue analysis has been carried out for MLG and NLG using minimum wall thickness.

4.4.1 Fatigue Analysis Results of MLG

Stress analysis of MLG shows that the strut is most critical therefore fatigue analysis is carried out only on strut. Figure 4.54 & 4.55 shows the cumulative fatigue life plot & fatigue hot spots on the strut. From the plot it can be seen that the strut has minimum fatigue life of $10^{1.93}$ blocks = 85 blocks. This is equivalent to 27625 landings after considering a scatter factor of 4.

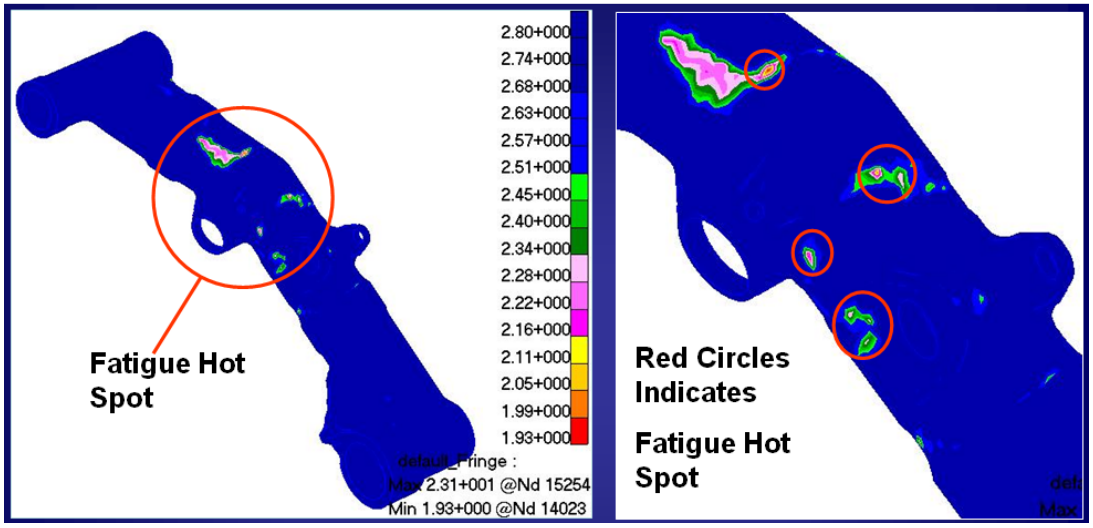

Figure 4.54 Fatigue Life Plot

Figure 4.55 Fatigue Hot Spots

4.4.2 Fatigue Analysis Results of NLG

Figure 4.56 shows the cumulative fatigue life plot on NLG assembly & Figure 4.56to 4.56 shows the cumulative fatigue life plot on various components. From the plot it can be seen that the Semi-fork has minimum fatigue life of $10^{2.03}$ blocks = 107 blocks. This is equivalent to 29425 landings after considering a scatter factor of 4.

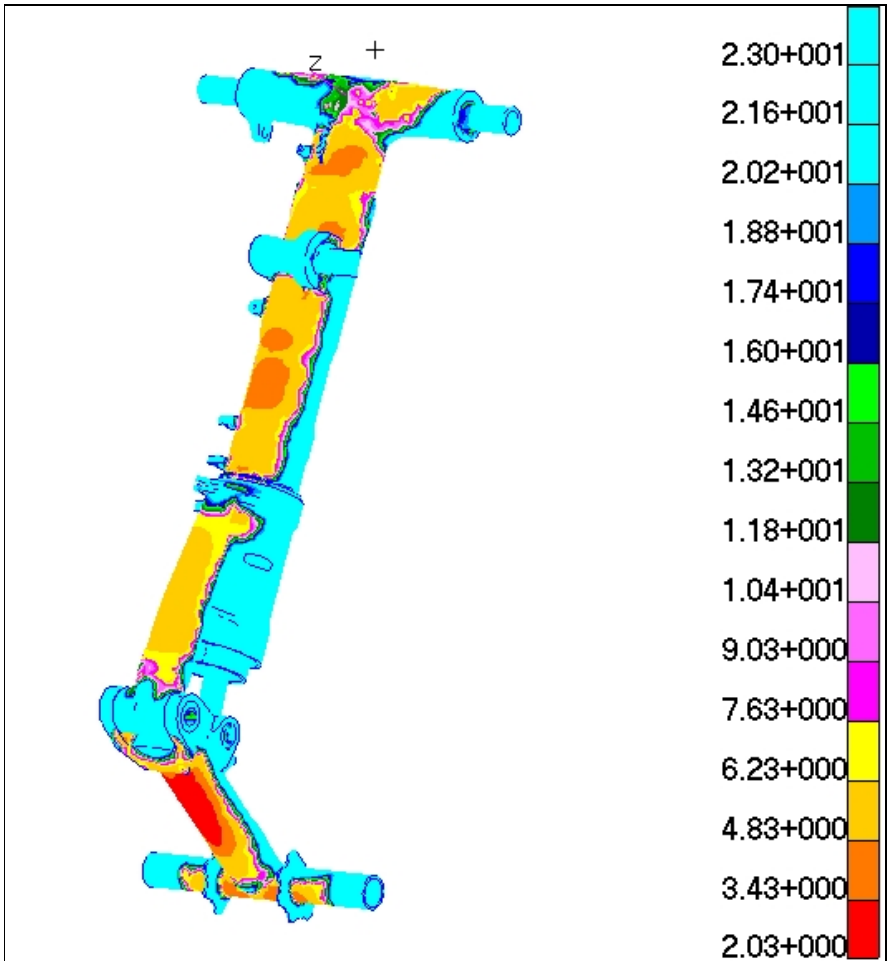

Figure 4.56 Fatigue Life plot on NLG assembly NLG assembly

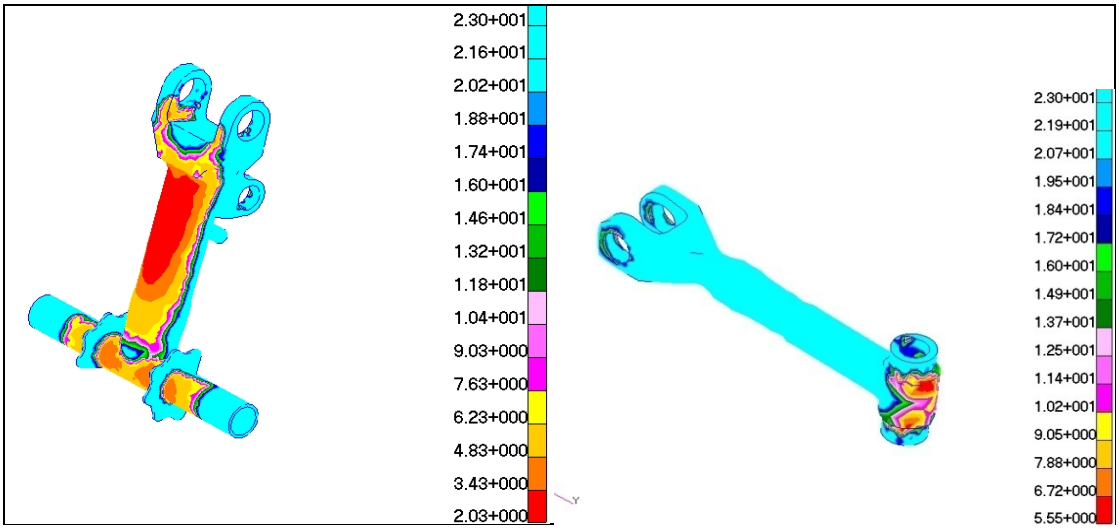

Figure 4.57 Fatigue Life plot on NLG Semi-fork & Connecting rod

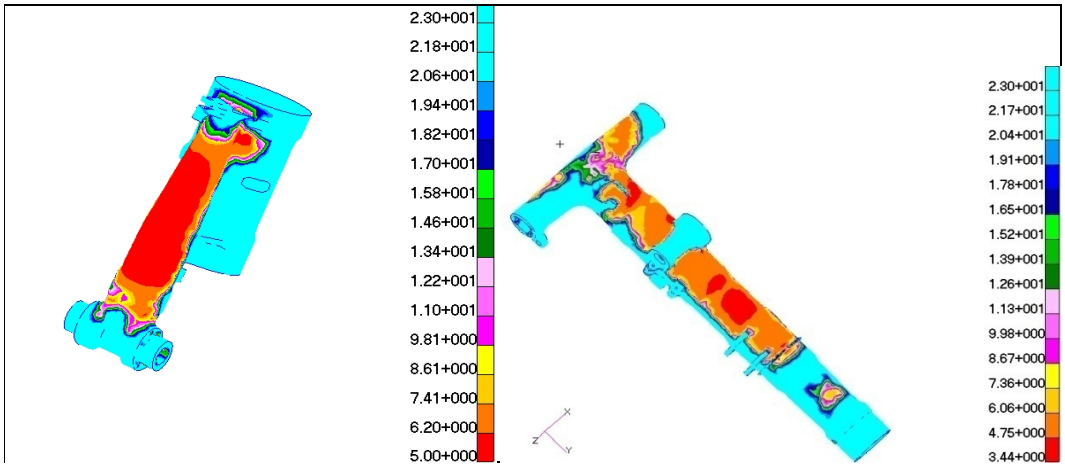

Figure 4.58 Fatigue Life plot on NLG Swivel Unit & Strut

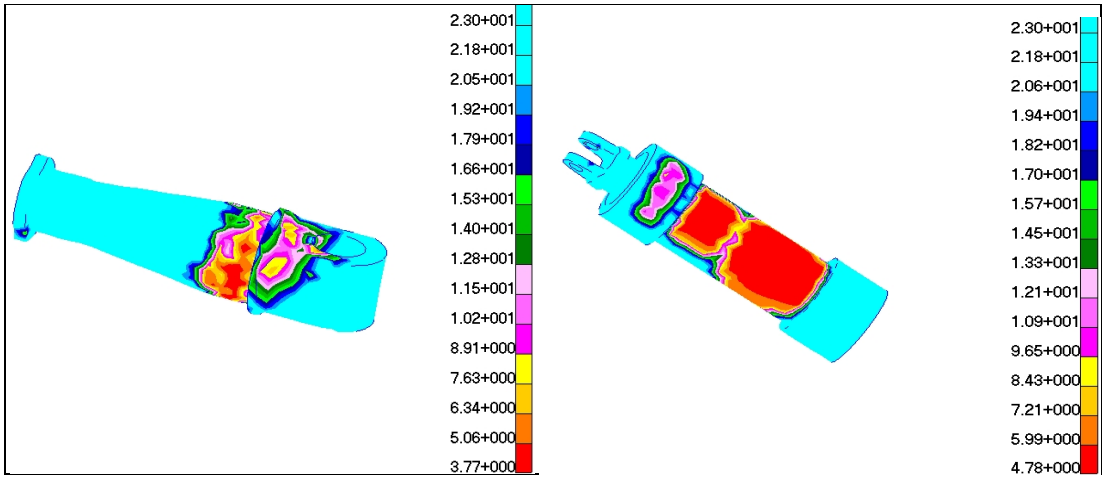

Figure 4.59 Fatigue Life plot on NLG Brace Bolt & Cylinder

4.4.3 Stress & Fatigue Analysis of Rejuvenated MLG

To consider the effect of thickness reduction at the rejuvenation zones, analysis was repeated considering 1mm thickness reduction due to rejuvenation (Ref Table-4.1), although there is a requirement of only 0.5mm thickness reduction for rejuvenation, we have considered 1.0mm reduction on rejuvenated areas as shown in Figure 4.60. Stress levels at different zones has been compared with minimum wall thickness case and results are been tabulated in Table 4.5

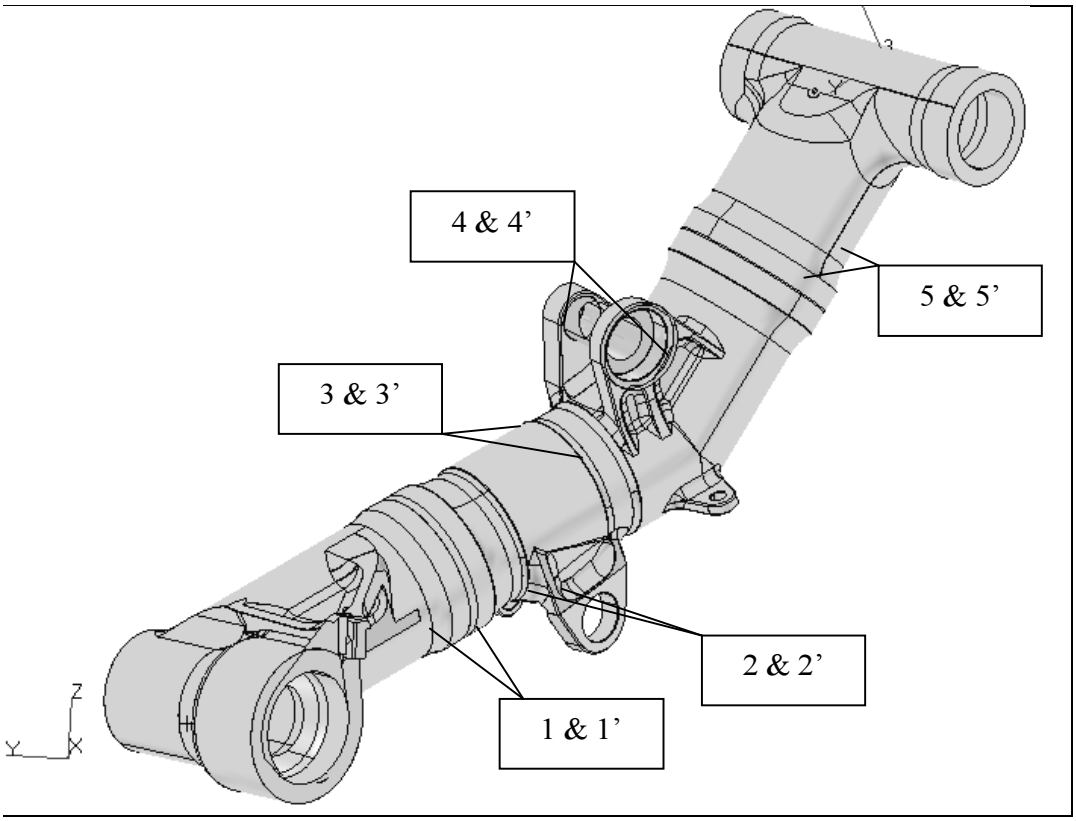

Figure 4.60 Zones for Stress Comparison

Table 4.5 Stress levels at different zones with minimum wall thickness

	Thickness Reduction	**1**	**1'**	**2**	**2'**	**3**	**3'**	**4**	**4'**	**5**	**5'**
CASE_1	Min. Rqd	-	-	-	-	108,*	-	-	-	-	108,118
	1mm			93,97		117,*					115,125
CASE_2	Min. Rqd	-	-	90 ,99	-	-	-	-	-	-	-
	1mm			103,114							
CASE_3	Min. Rqd	-	-	92,105	-	-	-	-	-	-	-
	1mm			106,121							
CASE_4.1	Min. Rqd	-	-	109,120	-	-	-	-	-	-	-
	1mm			126, 138							
CASE_4.2	Min. Rqd	-	-	* , 50	-	48 ,*	-	-	-	-	-
	1			*,52							

Note: - In above table first & second value indicate Von-Mises & Max. Principal respectively

4.4.4 Fatigue Analysis Results with 1 mm thickness reduction

Figure 4.61 shows the cumulative fatigue life plot on the strut. The corresponding minimum fatigue life is $10^{1.91}$blocks = **81 blocks**. This is equivalent to 26325 landings after considering a scatter factor of 4.

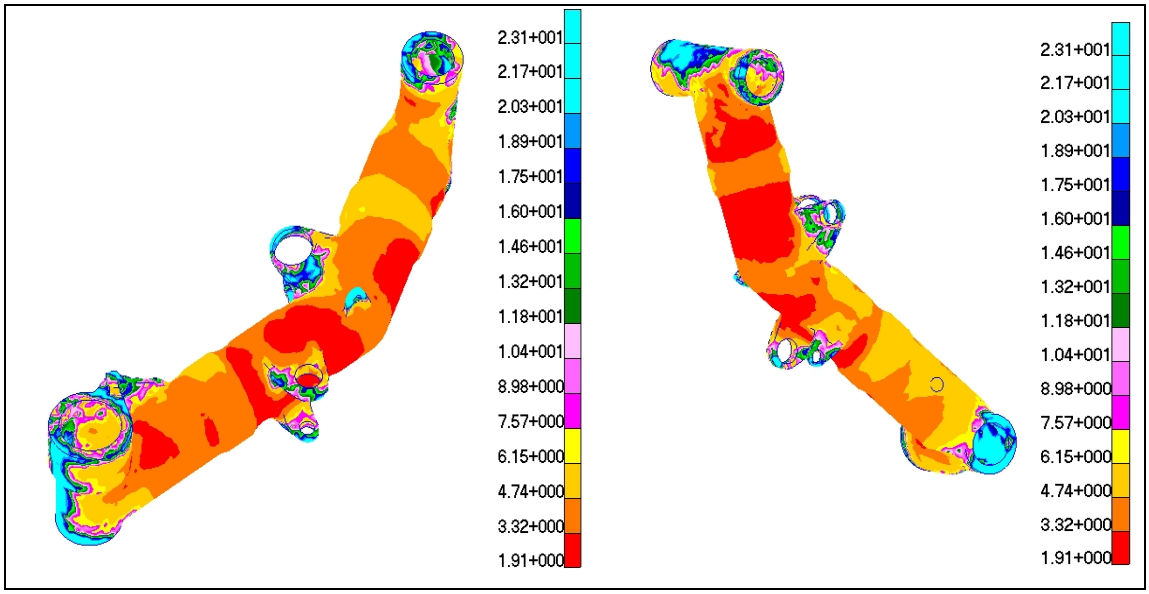

Figure 4.61 Fatigue life plot on the MLG strut with 1mm reduction in thickness

4.5 DISCUSSIONS

The results obtained shows that FEA can be used as powerful tool for numerical solution to a wide range of engineering problems. Also with aid of statistical design and advances in computer technology, FEA can play a vital roll to provide quick and accurate solution to complex problem with relative ease.

Using this numerical procedure, the uncertainties associated with experiments can be avoided and cost can be significantly reduced.

The FEA is employed to analyze fatigue life of MLG & NLG of Article 29L are furnished below for discussion.

1. Stress/Fatigue Analysis Results of MLG & NLG of article 29L are placed at table 4.6.

Table-4.6 Stress/Fatigue Analysis Results

S. No.	MLG		NLG	
	Max. Principal Stress	**No. of Cycles**	**Max. Principal Stress**	**No. of Cycles**
Case-1	118.0	100	92.7	100
Case-2	99.3	100	39.4	100
Case-3	105.0	400	47.4	400
Case-4(-Pz)	120.0	200	51.3	250
Case-4(+Pz)	53.0	500	55.8	250
Total No. of landing/block	1300		1100	
Fatigue life before crack initiation with minimum wall thickness	85 block or 27625 landing with scatter factor of 4		107 block or 29425 landing with scatter factor of 4	

2. MSC.FATIGUE Fatigue analysis shows life of 85 & 107numbers of blocks before crack initiation, considering minimum wall thickness for MLG & NLG respectively.

3. Maximum stress 120Kg/mm^2 is observed in load case 4 (-Pz) for MLG and 92.7 Kg/mm^2 is observed in load case 1 for NLG.

4. From this analysis it can be thrash out that life of NLG is better as compare to MLG.

5. Stress & Fatigue Analysis with 1mm wall thickness reduction against the requirement of maximum 0.5mm reduction shows Maximum Principal Stress 138kg/mm^2 which is still below the yield stress. Therefore, if

rejuvenation is to be done after 2000 landings, then it will further add to the life of strut.

6. Above analysis is done without considering effect of residual compressive stress on assembly therefore the rejuvenation of MLG is not required.

7. The estimated fatigue life of MiG-27 MLG is 27625 landings with minimum wall thickness mentioned in drawings and 26325 landings considering thickness reduction of 1.0 mm due to rejuvenation. The above estimated life of landings considers a scatter factor of 4 with stress ratio R=0,where

R= $\frac{\sigma_{min}}{\sigma_{max}}$

8. Considering reverse loading (stress ratio R= -1where R= $\frac{\sigma_{min}}{\sigma_{max}}$) & scatter factor 4, theoretical fatigue life estimation by miner's shows a life of 10,812 landings. This theoretical estimated life is highly conservative since actual loading spectrum is of fluctuating nature. Considering these aspects, actual fatigue life should be at least two times than the estimated life by Miner's Equation

CHAPTER 5: CONCLUSIONS

5.1 CONCLUSIONS

Stress hot spots identified by the present analysis is in agreement with six rejuvenation zones and as well as with classical calculations. This proves that FE modeling, Loads & Boundary Conditions for FE analysis defined are accurate.

From this analysis it can be seen maximum stress 120Kg/mm^2 is observed in load case 4 (-Pz) for MLG and 92.7 Kg/mm^2 is observed in load case 1 for NLG. It can also be seen that Maximum stress is 23% more in MLG as compare to NLG. Thus NLG is better than NLG.

Analysis shows that all the stress levels are below yield stress of the material, therefore there is no possibility of permanent set, which indicates that there is no possibility of change of the sign of residual compressive stress induced during rejuvenation.

MSC.FATIGUE Fatigue analysis shows life of 27625 landing & 29425 landing with scatter factor of 4 before crack initiation, considering minimum wall thickness for MLG & NLG respectively.

Number of strain gauges can be optimize i.e installation of minimum number of strain gauges during full scale fatigue testing with the help of stress result i.e strain gauge need to install near the hot spots only.

FEM can provide quick and accurate solutions to complex problem with relative ease as well as economically and should be used in vide range in future.

5.2 RECOMMENDATIONS/FUTURE SCOPE OF WORK

The stress obtained from fatigue analysis can be validated by experiment i.e. full scale fatigue testing result.

The determined cumulative fatigue damage hot spots can be rejuvenated locally and more no of landing (life of LGs) can be extended accordingly and avoid the experimental stress analysis approach and testing for life extension.

In future during design & development of new MLG & NLG of any fighter or civil aircraft this approach can be used to optimize the weight and estimate the fatigue life of MLG & NLG.

This approach can also be helpful for handpicked selection of material as well as critical dimensions of MLG & NLG components.

BIBLIOGRAPHY

LIST OF REFERENCES

1. Azevedo C.R. de Farias, Hippert E. Jr., 2002, Fracture of an aircraft's landing gear, Journal of Engineering Failure Analysis 9 (2002) 265-275

2. Bagnoli F. *, Dolce F., Colavita M., Bernabei M., 2008, Fatigue fracture of a main landing gear swinging lever in a civil aircraft, Journal of Engineering Failure Analysis 15 (2008) 755–765

3. Kaplan Mitchell P. and Wolff Timothy A.,2001, Fatigue-Life Assessment, International Journal of Fatigue (2001) 856-868

4. L.A.L.,*, Lourenco N.J. , Graca M.L.A., Silva O.M.M. , Campos P.P. de , Dollinger C.F.A. von, 2006 Fatigue fracture of a nose landing gear in a military transport aircraft Franco, Journal of Engineering Failure Analysis 13 (2006) 474–479.

5. Leea Hong-Chul, Hwanga Young-Ha, Kimb Tae-Gu, 2003, Failure analysis of nose landing gear assembly, Journal of Engineering Failure Analysis 10 (2003) 77–84

6. La Rue J.E., Daniewicz S.R., 2006, Predicting the effect of residual stress on fatigue crack growth, International Journal of Fatigue (2006) 956–966.

7. Messier-Dowty Ltd (2001), Description of Main landing gear leg part number 201383001 and 201383002, CMM 32-11-83, Gloucester, Messier-Dowty Ltd.

8. Messier-Dowty Ltd (2001), Description of Shock absorber, CMM 32-27-21, Gloucester, Messier-Dowty Ltd.

9. Morrow J, Society of Automotive Engineers, 1968, Fatigue Design hand book. 21-29

10. Ossa E.A., 2006, Failure analysis of a civil aircraft landing gear, Journal of Engineering Failure Analysis 13 (2006) 1177–1183

11. Astakhove M. F.: USSR & HAL, Nasik, Aircraft stress analysis (Vol –I)

12. Chandrupatala T R: 1981, Prentice Hall New Delhi, Introduction to Finite Element Analysis

13. Currey Norman S., 1988: Aircraft Landing Gear Design: Principal and Practices, American institute of aeronautics & Astronautics Inc.

14. Cook Robert D., Malkus David S., Plesha Michael E. & Witt Robert J.: Concepts & Applications of Finite Element Analysis

15. Maintenance Manual Book 3 of Article 29L

16. Stress Album of aircraft article 29L MLG

17. Stress Album of aircraft article 29L NLG

18. HYPERMESH User Guide

19. MSC. PATRAN/NASTRAN 2004 User Guide

20. Tumnov A T: USSR, Russian material handbook MMT-12 Vol-1

21. Report On Classical Stress Analysis of Article 29L under carriages MLG & NLG

22. Report No. IGC/NDED/EMSIS/RS-MIG-27-LG1-DEPTH/09/01-B. Report on Residual Stress measurement in MLG of article 29L.

23. Test Program for LG's of Article 29L Reg. No. I/29/3228/318.

24. Technical description of Article 29L aircraft book-3.

APPENDIX-A

1. Material Specification and its properties

Following is the list of material and its properties. The materials common to MLG & NLG are compiled and the data is as follows.

Table 1 Material property specification

Sl No	Material Used	E (KG/MM^2)	Poission Ratio	Density (KG/MM^3)
1.	30KHGSN2A	19000	0.3	7850
2.	30KHGSA	20000	0.3	7850
3.	BRAZHMTS 10-3-1.5	10500	0.3	7500
4.	STEEL20	21000	0.3	7860
5.	STEEL45	20000	0.3	7850
6.	STEEL20A	21000	0.3	7850
7.	CAST IRON MN	16000	0.3	7800
8.	18KHNVA	20400	0.3	7800
9.	M2	12000	0.3	8950
10.	3M3	12000	0.3	8950
11.	40KHN2SMA (EI-643)	19000	0.3	7810
12.	12KHN3A	20400	0.3	7800
13.	STEEL10	20000	0.3	7860
14.	BRAZHN-10-4-4	12500	0.3	7700
15.	STEEL 65 S2VA	19000	0.3	7850
16.	AK4-1	7200	0.3	2840
17.	BRB2-T	11700	0.3	8250
18.	MILD STEEL	20000	0.3	7850

2. Fatigue property data

Following Figures (from Figure 1 to 3 Shows the S-N curve of different material

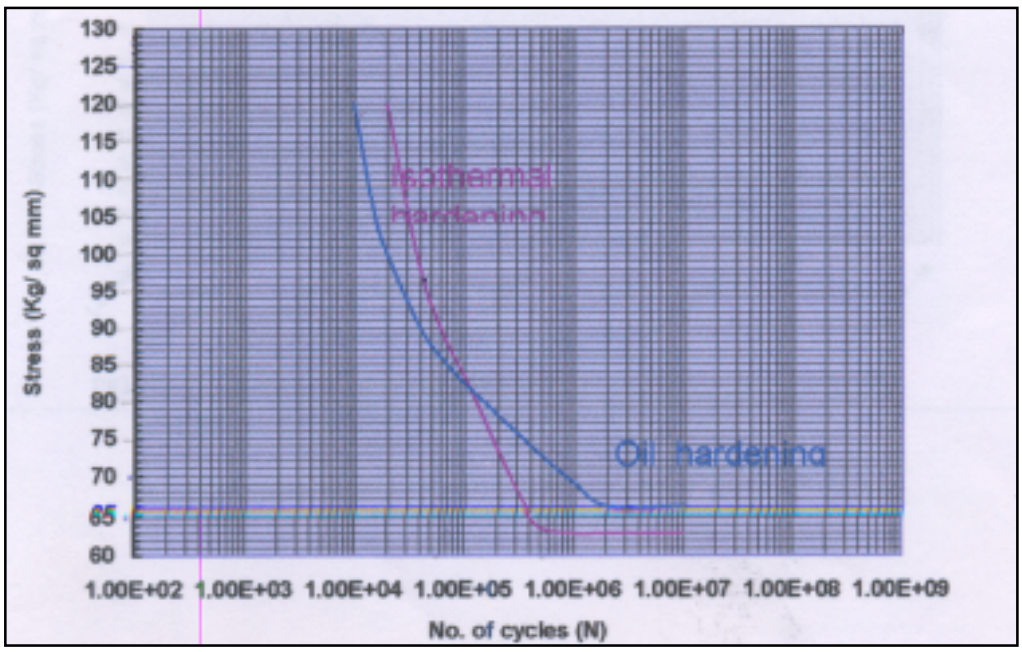

Figure 1 S-N curve of 30KhSNA2A steel in bending for plain specimen.

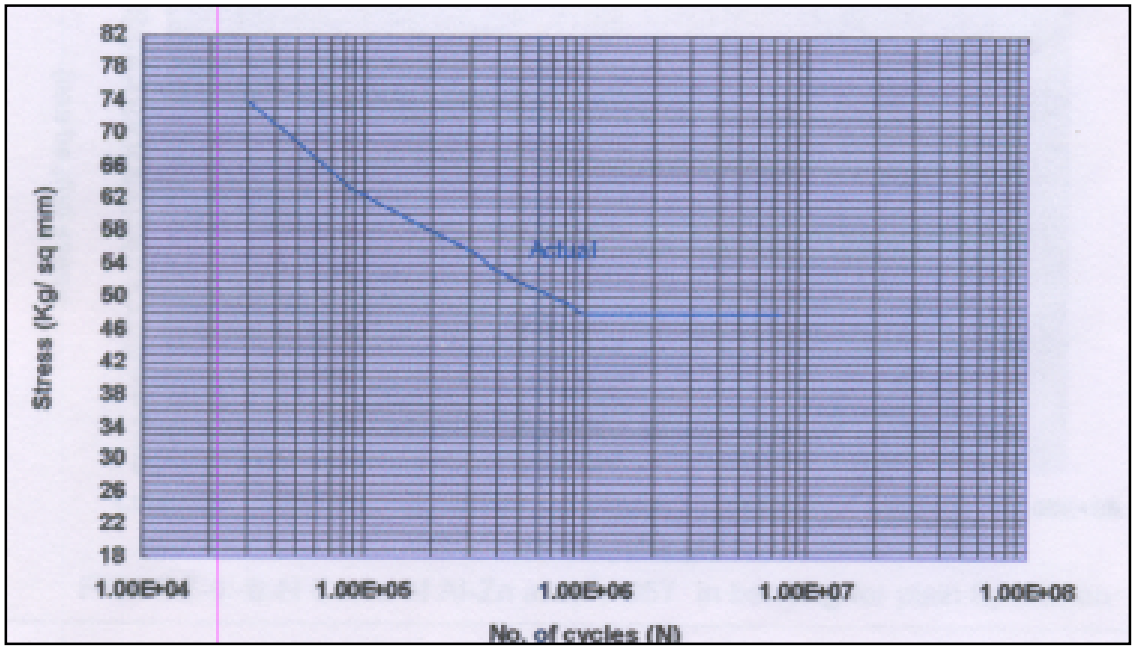

Figure 2 S-N curve of 30KhSA steel in bending for plain specimen

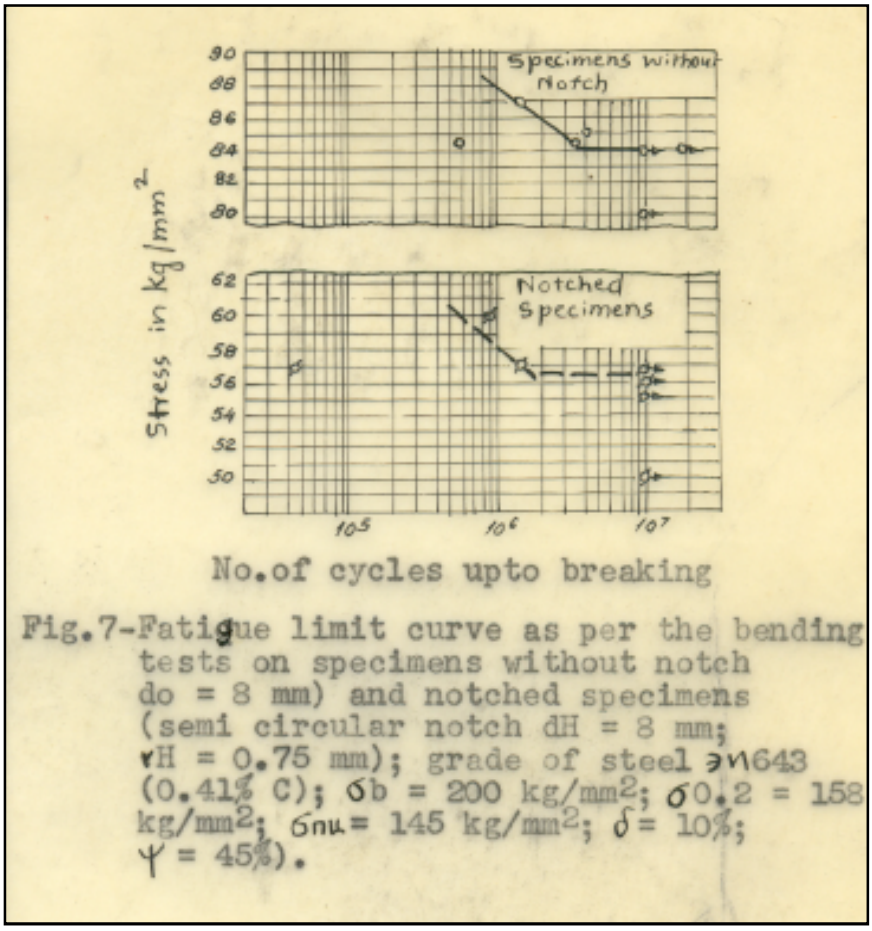

Fig.7-Fatigue limit curve as per the bending tests on specimens without notch do = 8 mm) and notched specimens (semi circular notch dH = 8 mm; rH = 0.75 mm); grade of steel EN643 (0.41% C); σb = 200 kg/mm^2; $\sigma 0.2$ = 158 kg/mm^2; σnu = 145 kg/mm^2; δ = 10%; ψ = 45%).

Figure 3 S-N curve of EN643 steel in bending for plain specimen.

APPENDIX-B

1. Solid isoparametric quadrilaterals and hexahedra Element

The library of solid elements in HYPERMESH contains first- and second-order isoparametric elements. The first-order elements are the 4-node quadrilateral for plane and axisymmetric analysis and the 8-node brick for three-dimensional cases. The library of second-order isoparametric elements includes "serendipity" elements: the 8-node quadrilateral and the 20-node brick, and a "full Lagrange" element, the 27-node (variable number of nodes) brick. The term "serendipity" refers to the interpolation, which is based on corner and midside nodes only. In contrast, the full Lagrange interpolation uses product forms of the one-dimensional Lagrange polynomials to provide the two- or three-dimensional interpolation functions. All these isoparametric elements are available with full or reduced integration. Gauss integration is almost always used with second-order isoparametric elements because it is efficient and the Gauss points corresponding to reduced integration are the Barlow points (Barlow, 1976) at which the strains are most accurately predicted if the elements are well-shaped.

The three-dimensional brick elements can also be used for the analysis of laminated composite solids. Several layers of different material, in different orientations, can be specified in each solid element. The material layers or lamina can be stacked in any of the three isoparametric coordinates, parallel to opposite faces of the master element. These elements use the same interpolation functions as the homogeneous elements, but the integration takes the variation of material properties in the stacking direction into account. Hybrid pressure-displacement versions of these elements are provided for use with incompressible and nearly incompressible constitutive models.

2. Fully integrated first-order isoparametric elements

For fully integrated first-order isoparametric elements (4-node elements in two dimensions and 8-node elements in three dimensions) the actual volume

changes at the Gauss points are replaced by the average volume change of the element. This is also known as the selectively reduced-integration technique, because the order of integration is reduced in selected terms, or as the $\bar{\beta}$technique, since the strain-displacement relation (β-matrix) is modified. This technique helps to prevent mesh locking and, thus, provides accurate solutions in incompressible or nearly incompressible cases: see Nagtegaal et al. (1974). In addition, HYPERMESH uses the average strain in the third (out-of-plane) direction for axisymmetric and generalized plane strain problems. Hence, in the two-dimensional elements only the in-plane terms need to be modified. In the three-dimensional elements the complete volumetric terms are modified. This may cause slightly different behavior between plane strain elements and three-dimensional elements for which a plane strain condition is enforced by boundary conditions.

3. Triangular, tetrahedral, and wedge elements

The library of solid elements in HYPERMESH includes first- and second-order triangles, tetrahedra, and wedge elements for planar, axisymmetric, and three-dimensional analysis.

Hybrid versions of these elements are provided for use with incompressible and nearly incompressible constitutive models (see “Hybrid incompressible solid element formulation,” for a detailed discussion of the formulation used). However, these hybrid forms should be used only to fill in regions in meshes made of brick elements; otherwise, too many constraint variables may be introduced.

Second-order tetrahedra are not suitable for the analysis of contact problems: a constant pressure on an element face produces zero equivalent loads at the corner nodes. In contact problems this makes the contact condition at the corners indeterminate, with failure of the solution likely because of excessive gap chatter. The same argument holds true for contact on triangular faces of a wedge element.

4. Beam elements

The element library in HYPERMESH contains several types of beam elements. A “beam” in this context is an element in which assumptions are made so that the problem is reduced to one dimension mathematically: the primary solution variables are functions of position along the beam axis only. For such assumptions to be reasonable, it is intuitively clear that a beam must be a continuum in which we can define an axis such that the shortest distance from the axis to any point in the continuum is small compared to typical lengths along the axis. This idea is made more precise in the detailed derivations in “Beam element formulation”. There are several levels of complexity in the assumptions upon which the reduction to a one-dimensional problem can be made, and different beam elements in HYPERMESH use different assumptions.

The simplest approach to beam theory is the classical Euler-Bernoulli assumption, that plane cross-sections initially normal to the beam's axis remain plane, normal to the beam axis, and undistorted. The beam elements in HYPERMESH that use cubic interpolation (element types B23, B33, etc.) all use this assumption, implemented in the context of arbitrarily large rotations but small strains. The Euler-Bernoulli beam elements are described in “Euler-Bernoulli beam elements,” This approximation can also be used to formulate beams for large axial strains as well as large rotations. The beam elements in HYPERMESH that use linear and quadratic interpolation are based on such a formulation, with the addition that these elements also allow “transverse shear strain”; that is, the cross-section may not necessarily remain normal to the beam axis. This extension leads to Timoshenko beam theory (Timoshenko, 1956) and is generally considered useful for thicker beams, whose shear flexibility may be important. (These elements in HYPERMESH are formulated so that they are efficient for thin beams-where Euler-Bernoulli theory is accurate—as well as for thick beams: because of this they are the most effective beam elements in HYPERMESH.) The large-strain formulation in these elements allows axial strains of arbitrary magnitude; but quadratic terms in the nominal torsional strain are neglected compared to unity, and the axial strain is assumed to be small in

the calculation of the torsional shear strain. Thus, while the axial strain may be arbitrarily large, only “moderately large” torsional strain is modeled correctly, and then only when the axial strain is not large. We assume that, throughout the motion, the radius of curvature of the beam is large compared to distances in the cross-section: the beam cannot fold into a tight hinge. A further assumption is that the strain in the beam's cross-section is the same in any direction in the cross-section and throughout the section. Some additional assumptions are made in the derivation of these elements: these are introduced in the detailed derivation in “Beam element formulation,”.

For certain important designs the beam is constructed from thin segments made up into an open section. The response of such open sections is strongly effected by warping, when material particles move out of the plane of the section along lines parallel to the beam axis so as to minimize the shearing between lines along the wall of the section and along the beam axis. The beam element formulation (“Beam element formulation,”) includes provision for such effects. Beam elements that allow for warping of open sections (B31OS, B32OS etc.) are also derived. The particular approach used for modeling open-section warping in HYPERMESH is based on the assumption that the warping amplitude is never large anywhere along the beam axis because the warping will be constrained at some points along the beam-perhaps because one or both ends of the beam are built into a stiff structure or because some form of transverse stiffeners are added.

The regular beam elements can be used for slender and moderately thick beams. For extremely slender beams, for which the length to thickness ratio is $O(10^3)$or more and geometrically nonlinear analysis is required (such as pipelines), convergence may become very poor. For such cases use of the hybrid elements, in which the axial (and transverse) forces are treated as independent degrees of freedom, can be beneficial. The hybrid beam formulation is described in “Hybrid beam elements,”. Distributed pressure loads applied to beams (for example, due to wind or current) will rotate with the beam, leading to

follower force effects. The derivation of the load stiffness that accounts for this effect is presented in “Load stiffness for beam elements,”

In some piping applications thin-walled, circular, relatively straight pipes are subjected to relatively large magnitudes of internal pressure. This has the effect of creating high levels of hoop stress around the wall of the pipe section so that, if the section yields plastically, the axial yield stress will be different in tension and compression because of the interaction with this hoop stress. The PIPE elements allow for this effect by providing uniform radial expansion of the cross-section caused by internal pressure.

In other piping cases thin-walled straight pipes might be subjected to large amounts of bending so that the section collapses (“Brazier collapse”); or a section of pipe may already be curved in its initial configuration-it might be an “elbow.” In such cases the ovalization and, possibly, warping, of the cross-section may be important: these effects can reduce the bending stiffness of the member by a factor of five or more in common piping designs. For material linear analysis these effects can be incorporated by making suitable adjustments to the section's bending stiffness (by multiplying the bending stiffness calculated from beam theory by suitable flexibility factors); but when nonlinear material response is a part of the problem it is necessary to model this ovalization and warping explicitly. Elbow elements are provided for that purpose; they are described in “Elbow elements,” . Elbow elements look like beam elements to the user, but they incorporate displacement variables that allow ovalization and warping and so are much more complex in their formulation. In particular, ovalization of the section implies a strong gradient of strain with respect to position through the wall of the pipe: this requires numerical integration through the pipe wall, on top of that used around the pipe section, to capture the material response. This makes the elbow elements computationally more expensive than beams. Since consideration of planar deformation only provides considerable simplification in formulating beam elements, for each beam element type in HYPERMESH a corresponding beam element is provided that only moves in the (X, Y) plane. However, the open-section beams are provided only in three dimensions for reasons that are obvious.

APPENDIX-C

1. Kinematic coupling constraints

Kinematic coupling constrains the motion of the coupling nodes to the rigid body motion of the reference node. The constraint can be applied to user-specified degrees of freedom at the coupling nodes with respect to the global or a local coordinate system.

Kinematic constraints are imposed by eliminating degrees of freedom at the coupling nodes. In HYPERMESH/Standard once any combination of displacement degrees of freedom at a coupling node is constrained, additional displacement constraints-such as MPCs, boundary conditions, or other kinematic coupling definitions-cannot be applied to any coupling node involved in a kinematic coupling constraint. The same limitation applies for rotational degrees of freedom.

2. Translational degrees of freedom

Translational degrees of freedom are constrained by eliminating the specified degrees of freedom at the coupling nodes. When all translational degrees of freedom are specified, the coupling nodes follow the rigid body motion of the reference node.

3. Rotational degrees of freedom

Rotational degrees of freedom are constrained by eliminating the specified degrees of freedom at the coupling nodes. All combinations of selected rotational degrees of freedom result in rotational behavior identical to existing MPC types:

- Selection of three rotational degrees of freedom along with three displacement degrees of freedom is equivalent to MPC type BEAM.
- Selection of two rotational degrees of freedom is equivalent to MPC type REVOLUTE in HYPERMESH/Standard.
- Selection of one rotational degree of freedom is equivalent to MPC type UNIVERSAL in HYPERMESH/Standard.

In HYPERMESH/Standard internal nodes are created by the kinematic coupling to enforce the constraints that are equivalent to MPC types REVOLUTE and UNIVERSAL. These nodes have the same degrees of freedom as the additional nodes used in these MPC types and are included in the residual check for nonlinear analysis.

4. Specifying a local coordinate system

The kinematic coupling constraint can be specified with respect to a local coordinate system instead of the global coordinate system (see “Orientations,”). Figure 28.3.2–1 illustrates the use of a local coordinate system to constrain all but the radial translation degrees of freedom of the coupling nodes to the reference node. In this example a local cylindrical coordinate system is defined that has its axis coincident with the structure's axis. The coupling node constraints are then specified in this local coordinate system.

5. Constraint direction and finite rotation

In geometrically nonlinear analysis steps the coordinate system in which the constrained degrees of freedom are specified will rotate with the reference node regardless of whether the constrained degrees of freedom are specified in the global coordinate system or in a local coordinate system.

6. Distributing coupling constraints

Distributing coupling constrains the motion of the coupling nodes to the translation and rotation of the reference node. This constraint is enforced in an average sense in a way that enables control of the transmission of loads through weight factors at the coupling nodes. Forces and moments at the reference node are distributed either as a coupling node-force distribution only (default) or as a coupling node-force and moment distribution. The constraint distributes loads such that the resultants of the forces (and moments) at the coupling nodes are equivalent to the forces and moments at the reference node. For cases of more than a few coupling nodes, the distribution of forces/moments is not determined by equilibrium alone, and distributing weight factors are used to define the force distribution.

The moment constraint between the rotation degrees of freedom at the reference node and the average rotation of the cloud nodes can be released in one direction in a two-dimensional analysis and one, two, or three directions in a three-dimensional analysis. In a three-dimensional analysis you can specify the moment constraint directions in the global coordinate system or in a local coordinate system. All available translational degrees of freedom at the reference node are always coupled to the average translation of the coupling nodes.

In a three-dimensional HYPERMESH/Standard analysis if all three moment constraints are released by specifying only degrees of freedom 1–3, only translation degrees of freedom will be activated on the reference node. If only one or two rotation degrees of freedom have been released, all three rotation degrees of freedom are activated at the reference node. In this case you must ensure that proper constraints have been placed on the unconstrained rotation degrees of freedom to avoid numerical singularities. Most often this is accomplished by using boundary conditions or by attaching the reference node to an element such as a beam or shell that will provide rotational stiffness to the unconstrained rotation degrees of freedom.

7. Fatigue algorithm details

Brown Miller analysis

This is a critical plane multi-axial fatigue algorithm, using planes perpendicular to the surface, and at 45° to the surface. Stress results from an elastic FEA are required. A multi-axial elastic-plastic correction is used to calculate elastic-plastic stress-strains from the elastic FEA stresses

On each of three planes, fatigue lives are calculated on eighteen subsidiary planes, spaced at 10 degree increments. On each plane

- the principal strains are used to calculate the time history of the shear strain and the strain normal to the plane
- fatigue cycles are extracted and corrected for the effect of the mean normal stress
- the fatigue life is calculated

The fatigue life is the shortest life calculated for the series of planes

This algorithm uses the strain-life curve defined by the equation:

$$\frac{\Delta\gamma}{2}+\frac{\Delta\varepsilon_n}{2}=1.65\frac{\sigma_f'}{E}(2N_f)^b+1.75\varepsilon_f'(2N_f)^c$$

Morrow, User Defined or no mean stress correction may be selected. See section 14.6 for a definition of the used-defined MSC. For the Morrow mean stress correction the strain-life equation is modified to:

$$\frac{\Delta\gamma}{2}+\frac{\Delta\varepsilon_n}{2}=1.65\frac{(\sigma_f'-\sigma_m)}{E}(2N_f)^b+1.75\varepsilon_f'(2N_f)^c$$

This algorithm can be also be used for fatigue analysis of elastic-plastic FEA results. (See section 15).

The Brown Miller algorithm is the preferred algorithm for most conventional metals at room temperature and is the default algorithm for most materials in the *fe-safe* materials data base. See Volume 2, section 7 for the background to this algorithm.

Maximum principal strain analysis

This is a critical plane multi-axial fatigue algorithm, using planes perpendicular to the surface. Stress results from an elastic FEA are required. A multi-axial elastic-plastic correction is used to calculate elastic-plastic stress-strains from the elastic FEA stresses

Fatigue lives are calculated on eighteen planes, spaced at 10 degree increments. On each plane

- the principal strains are used to calculate the time history of the strain normal to the plane.
- cycles of normal strain are extracted and corrected for the mean stress
- the fatigue life calculated

The fatigue life is the shortest life calculated for the series of planes

This algorithm uses the strain-life curve defined by the equation:

$$\frac{\Delta\varepsilon}{2}=\frac{\sigma_f'}{E}(2N_f)^b+\varepsilon_f'(2N_f)^c$$

Morrow, User Defined or no mean stress correction may be selected. See section 14.6 for a definition of the used-defined MSC. For the Morrow mean stress correction the strain-life equation is modified to:

$$\frac{\Delta\varepsilon}{2}=\frac{(\sigma_f'-\sigma_m)}{E}(2N_f)^b+\varepsilon_f'(2N_f)^c$$

Alternatively, an FRF calculation can be used with this algorithm - see section 17.3.

This algorithm can be also be used for fatigue analysis of elastic-plastic FEA results. (See section 15).

Fatigue analysis using principal strains can give very non-conservative results for ductile metals. See Volume 2, section 7 for the background to this algorithm.

APPENDIX-D

1. Figure 4 & 5 shows MLG in extended and retracted condition

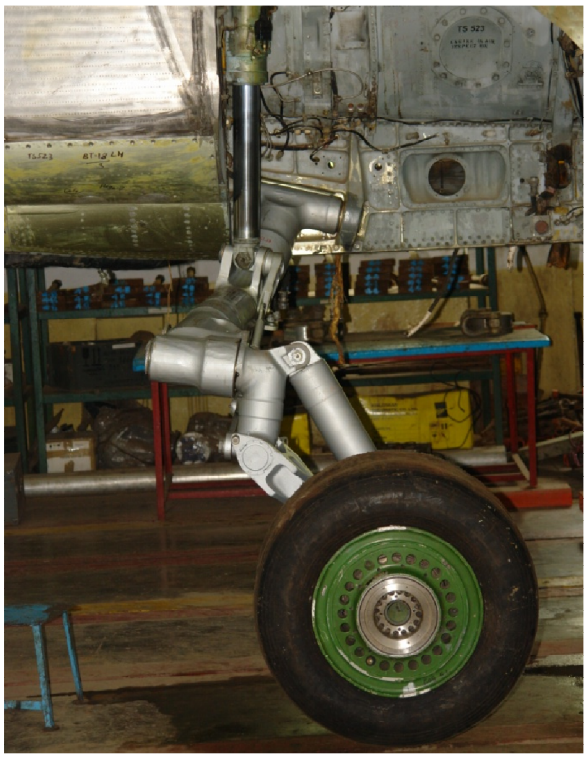

Figure 4 MLG at Extended condition

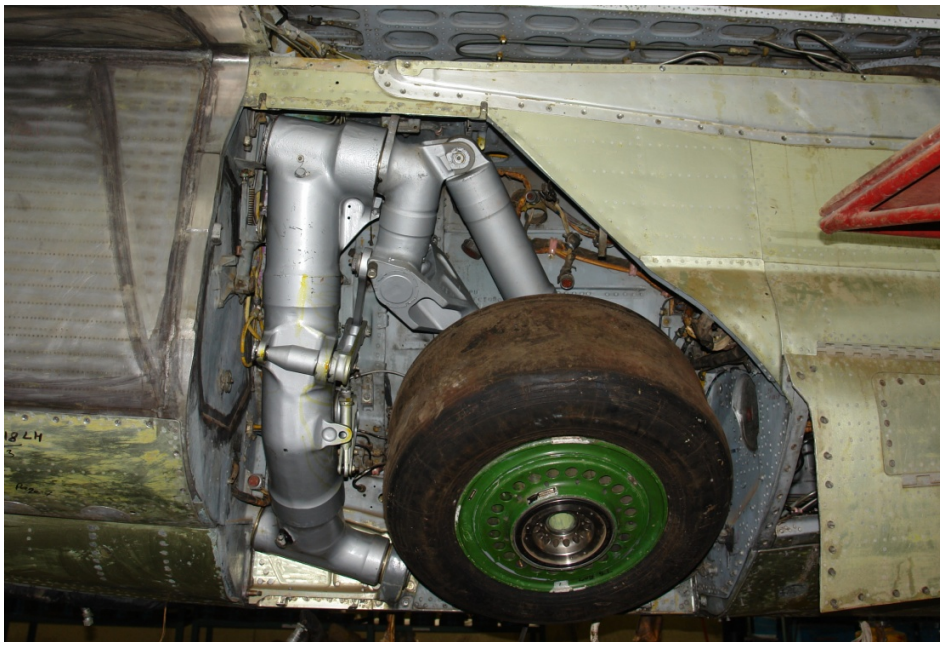

Figure 5 MLG at retracted condition”

2. Figure 6 & 7 shows Article 29L in flying & ground mode with MLG & NLG extended

Figure 6 Fighter Aircraft “Article 29L” in Flying Mode

Figure 7 Fighter Aircraft “Article 29 on Grounds